THESIS

ASSESSING THE ON-FARM EFFECTS OF REMOVING SALTS FROM IRRIGATION WATER

Submitted By

Sanskriti Shrestha

Department of Civil and Environmental Engineering

In partial fulfillment of the requirements

For the Degree of Master of Science

Colorado State University

Fort Collins, Colorado

Spring 2023

Master's Committee:

Advisor: Ryan Bailey

Sybil Sharvelle
Gregory Butters

ABSTRACT

ASSESSING THE ON-FARM EFFECTS OF REMOVING SALTS FROM IRRIGATION WATER

In dry and semi-arid places where precipitation is insufficient to sustain a regular percolation of water through the soil, salt-induced land degradation is frequent. Desalination of irrigation water is an emerging alternative that can be utilized to repurpose our salt-affected agricultural lands, thus providing an avenue for sustaining the growing production demands with limited water and land resources. Therefore, a combination of fieldwork, modeling and soil sensor records was implemented to evaluate the feasibility of an on-farm Reverse Osmosis (RO) system, in terms of crop yield and soil salinity, for the desalination of irrigation water over three growing periods. Four types of treatment systems were applied to 16 experimental field plots at the Arkansas Valley Research Center (Rocky Ford, CO), representing soil conditions of the Lower Arkansas River Valley (LARV), a region of which approximately 70% is affected by salt-induced crop yield loss. Statistical t-tests done on the data of the three seasons did not show any significant differences in the VMC, EC and biomass of the plots irrigated with the different treatments. Results of the tests for season 3, which showed an increase in t-values and a decrease in p-values demonstrated the need for a longer study period to gauge any significant effects. Similarly, the results of sensor data did not show a significant decrease in soil salinity for the study period. The average soil electrical conductivity (EC) showed a 20% to 26% reduction in soil salt mass in the fields irrigated with desalinated water over the three seasons, however, the EC results did not show a consistent decreasing trend across the 16 plots. A 6-year numerical modeling forecast done by the hydro-chemical model HYDRUS 1D simulating dry, average, and wet weather showed a 6% to 20% reduction in EC when desalination was applied to the fields. These preliminary results of the field and modeling approaches

provide encouragement for the continuation of desalination treatments to see any substantial long-term effects.

ACKNOWLEDGMENTS

This thesis would not have been possible without the people who supported me along the way. I would like to express my warmest thanks to my advisor, Dr. Bailey for giving me this opportunity and for your calm and consistent guidance that helped shape this study. I would also like to sincerely acknowledge the invaluable support and guidance from our collaborators at AVRC, UNT, NMSU and CSU campuses, particularly Dr. Miguel Acevedo and Breana Smithers for coming down and helping with all the field trips and the desalination trailer setup at AVRC, a special thanks to Breana for helping me with the desalination trailer writeup for this thesis. I am incredibly grateful to all my peers who worked alongside me in the fields during harvest and seeding every season. I would like to thank my committee members Dr. Sybil Sharvelle and Dr. Gregory Butters for their guidance and encouragement. I would also like to thank the INFEWS project (grant #185605) of the National Science Foundation for providing financial support for this study. My heartiest gratitude goes to my close-knit friends in Fort Collins for being my unwavering pillars of support for the past two years. Last but not the least, I am appreciative of my family who have been there always, whose love has sustained me so far along my journey to gain this Master's degree at CSU.

TABLE OF CONTENTS

LIST OF TABLES

LIST OF FIGURES

1. INTRODUCTION

Agricultural losses brought on by salinity are evidenced to be significant and are anticipated to rise as more intensive irrigation methods are implemented to meet increasing food demands. Saline soils contain excess of soluble salts like Cl^-, Ca^+, Na^+, Mg^{2+} and SO_4^{2-}, which in normal conditions would assist in plant growth, but in excess amounts are detrimental to it [1]. Conventionally, soils having an EC greater than 4 mS/cm in the soil saturation extract are borderline saline with some sensitive high value crops such as citrus, tomato, capsicum and potatoes being affected at half the concentration [2]. Plant nutrition, photosynthesis and cellular metabolism are affected by osmotic stress and ionic toxicity which are associated with accumulation of salts in the soil [3]. The impediment caused by increasing soil salinity for a particular species can be assessed through their rate of survival, vegetative growth and seed production [4]. Globally, agricultural lands have been shrinking due to industrialization and/or habitat use, therefore, it is of utmost importance to utilize the available land affected by salinity to meet the food demand.

Salt mass in soil and soil water can have a detrimental effect on crop growth and yield by preventing plants from absorbing water and by impeding transpiration and photosynthetic activity on the surface of leaves [5] [6] [7] . To cope with this, plants can develop defense mechanisms such as increase in chlorophyll content along with changes in the leaf anatomy to prevent leaf ion toxicity, increases in the root/ canopy ratio to maintain the water status and prevent water loss [6]. The physical effects in plants can be seen in slow growth, smaller leaves, darker leaves and waxy coatings, or they may not show any symptoms unless they are compared with normal plants [1]. In locations with intense agricultural operations, high saline levels can reduce agricultural productivity [8] [9].

Some examples of salt-induced land degradation caused by anthropogenic activities that decreased the agricultural yields include the Indo-Gangetic Basin in India, the Indus Basin in Pakistan, the Yellow River Basin in China, the San Jaoquin Valley in the US, the Aral Sea Basin in Central Asia, and the Euphrates

Basin in Syria [10]. The Food and Agriculture Organization (FAO) identified 932 million ha of salt-affected soils in 1988; and 32 million ha of dryland agriculture are salt-affected. As per recent reports considering salt induced land degradation, economic losses could total $27 billion annually [11]. Historically, salinity has affected human civilization for centuries, a prime example comes from Mesopotamia, where the early civilizations first thrived before collapsing as a result of salinization brought on by humans. Kuwait, the United Arab Emirates, the Middle East, Australia, Spain and many other nations have evaluated their soils and soil salinization on a national scale. Their reports have scientists predicting that salinity and sodicity affect 10% of all arable land; one billion hectares are covered by saline and/or sodic soils; 25% to 30% of irrigated lands are salt-affected and essentially commercially unproductive; 954 million ha are salt-affected soils globally [12].

Salt buildup in soils can be due to high salt concentration in irrigation water, lack of flushing events, poor soil drainage, and high evapotranspiration, with the latter concentrating salts in the remaining soil water [13]. Furthermore, poor soil drainage can lead to high groundwater levels, with two detrimental impacts: high-salinity groundwater can transport large quantities of salt mass into the root zone of crops; and induces higher rates of groundwater flow into nearby streams, which can load high quantities of salt mass to downstream areas. The impact of salts and sodium on soils is determined by the salinity (EC) to sodicity (SAR) ratio. Sodicity and salinity both encourage soil dispersion and flocculation, respectively. The swelling factor, or the amount a soil is anticipated to swell with various combinations of salinity and sodicity, is used to measure the salinity and sodicity of soils. In essence, the swelling factor determines whether salinity-induced flocculation or sodium-induced dispersion will have a greater impact on the physical qualities of soil [14]. Agricultural practices in semi-arid and arid regions often implement strategies for combating soil salinity buildup and consequent decrease in crop yield. One set of strategies focuses on desalination technology to remove salt mass from irrigation water before application to fields.

Alkali metal salts at high concentrations are harmful to plant growth and productivity. Agronomists and soil testing labs regularly utilize the soil Saturated Paste Extract (SPE) method to evaluate soil salinity, salt components, and their effects on soils. The method quantitatively determines the concentration of dissolved chemical ions in the soil solution that are not associated with soil minerals and organic matter [15]. The SPE is the best indicator of plant response to salinity compared with other ratio extractions that provides relevant information on qualitative assessment of soil texture, soil pH, dissolved salts, salt chemical constituents, potential management information on salinity, sodicity, and/or B toxicity [16]. To determine a soil's relative alkalinity or acidity, the pH of the soil can be measured at saturation. Salinity is assessed based on the chemical makeup of the soluble salts as well as their electrical conductivity. The soil sodicity can be determined from the examination of the salt contents based on the SPE sodium absorption ratio (SAR) [15].

There have been numerous field and modeling studies to evaluate the effects of desalination on farms. An example is a study to assess the shallow aquifers present in Tunisia with Geospatial Multi-Criteria Approach to rank the feasibility of installation of a solar-PV desalination system for sustainable agriculture in small-scale farms. The primary markers of the highest appropriateness of the aquifers in this study were the lower salinity, the greater agricultural area, and the water availability[17]. Other Mediterranean countries like Spain and Israel have been at the forefront of desalination technology and its application as an alternative water resource for agriculture. A mid 1990s drought forced Spanish mainland farmers to install more than 200 small scale brackish water desalination plants [18]. Later, to protect aquifers from overexploitation, they shifted to large scale seawater desalination plants (SWDPs). Their proposed SWDPs planned to use RO technology with 40 to 50% efficiency. The main concern for their irrigation districts has been the price which is considered too high for farms' economy and discussion between the government and farmers have led to the proposals for 'social price' to curb the desalination costs for farmers.

Similarly, the arid climate of Israel has forced their agricultural water users to practice brackish water irrigation as an option for agriculture, with specific criteria governing DSW production for agricultural use [19]. Israel has created a sophisticated water supply system that includes freshwater extraction, agricultural reuse of TWW, and considerable brackish and ocean water desalination [20]. The results of the scientific monitoring of these early farming experiences were not entirely encouraging though, demonstrating that irrigation with DSW could be difficult and that there were some significant issues to consider when planning its agricultural use.

In Australia, another desalination technology, Membrane Capacitive Deionization (MCDI), showed a profit of AU$2500/ha/yr to AU$44,200/ha/yr when compared to the use of brackish water for irrigation [21]. For salinities larger than from 1.2 to 4.7 dS/m depending on the crop and region, the MCDI desalination system was deemed to be more profitable than brackish irrigation over the course of a 10-year investment. The study also found that profitability of the desalination system depended on climatic and geographic factors like rainfall and soil type, with areas receiving higher rainfall having higher profitability due to flushing of the soil resulting in less solute buildup and less irrigation required, unlike drier areas where higher irrigation was required resulting in less profitability. Along with that, protective cropping like greenhouse generated more profit than when the crops were grown in open fields; however, increased capital costs of protective cropping need to be considered when analyzing the net profit.

Desalinating brackish groundwater before using it for irrigation, utilizing salt-tolerant crops, and controlling soil conditions are all ways to deal with the problem of high soil salinity [22], [23]. High quality irrigation water is necessary for current methods of managing and rehabilitating soil salinity; this additional need could be satisfied by desalination. Desalination of brackish water, however, necessitates substantial energy inputs, increasing both the cost to the farmer and CO_2 emissions if this energy were to come from burning fossil fuels or another carbon-based source of electric power. In order to mitigate environmental concerns associated with the disposal of desalination concentrate, it is also commonly

acknowledged that it is critical to reduce the volume of concentrate from desalination procedures, particularly from inland areas [24], [25]. Together, these three issues—soil salinity control, concentration management, and energy supply—remain a barrier to technological advancements that would permit the widespread use of alternate water sources for agricultural production, notably brackish groundwater desalination. This study is a part of a bigger project by the NSF that focuses on the Food-Energy-Water nexus that has been engaged in addressing these issues, by developing off-grid sustainable desalination pilot projects, powered by photovoltaic (PV) and wind generators. In particular, the focus is on addressing the soil salinity issue for this study.

With limited and inconsistent supply of water, much of the western United States extending from the Continental Divide of the Rocky Mountains to the shores of California is arid, characterized by desert land and vegetation and semi-arid, characterized by prairie land [26]. Western agriculture increases the variety of agricultural production across the country and further guarantees that domestic customers have access to a steady supply of a variety of foods. Many production innovations were developed in the dry and semi-arid parts of the United States before being exported to more humid regions or other nations [27]. Southeastern Colorado is an important region in western agriculture and has benefited from irrigation by the Arkansas river by the web of over 1000 miles of channels that diverts the water and distributes it to the fertile alluvial lands [28]. The side effect of this is that the groundwater table has risen so high that the salts are unable to leach back into the deeper layers and are accumulated in the root zone of the crops, a growing concern common to similarly irrigated regions around the world. The reasons for this can be attributed to excessive irrigation, seepage from the earthen canals, and inadequate drainage facilities. The direct effects of the increase in soil salinity can be seen in the reduced crop and biomass yield in the region which is also a common pattern globally.

Table 1 summarizes the Soil Salinity (as *ECe*) Measured with EM38 Probes in Fields in the Lower Arkansas River Valley [29]. While evaluating the results in this table, it should be noted that the region's

principal crops, alfalfa and corn, have considerable yield losses at a value between around 2 and 4 dS/m [30]. The average values during that study period was around or more than 4 dS/m, which shows the need for remediation efforts in the region.

Table 1: Salinity in the upstream region of LARV throughout the years [29]

		Number of fields surveyed	Number of locations surveyed per field			Average ECe (dS/m) measured over field		
Season	Year		Minimum	Maximum	Mean	Minimum	Maximum	Mean
Early	1999	68	31	86	63	2.35	10.14	4.24
Late	1999	67	31	89	67	2.4	9.66	3.96
Early	2000	73	17	99	59	2.32	8.28	3.49
Late	2000	77	32	117	64	0.78	12.51	3.81
Early	2001	80	27	123	62	1.16	17.22	4.83
Late	2001	76	30	97	60	1.34	12.07	4.43
Early	2002	80	30	128	72	1.5	17.94	3.67
Late	2002	32	16	107	64	1.74	15	4.28
Early	2003	52	24	107	62	1.88	15.31	4.19
Late	2003	37	24	120	65	2.03	5.98	3.26
Early	2004	66	23	142	69	1.77	12.81	4.2
Late	2004	61	30	102	63	1.72	12.35	4.2

The objective of this thesis is to quantify the effects of small-scale, on-farm, off-grid desalination technology on crop yield and soil salinity in a semi-arid environment. The LARV, a region in the Southeastern Colorado, is selected in the study due to high soil salinity and estimated crop damages in recent decades. The research plan includes 16 experimental 10 ft x 20 ft field plots with two 5 ft wide planting beds at the Arkansas Valley Research Center (AVRC) in Rocky Ford, Colorado, with each plot receiving either direct groundwater or desalinated groundwater for irrigation, and half of the plots receiving a compost inoculation mixture to stimulate biological activity in the soil profile. Desalination is accomplished using a RO system, developed by project collaborators at the University of North Texas. The approach is conducted over three growing periods (summer, 2021; fall-winter 2021-2022; summer, 2022).

Crop yield is quantified through harvesting, soil sodicity and salinity are quantified through soil sampling and within-plot soil sensors (soil moisture, EC), placed at depths of 6 in and 12 in. Statistical measures are used to determine the effects of desalinated irrigation water and compost. Finally, we used the field-based hydro-chemical numerical model HYDRUS 1D to forecast the effects of ongoing desalination on soil salinity and salinity leaching. The model used the combination of field data in the form of salt ion concentrations obtained from the soil test results as well as the sensor data that recorded water content, EC and temperature. Therefore, this research is an amalgamation of physical, numerical and scientific methods to assess and address the concerns regarding salinity in agricultural fields. The results of this thesis provide preliminary conclusions for on-farm desalination technology, and methods can be used for other irrigated areas experiencing soil salinity buildup.

2. MATERIALS AND METHODS

Desalination through RO removes ions that are necessary for plant growth in addition to the unwanted salts from the water. Desalinated water usually replaces irrigation water that had previously supplied essential nutrients like Calcium (Ca^{2+}), Magnesium (Mg^{2+}), and Sulfate (SO_4^{2-}) at levels high enough to prevent further fertilization of these elements. Therefore, in order to supply necessary nutrients in sufficient amounts, the RO permeate was mixed with raw well water. In this thesis, three kinds of approaches were used to study and quantify the effects of removing salt mass from irrigation water. More details will be provided in later sections.

1. The first approach was field based with seasonal seeding and harvesting of crops on the experimental field plots at AVRC. Four types of treatments were applied to the field: - 1. Irrigation with agricultural water (AW) with inoculation of compost (0.8 mS/cm), 2. Irrigation with AW without the inoculation of compost, 3. Irrigation with well water (WW) with the inoculation of compost (3.116 mS/cm), 4. Irrigation with WW without the inoculation of compost. Here, agricultural water refers to RO permeate mixed with a small amount of well water to replenish deficient nutrients, and well water refers to the pumped groundwater applied without any desalination. These four treatments were replicated four times, resulting in a total of 16 plots. Crop biomass was quantified at the end of each growing period via harvesting and weighing.
2. The second approach was soil profile based, using soil sampling and soil sensors to track the soil water content, soil temperature and soil salinity. Soil samples were taken each growing period, and soil sensors were placed, one in each plot at 6 or 12 inches. Soil salinity was assessed on the basis on laboratory tests and tracking through the sensors. The sensors recorded these three types of data continuously every 15 minutes during each growing period. Comparing the results of these two methods provided preliminary results to assess the effectiveness of the treatments.

3. The third approach was numerical modeling based, using the 1D finite element hydro-chemical model HYDRUS [31] to estimate the impact of decadal implementation of desalination on soil water content and salt ion concentrations in the soil profiles of the experimental plots.

2.1 Study Region

The study region is in the Lower Arkansas River Valley near Rocky Ford in Otero County, Colorado (Figure 1). The average monthly precipitation in the region ranges from a high of 5.0 cm during the summer months (April-September) to 0.7 cm during the winter months (October-March). Despite arid climate, the market value of product sold comes around $121.5 million with 687.53 acres of farm spread across the county [32]. Irrigators divert water through various irrigation canals from the Arkansas River or pump the water from the alluvial aquifer [33]. The region is primarily known for agricultural productions of crops like cantaloupe, melons, corn, squash, beans and several other vegetables [34]. The water quality of the river valley has been impaired due to contamination by selenium, uranium, sulfates, and salts [29]. Field scale mapping of salinity in Arkansas River showed salinity levels of the canal systems along the river increasing from 300 ppm Total Dissolved Solids (TDS) near Pueblo to nearly 4000 ppm TDS near the Colorado Kansas Border [35]. Approximately 70% of the region has experienced a decrease in crop yield due to elevated soil salinity [28], [36].

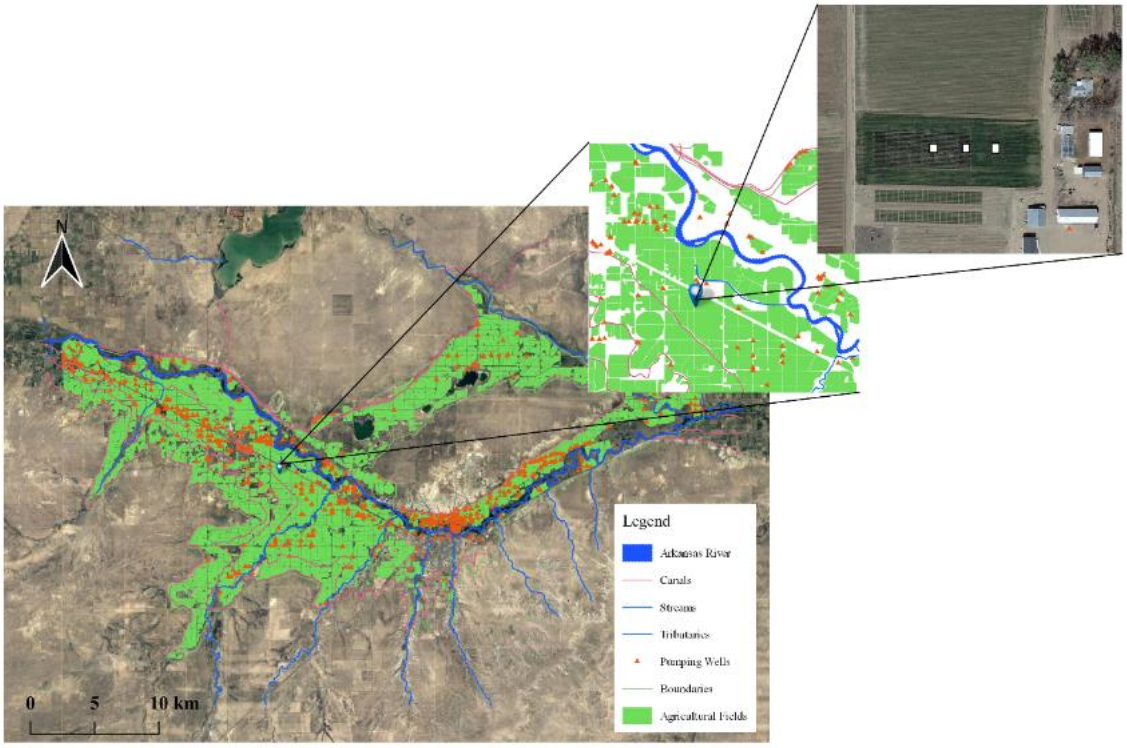

Figure 1 Map of the Study area showing the upstream section of Arkansas River Basin, Arkansas River and its major tributaries, canals, fields and pumping wells. Second inset displays the position of soil sensors at the experimental site.

This project is based on a 3200 ft² section of Colorado State University Arkansas Valley Research Centre (AVRC) in Rocky Ford, Colorado. The soil sensors are installed in the plots at 6 and 12 inches. Each plot is irrigated with the different treatments. The seeding and harvesting are done twice a year, around May for summer crops and around October for winter crops. A solar powered desalination trailer located right beside the plots has the system installed in situ that supplies the irrigation water to the fields using drip irrigation. The RO system was designed and installed by project collaborators at the University of North Texas. The drip tapes are buried at 4-5 inches depths. A layout of the 16 experimental plots, along with treatments and depth of soil sensors, is shown in Figure 2.

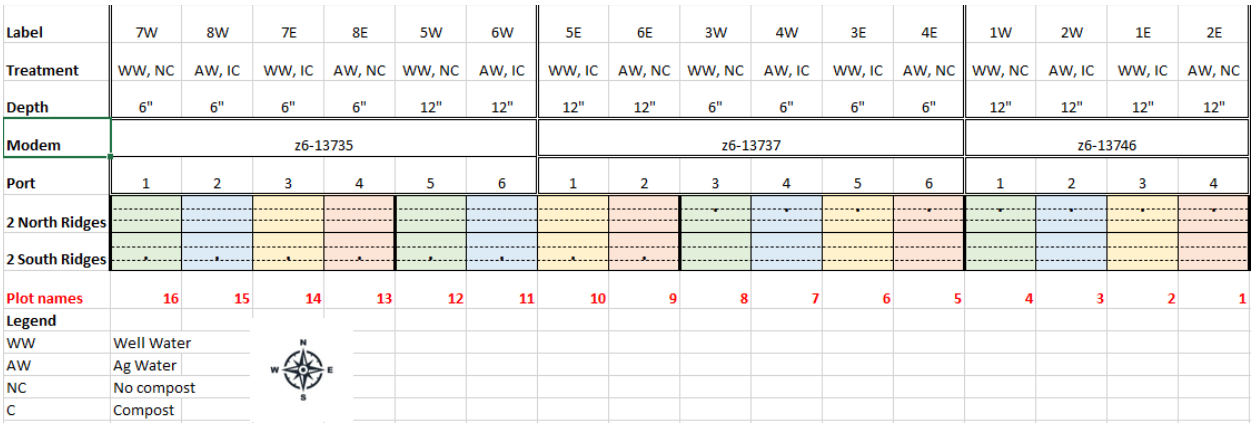

Figure 2 Experimental plots with respective treatments at AVRC, four treatments ((AW, IC), (AW,NC), (WW,IC), (WW, NC)) were replicated four times each; depth is the depth of soil sensors, modem is the device connected to the online database ZENTRA, there are six ports each connected to the first and second modem and four ports connected to the third modem. The north and south ridges represent the location of the buried soil sensors, and the plots are named 1 to 16 from the east.

2.1.1 Water quality conditions at AVRC

According to element analysis, AVRC had non-detectable and lower quantities of elements like Al, As, Ba, Be, Cd, Co, Cr, Fe, Mn, Mo, Ni, Pb, Se, Tl, V, Zn, Bi, Li, P, and Cu. The analysis was also done on the RO permeate and brine water. Table 2 presents the initial water quality conditions of the three types of water. From the tests done at the start of season 2, the RO permeate from the AVRC, showed high removal of Ca (96.6%), Mg (96.5%), SiO2 (93.2%), Na (91.5%), and S (97.1%) from the well water where Ca, Mg, K, SiO2, Na and S were measured with 429.4, 105.6, 7.4, 22, 150.2 and 449.1 mg/L respectively. They were measured at 955, 305, 410, 65.9, 19.9, and 1102 mg/L, respectively, in brine water. SiO_2, Sr, S, Na, Mg and Li were rejected by RO membrane with more than 90% removal rate.

Table 2: Chemistry of the three types of water at AVRC

	AVRC, Colorado				
	RO permeate	**Agricultural water**	**Well water**	**Brine water**	**Rejection %**	***MDL**
B (mg/L)	0.12	0.17	0.26	0.51	53.8	0.007
Ba (mg/L)	0.05	0.00	0.01	0.05	-	0.001
Ca (mg/L)	14.8	67.2	429.4	955	96.6	0.016
Cu (mg/L)	0.1	0.0	ND	0.2	-	0.003

Fe (mg/L)	0.05	ND	ND	0.81	-	0.037
K (mg/L)	ND	0.5	2.7	7.4	-	0.304
Li (mg/L)	0.0	0.0	0.1	0.3	100	0.008
Mg (mg/L)	3.7	16.4	105.6	305	96.5	0.241
Na (mg/L)	12.7	29.2	150.2	410	91.5	0.0483
Ni (mg/L)	0.01	0.00	0.01	0.04	0	0.002
S (mg/L)	13.0	66.8	449.1	1102	97.1	0.5
SiO_2 (mg/L)	1.5	3.8	22.0	65.9	93.2	0.0151
Sr (mg/L)	0.3	1.2	7.4	19.9	95.9	0.0012
Zn (mg/L)	1.7	0.0	ND	0.4	-	0.006

2.2 Quantifying the effect of Desalination Technology on soil salinity and crop production

2.2.1 Off-Grid Desalination System

The desalination system used in our research performed the softening by cation exchange resins (CEX), nanofiltration (NF), smart use of available water, hybrid photovoltaic and wind power renewable energy, and reduced electrical power consumption and costs. The system at AVRC is based on reverse osmosis (RO) desalination technology and blending of RO permeate with raw well water to produce irrigation water with reduced values of electrical conductivity (EC) compared to the brackish water from the well at AVRC (Figure 3). The system can produce about 3.5 liter/min (~ 1 gpm) of permeate and is operated at low recovery ratio (50-60%) to avoid scaling due to the high calcium sulfate concentration of the AVRC well water. Upon blending of permeate with well water, the system produces about 7-8 liters/min (~2 gpm) of irrigation water at about 800 μS/cm, which is about a 0.25-0.3 of that of well water (~2,600 -3,000 μS/cm).

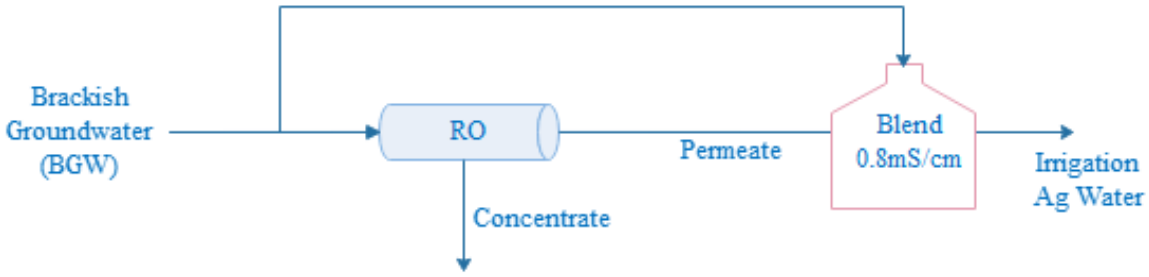

Figure 3 AVRC Desalination system schematic

To further prevent membrane scaling, the process water is dosed with anti-scalant as well as HCl acid (reducing pH to 5.8). On a regular basis, the membranes are cleaned and then flushed with permeate using two cleaning-in-place (CIP) tanks. The system is controlled automatically by a programmable logic controller (PLC), which we can access remotely to program sensors (level switches, pressure transducers, temperature sensors, level switches, flow meters, shunts, pH and EC transmitters) and actuators (valves, pumps, motors). The system is completely off-grid powered by photovoltaic (PV) panels, and it is designed to minimize electrical power consumption and costs. The electric power system is designed for 24 V comprised of 1.3 kW PV array installed generation capacity, along with a battery bank of 600 Ah storage capacity.

2.2.2 Effects on crop yield

The focus while selecting the crops for this study has been on crops grown in saline soils and irrigated with brackish water, developing a Soil Microbial Community solution to improve crop yield and soil salinity. Enhanced soil improvement, and concomitant reduction of atmospheric CO_2, is sought by inclusion of crops able to sequester carbon in the soil. Crop mixes used in this study containing crops like Daikon radish, Purple Vetch, Winter wheat, Black oilseed sunflower, etc. fulfill these needs to sequester Carbon in the soil and reducing fertilizer use.

Mixtures of winter and summer cover crops contained a variety of species. Every year, two plantings (spring and autumn) were conducted. The trial site was ripped, disked, and planted in the first

year of the tests. The area was mowed the following years before being ripped, disked, and planted [37]. The first seeding at AVRC was done in June 2021 when summer cover crops were planted in the 16 experimental plots. Custom Crotalaria mix containing Daikon Radish, black sunflowers, grain sorghum and sun hemp were planted in the fields. The planting rate was 30 per acre with 468 K seeds/ac and approximately 11 seeds/sq ft coverage. The grown plants were then harvested using a tractor at the end of September 2021 and another set of winter cover crops was seeded. The winter crop mix included fewer plants like Red Winter Wheat, Cereal Rye and Purple Vetch. Comparing the two seasons, the summer crops were more abundant with higher biomass weight. During the summer growing season, the plots were irrigated according to the different treatments to meet the potential evapotranspiration rates as recorded by the CoAgMet weather station at AVRC. During winter, the irrigation was stopped, and the irrigation lines were winterized to prevent the bursting of pipes due to freezing winter temperatures. The soil sensors installed at 6 and 12 inches recorded soil hydrologic properties throughout the growing season. The 15-minute interval data could be accessed and stored online through a remote server, ZENTRA Cloud. In the summer of 2022, which was the third season, the crop seed mix included crimson clover, proso millet, smart radish and black oilseed sunflower.

After harvesting each plot, the weights of biomass were recorded and summed up as the total biomass produced by the plot with a particular treatment. The grown crops were collected in a bucket and weighed on a tared scale. A small amount of cut sample was collected in a paper bag from each plot and transported to the nearby greenhouse as soon as possible. The initial weight of the sample was recorded using a tared scale. It was left in the greenhouse to dry for nearly two weeks. At that point, the dry weights of the samples were recorded. The difference between the initial weights and the final weights helped estimate the moisture content of the samples collected from each plot. The seeding and harvesting were performed again in June 2022 and October 2022, respectively. Same process was repeated throughout the plots.

2.2.3 Effects on soil salinity and sodicity

To gauge the effects of the trial treatments on soil salinity and properties, soil samples were taken after each harvest and before planting the next batch of crops. The samples were collected at two depths during the first harvest from each plot. During the second harvest, only one sample was taken. They were collected at the depths of the sensors in that respective plot. During the third harvest in October 2022, two samples were collected again. Those were then sent to Ward Laboratories (Kearney, Nebraska) for the analysis of concentrations of major salts using the soil SPE method and the Cation Exchange Capacity. The primary salts in all the soil tests were Ca^{++}, Na^{+}, Mg^{++}, Cl^{-}, S^{2+}. The soil Organic Matter content, the SAR, the total Carbon and total Nitrogen were also included in the soil tests of the second season. The change in the soil chemistry was tracked every season to gauge the effect on soil salinity.

2.2.4 Long-term effects of desalination

Since the study period (2021-2022) in this thesis is not long enough to determine long-term effects in the soil salinity for our field tests, hypothetical scenarios were created to test the efficacy of our treatment system over multiple years. In order to prepare regulations to control the soil salinity, numerous steady-state as well as transient models have been developed. Traditionally, steady state assumptions have been used to calculate the leaching requirements, which are then used to prepare guidelines for the application of irrigation water, as more than enough water for evaporation should be applied to the fields to leach salts from the root zone. The distribution of root balls and root water uptake are important factors to determine the crop yield for salinity stress [13]. Widely used steady state models like WATSUIT, WPF and transient models like HYDRUS, UNSATCHEM, ENVIRO-GRO, SALTMED and SWAP use these approaches to predict the leaching requirements when brackish irrigation water is used. By quantifying the long-term effects of removing salts from irrigation water on soil salinity, we seek to analyze whether small-scale field-based desalination systems can help mitigate the water quality deterioration in the region.

For this study, the HYDRUS 1D model was used to simulate the water flow and salt ion chemical transport in the soil profile. The model can be used to examine how water and other substances travel through porous medium that is either completely or partially saturated. The soils in the flow region might not be uniform. Transport and flow were in a horizontal direction for this study. The water flow portion of the model is capable of handling boundaries governed by atmospheric conditions, prescribed head and flux bounds, and free drainage boundary conditions [31]. The model simulates the process of plant water uptake by coupling potential transpiration, which depends on plant and atmospheric conditions, with soil restriction to water flow, or the root-water uptake water stress response function [38]. The model uses mechanistic equations and the Richards equation (flow in variably saturated porous media) to reproduce the osmotic and matric potential of soil. The plant water uptake is simulated based on root size and distribution and the crop yield by Maas and Hoffman equations for salinity stress [39]. Following is a brief theoretical description of all the model processes used in the simulations with equations [31].

2.2.4.i. Water transport in HYDRUS

The governing flow equation for one-dimensional isothermal Darcian flow in a variably saturated rigid porous medium is given by the following modified form of the Richards equation:

$$\frac{\partial \theta}{\partial t} = \frac{\partial}{\partial z}\left(k\frac{\partial h}{\partial z} + \cos\alpha\right) - S \quad (1)$$

where θ is the volumetric water content, h is the soil-water pressure head, K is the hydraulic conductivity, z is the vertical coordinate positive upward, and t is the time.

2.2.4.ii. Solute Transport in HYDRUS

The partial differential equations governing one-dimensional nonequilibrium chemical transport of solutes involved in a sequential first-order decay chain during transient water flow in a variably saturated rigid porous medium are taken as

$$\frac{\partial \theta c}{\partial t} + \frac{\partial \rho s}{\partial t} = \frac{\partial}{\partial z}\left(\theta D\frac{\partial c}{\partial z}\right) - Scr - \mu_w\theta_C - \mu_s\rho s + \gamma w\theta + \gamma s^{\rho} \quad (2)$$

where c and s are solute concentrations in the liquid and solid phases, respectively; ρ is the soil bulk density, μ_w and μ_s are first-order rate constants for solutes in the liquid and solid phases, respectively; γ_w and γ_s are zero-order rate constants for the liquid and solid phases, respectively; S is the sink term in the flow equation, c_r is the concentration of the sink term, and D is the dispersion coefficient for the liquid phase:

$$D = Dw\tau + \lambda|\mathrm{v}| \quad (3)$$

where D_w is the molecular diffusion coefficient, τ is a tortuosity factor, λ is the longitudinal dispersivity, and v is the average pore water velocity.

2.2.4.iii. Heat transport in HYDRUS

Neglecting the effect of water vapor diffusion on transport, one-dimensional heat transfer can be described with a convection-dispersion equation of the form

$$\frac{\delta C_p(\theta)T}{\delta t} = \frac{\delta}{\partial x}\left[\lambda(\theta)\frac{\delta T}{\delta x}\right] - C_\omega\frac{\delta qT}{\partial x} - C_w ST \quad (4)$$

where $\lambda(\theta)$ is the coefficient of the apparent thermal conductivity of the soil and $C_p(\theta)$ and C_w are the volumetric heat capacities of the porous medium and the liquid phase, respectively.

2.2.4.iv. Root water uptake and root growth in HYDRUS

The water stress response function suggested by Feddes [40]and an S-shaped function suggested by van Genuchten [41] can be used to calculate the potential root water uptake and the actual root water uptake. Root water uptake with compensation can be simulated when the Critical Stress Index is smaller than one [31]. The effect of salinity stress on root water uptake can be ignored (No Solute Stress) or taken into account using the Additive or Multiplicative models.

The root water uptake in response to transpirational demand is distributed over the root-zone and should be reduced in response to matric and salinity stress. HYDRUS uses a simple root growth function

$$L_R(t) = L\,max\left[\frac{L_0}{L_0+(L_m-L_0)e^{-r_t}}\right] \quad (5)$$

where L_{max} is the maximum rooting depth, L_o is the initial (non-zero) rooting depth and r is a root growth factor.

2.2.4.v. Inverse Solution in HYDRUS

HYDRUS can be used in inverse mode to match observed data by modifying system parameters. For this thesis, we matched sensor-measured soil water content by modifying soil hydraulic parameters. For the estimation of the solute transport and reaction parameters, HYDRUS performs parameter optimization by inverse methods which describe the difference between the values observed and the expected system response and are based upon the minimization of a suitable objective function[31]. A correlation matrix that details the level of correlation between the fitted coefficients is produced by HYDRUS as part of the inverse solution. The correlation matrix compares similar changes as a result of changes in other parameters to changes produced by tiny changes in the final estimate of a given parameter.

The soil profile in our model was created according to the type of soil found in the region [42]. By creating observation points at the depths of soil sensors installed on the farm, the movement of salt in the profile was modeled using the sensor data of the three growing seasons. The UNSATCHEM module is inbuilt into HYDRUS and is used to simulate the chemical transport of salt ions in the profile. The main processes incorporated in the inverse simulation were Water Flow, Heat Transport, Root Water Uptake, and Root Growth. The model was run for 70 days (first season) for 15 of the 16 plots. Plot 4's inverse simulation could not be performed due to a prominent lapse in the periodic sensor data. The volumetric water content (VMC) (m^3/m^3) and temperature (°C) recorded daily at the sensor depths were used as the input values for the inverse simulation. The van Genuchten-Mualem single porosity model was used to estimate soil hydraulic properties and the Feddes model was used to simulate the root water uptake.

A 46-cm soil depth was selected to make the profile uniform because according to a report by the National Co-operative Soil Survey[1], the top layer of silty clay loam extends to that depth, and it includes both our sensor depths. For the inverse simulation, initial estimates of residual and saturated soil water content (θr and θs respectively), parameter alpha (α) and parameter (n) in the soil water retention function, saturated hydraulic conductivity (Ks) and tortuosity parameter (l) were used. These were estimated from the Neural Network Prediction model by providing the textural class of the soil profile. After that, the upper (UBC) and lower boundary conditions (LBC) were selected. For the UBC, atmospheric BC with a Surface Layer option was chosen and for the LBC, a free-draining soil profile was selected. The initial conditions were based on water content, the values of which were obtained from the sensors. Similarly, the initializing parameters for heat transport were provided based on the Chung and Horton Thermal Conductivity model values for loamy soil. For heat transport, both the upper and lower boundary conditions were based on temperature. The time variable input data contained the precipitation, evaporation and transpiration in cm/day, and the daily surface temperature (°C). These values were obtained from the Rocky Ford station of the CoAgMet, which operates a network of agricultural weather stations around the state of Colorado. Then the observation points were created at the depth of the installed soil sensor in the soil profile. Every step was repeated for 15 simulations with different treatments and depths of the observation points.

2.2.4.vi Forecasting simulations

Using the historical weather data collected from the CoAgMet website, dry, average, and wet periods of precipitation were chosen to run 3 types of forward simulations based on the results of parameter estimates from the inverse simulations. These three precipitation scenarios were chosen to emulate the different weather patterns. The dry period was modeled based on the years 2012-2013, the average period was modeled after 2007-2008 and the wet period was modeled after 2017-2018 precipitation data, all of which were repeated three times to create a 6-year data set for each of the simulations. For the forward

simulations, the Major Ion Chemistry Solute Transport option in HYDRUS, which uses the inbuilt UNSATCHEM model, was used to track the chemical mass balance of salt ions in the soil layers. The solution concentrations in meq/L and adsorption concentrations (Cation Exchange Capacities (CEC)) in meq/kg were input as the initial conditions for the salts in the soil, the values of which were obtained from the soil tests done after each harvest and before the beginning of the new season. The detailed calculations of the activity coefficients, Gapon coefficients, solution compositions are presented in Appendix A. The values of CEC of all the plots from the soil tests are presented in Table 3.

Table 3: CEC (meq/kg) of the 16 plots at AVRC and partition of Cations (%)

Plot #	CEC (meq/kg)	% K	%Ca	%Mg	%Na	Plot #	CEC (meq/kg)	% K	%Ca	%Mg	%Na
1	225	2	86	11	1	**9**	268	2	81	15	2
2	246	2	83	13	2	**10**	270	2	81	15	2
3	222	2	86	11	1	**11**	280	2	80	15	2
4	222	1	86	11	1	**12**	261	2	81	15	2
5	231	2	83	13	2	**13**	272	2	80	16	2
6	218	2	82	14	2	**14**	257	2	81	15	2
7	267	2	82	14	2	**15**	272	2	81	15	2
8	281	2	80	15	2	**16**	275	2	80	15	3

For the forecasting simulations, plots 12 and 13 were chosen to represent WW and AW treatment scenarios, respectively. The irrigation regime was patterned after the field modeled after our own project by adopting the same irrigation frequency as well as amount of water for the forecast. Each precipitation scenario was repeated for both plots and the parameters estimated through inverse modeling were plugged into the model.

RESULTS AND DISCUSSION

3.1 Crop Yield

The crop yields of the three seasons were tracked based on the biomass produced by the type of irrigation water used and whether the plots were inoculated with compost. Results presented in Figure 5 show that the plots that were irrigated with RO permeate mixed with well water (AW plots) produced biomass with a higher center of distribution than those irrigated with direct well water (WW plots) in all three seasons. The average biomasses were 2.73 kg (4.5%), 0.48 kg (2.7%), and 2.9 kg (8.75%) higher in AW plots than in the WW plots. Based on the inoculation of compost, mixed results were seen. The plots which were inoculated with compost (IC) produced less biomasses than those without compost (NC) in the two summer seasons by 2.5kg (4.14%) and 4.33 (13.08%) kg respectively. The distribution of NC was positively skewed as seen in Figure 4 (D) and (F). However, in the second season which was longer and cooler, the IC plots produced 1.63 kgs (8.9%) more biomass than the NC plots. The IC plot biomass distributions were more compact throughout the seasons than observed in the NC plots.

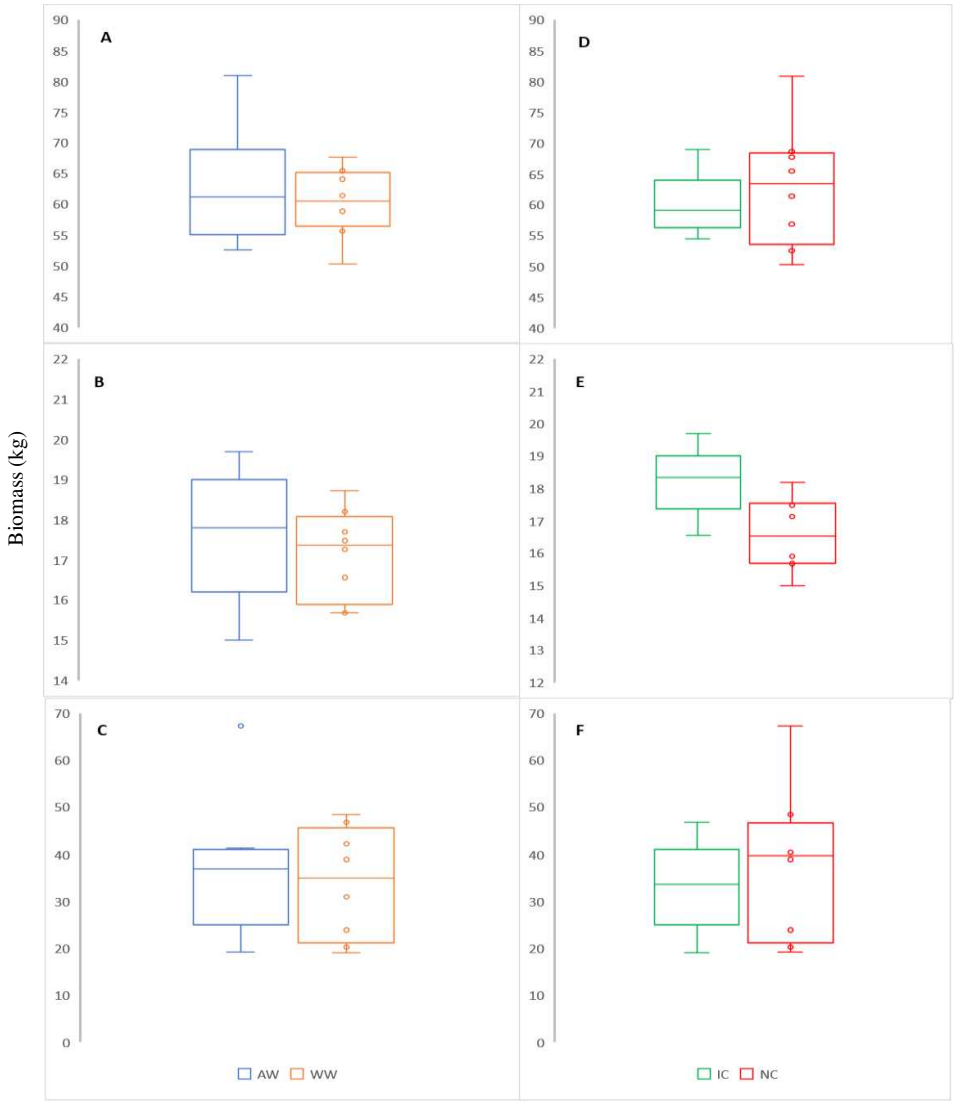

Figure 4 Biomass weights for the three seasons; A, B, C: AW vs. WW for season 1, season 2, season 3 respectively; D, E, F: IC vs NC for season 1; season 2 and season 3 respectively

No definitive results were seen in the comparison of the three seasons in AW-WW and IC-NC comparisons. This is further proved by the statistical t-test done to compare the mean biomasses between AW and WW and between IC and NC. The results of the t-test are presented in Table 4. The difference between biomass produced by AW (mean= 63.10 kg, SD= 9.47) and WW (mean= 60.37, SD=5.62) was not significant (t (11.39) =0.70; p=0.75) for season 1. The results of the other two seasons also did not show any significant differences. Similarly, comparisons of the t-test results for IC and NC plots showed that the differences between biomasses produced by IC vs NC plots were not significant between the three seasons.

Table 4: Results of two sample t-test for biomass

Results of t-test	**AW vs WW; biomass**			**IC vs NC; biomass**		
	Season 1	**Season 2**	**Season 3**	**Season 1**	**Season 2**	**Season 3**
t-value	0.70	0.69	0.44	-0.64	3.00	-0.65
Degree of freedom	11.39	12.50	13.40	10.13	13.82	11.17
p-value	0.75	0.74	0.66	0.26	0.99	0.26

Next, the moistures retained by the harvested crops were also compared based on the four types of treatments for the three seasons using the t-test. The results of average moisture content are presented in Table 5 and their distribution is shown in Figure 5. Crops irrigated with AW retained an average of 0.4% more moisture in the first two seasons. In the third season, however, the crops irrigated with well water had 5% more moisture. Similarly, crops inoculated with compost retained more moisture in the second and third seasons by 2.2% and 3.3% respectively. In the first season, the plots that were not inoculated had 0.72% more moisture. Statistically, the results did not show any significant differences when AW-WW and IC-NC comparisons were done, as shown by the t-test results, also presented in Table 5.

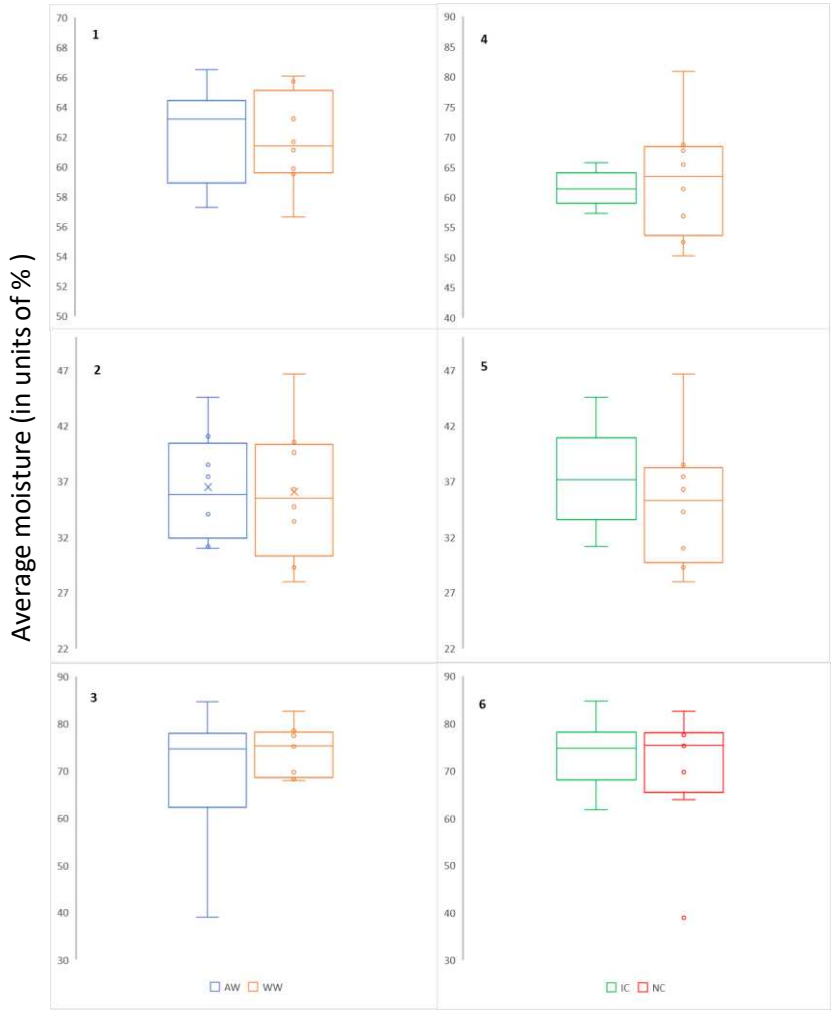

Figure 5 Average moisture percentages of collected samples for the three seasons; 1,2,3 are the AW vs. WW for seasons 1, 2, 3, respectively; 4, 5,6 are the IC vs NC for seasons 1,2, 3 respectively.

Table 5: Average moisture % and results of t-test for samples

	Average Moisture content in collected samples (%)				**Results of t-test**					
					AW vs WW			**IC vs NC**		
	AW	**WW**	**IC**	**NC**	**t-value**	**df**	**p-value**	**t-value**	**df**	**p-value**
Season 1	62.13	61.73	61.57	62.302	0.24	13.99	0.59	-0.452	13.53	0.3292
Season 2	36.51	36.07	37.40	35.19	0.159	13.198	8.8	0.81	13.17	10.574
Season 3	69.34	74.42	73.55	70.21	-0.93	8.8	0.18	0.6053	10.57	0.72

3.2 Soil Salinity and sodicity

3.2.1 Soil sample tests results

Soil tests were ordered to track the seasonal changes in salt ion concentrations present in the soil. SPE method was used to calculate the values. The results of major ion concentrations are displayed in Table 6. The average concentrations of salts were higher in WW plots than in AW plots throughout the study period, except for the concentration of Calcium in season 2. In season 1, WW plots contained around 24% more Ca^{++} and Mg++ in the soil profile, sulfate was 42.62% higher and Cl^{-} was only 18.16% higher in WW plots. This changed in season 2, where Cl^{-} had double the concentration in the WW plots than in the AW plots. The season was during the winter months when no irrigation was supplied through the drip pipes. The average Ca^{++} concentration was almost the same throughout the plots, with AW plots having a slightly greater concentration of 0.9%. In season 3, the system showed similar results to season 1 with all the WW plots showing higher salt ion concentrations than the AW plots, with Na^{+} ion having the highest percentages difference (36.23%) between the two kinds of treatments. Other salt ions like Potassium, Zinc, Iron, Manganese, Copper, Boron and Phosphorus were also tested for seasons 2 and 3, and total Carbon and total Nitrogen were tested for season 2; their average results for the 16 plots are presented in Appendix section A. Over the three seasons, 14.2% to 25.9% salt reduction in the soil profile was seen due to the application of AW. The SAR was measured for season 1 and the results showed an average of 7% higher SAR value in WW plots than AW plots. The average SAR in AW plot was 3 whereas it was 3.3 in WW plots. The range of SAR was 2.1 to 3.8. For the range of EC in our experimental plots (1.7-4.7 mS/cm), these values of SAR do not cause negative effects on the growth of our low to moderately sensitive plants.

Table 6: Soil test results for the three seasons

	Difference between AW and WW soil salt concentrations (WW-AW) (ppm)			Difference between AW and WW soil salt concentrations (%)		
	s1	s2	s3	s1	s2	s3
Ca	95.10	-39.25	116	24.31	-0.94	2.61
Mg	23.74	4.62	24.62	24.57	1.08	4.71
Na	39.21	23.75	55.75	20.15	23.06	36.23
SO_4	515.27	63.42	40.36	42.62	50.6	16.21
Cl	19.02	26.36	5.15	18.16	104.3	11.66
SAR	0.3	-	-	7	-	-

3.2.2 Soil Sensor results

The seasonal changes in soil characteristics were tracked using the sensors. The averages of moisture, EC and temperature of all three seasons are presented in Figure 6 and in tabular form are presented in Table 7. Throughout the study period, on average, the plots irrigated with AW had 0.2312 m^3/m^3 of moisture whereas the WW plots had 0.2325 m^3/m^3 of soil water. This trend varied with season, with AW plots containing a marginally higher volume of water than WW plots in the winter months (average values of 0.2325 m^3/m^3 vs 0.2303 m^3/m^3) whereas, during the summer of 2021 and 2022, WW plots retained 1.06% and 4.09% more water (0.227 m^3/m^3 in WW vs 0.224 m^3/m^3 in AW; 0.24 m^3/m^3 in WW vs 0.23 m^3/m^3 in AW, respectively). In all three seasons, WW plots had higher concentrations of salts and thus higher EC by 20.5%, 21.09%, 26.8% than AW plots (3.69 mS/cm vs 3.06 mS/cm; 3.23 mS/cm vs 2.67 mS/cm; 3.66 mS/cm vs 2.88 mS/cm in seasons 1, 2 and 3 respectively), an increasing trend showing improvement in soil salinity effects of AW treatment plots.

Table 7: Average VMC, temperature, EC in 16 plots

Plot #	Treatment type	Soil moisture (m^3/m^3)	Temperature (°C)	EC (mS/cm)
1	AW, NC	0.21	15.41	2.67
2	WW, C	0.22	14.79	2.41
3	AW, C	0.19	15.30	3.48
4	WW, NC	0.20	15.46	3.26
5	AW, NC	0.25	15.17	3.07

6	WW, C	0.20	14.91	3.84
7	AW, C	0.19	15.30	1.55
8	WW, NC	0.24	15.11	3.73
9	AW, NC	0.25	16.05	3.36
10	WW, C	0.25	15.76	3.92
11	AW, C	0.24	16.04	3.05
12	WW, NC	0.25	15.68	3.70
13	AW, NC	0.27	15.77	2.36
14	WW, C	0.24	15.36	3.15
15	AW, C	0.24	15.81	2.72
16	WW, NC	0.24	15.88	3.36

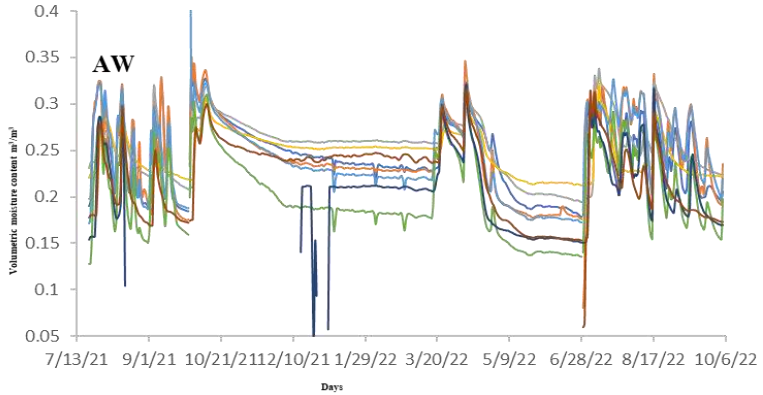
AW
Volumetric moisture content m³/m³
0.4
0.35
0.3
0.25
0.2
0.15
0.1
0.05
7/13/21 9/1/21 10/21/21 12/10/21 1/29/22 3/20/22 5/9/22 6/28/22 8/17/22 10/6/22
Days

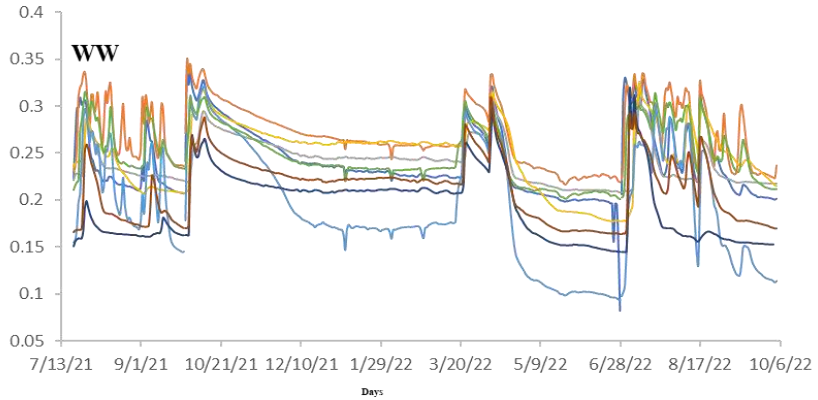
WW
0.4
0.35
0.3
0.25
0.2
0.15
0.1
0.05
7/13/21 9/1/21 10/21/21 12/10/21 1/29/22 3/20/22 5/9/22 6/28/22 8/17/22 10/6/22
Days

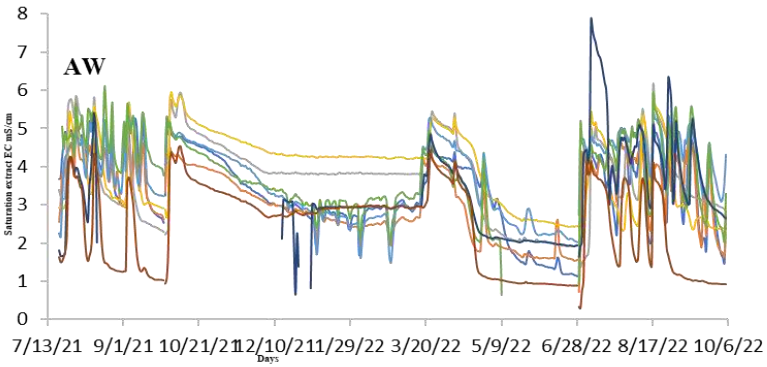
AW
Saturation extract EC mS/cm
8
7
6
5
4
3
2
1
0
7/13/21 9/1/21 10/21/21 12/10/21 1/29/22 3/20/22 5/9/22 6/28/22 8/17/22 10/6/22
Days

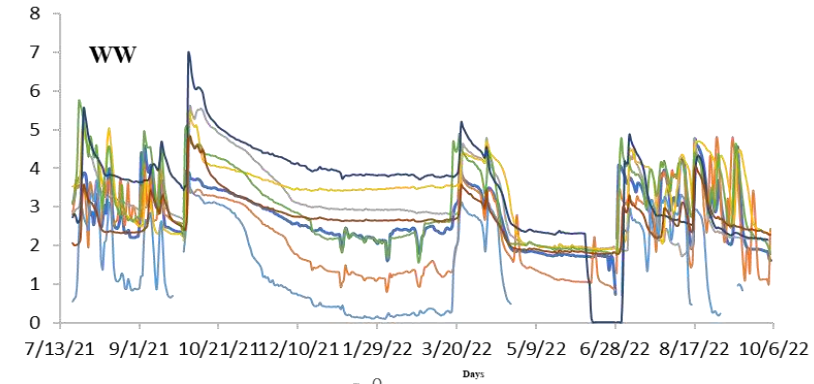
WW
8
7
6
5
4
3
2
1
0
7/13/21 9/1/21 10/21/21 12/10/21 1/29/22 3/20/22 5/9/22 6/28/22 8/17/22 10/6/22
Days

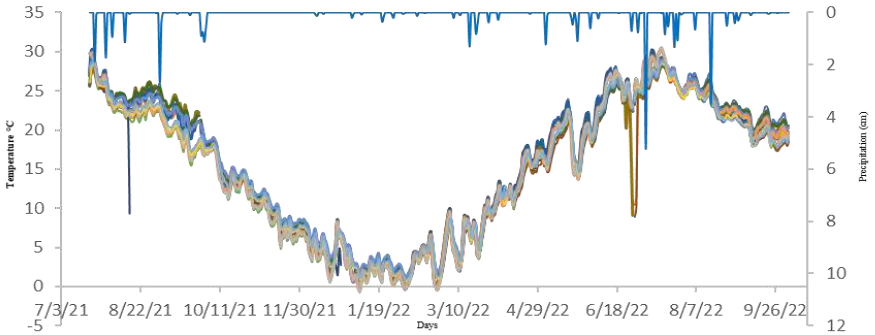
Temperature °C
35
30
25
20
15
10
5
0
-5
Precipitation (cm)
0
2
4
6
8
10
12
7/3/21 8/22/21 10/11/21 11/30/21 1/19/22 3/10/22 4/29/22 6/18/22 8/7/22 9/26/22
Days

Figure 6 Time series of VMC, EC and temperature, recorded by soil sensors over the period of 3 seasons. The top two graphs show the VMC of AW and WW plots respectively, each one has the data of 8 sensors; the middle two plots represent EC of AW and WW plots respectively, and the bottom graph represents the temperature at the sensor depths of the 16 plots.

3.2.3 Statistical tests results

3.2.3.i. Two sample t-test

Two sample t-tests were done on the daily average values of the sensor data to test the similarity or differences of conditions in the soil profile because of the different treatments. VMC and EC of AW plots were compared with WW plots for all three seasons. Similar tests were done to test the viability of IC plots versus the NC plots. The results of t-test are presented in Table 8.

Table 8: Two sample t-test results for AW/WW plots and IC/NC plots for three seasons

	AW vs WW						IC vs NC					
	VMC			EC			VMC			EC		
	Season 1	Season 2	Season 3	Season 1	Season 2	Season 3	Season 1	Season 2	Season 3	Season 1	Season 2	Season 3
t-value	-0.17	0.17	-0.65	-1.8	-1.7	-2.5	-1.5	-1.2	-1.9	-0.5	-0.0022	-1.8
df	10.56	13.70	11.95	13.58	12.36	11.72	13.99	13.97	13.45	10.64	11.74	13.45
p-value	0.431	0.56	0.26	0.046	0.054	0.01	0.07	0.11	0.036	0.31	0.49	0.04

Like the t-test results for biomass and sample moisture content, the t-test results for sensor data also did not show any significant differences between the soil conditions in the plots using different treatments. The t-values were not high enough to indicate any major differences. However, an important pattern can be seen emerging from the present results. The absolute values of t have shown a slow but steady increase and the p-values have shown a decrease in season 3 results of all the treatments, forecasting an increase in differences in the soil conditions in the plots as the seasons proceed and a new cycle of seeding and harvesting is done with consistent application of AW and WW. With this, we might be able to

hypothesize that as the study period proceeds, the effectiveness of salt removal by the RO system might become more distinct. These soils have a large salt load so it will take a lot of low salt water to change the soil chemistry in the long run.

3.2.3.ii. Distribution of fit

Skewness-Kurtosis tests were done to check how the sensor data were distributed seasonally and annually. The tests were done for VMC as well as the EC data. The resulting Cullen-Frey graphs for one of the plots, done annually as well as seasonally is shown in Figure 7.

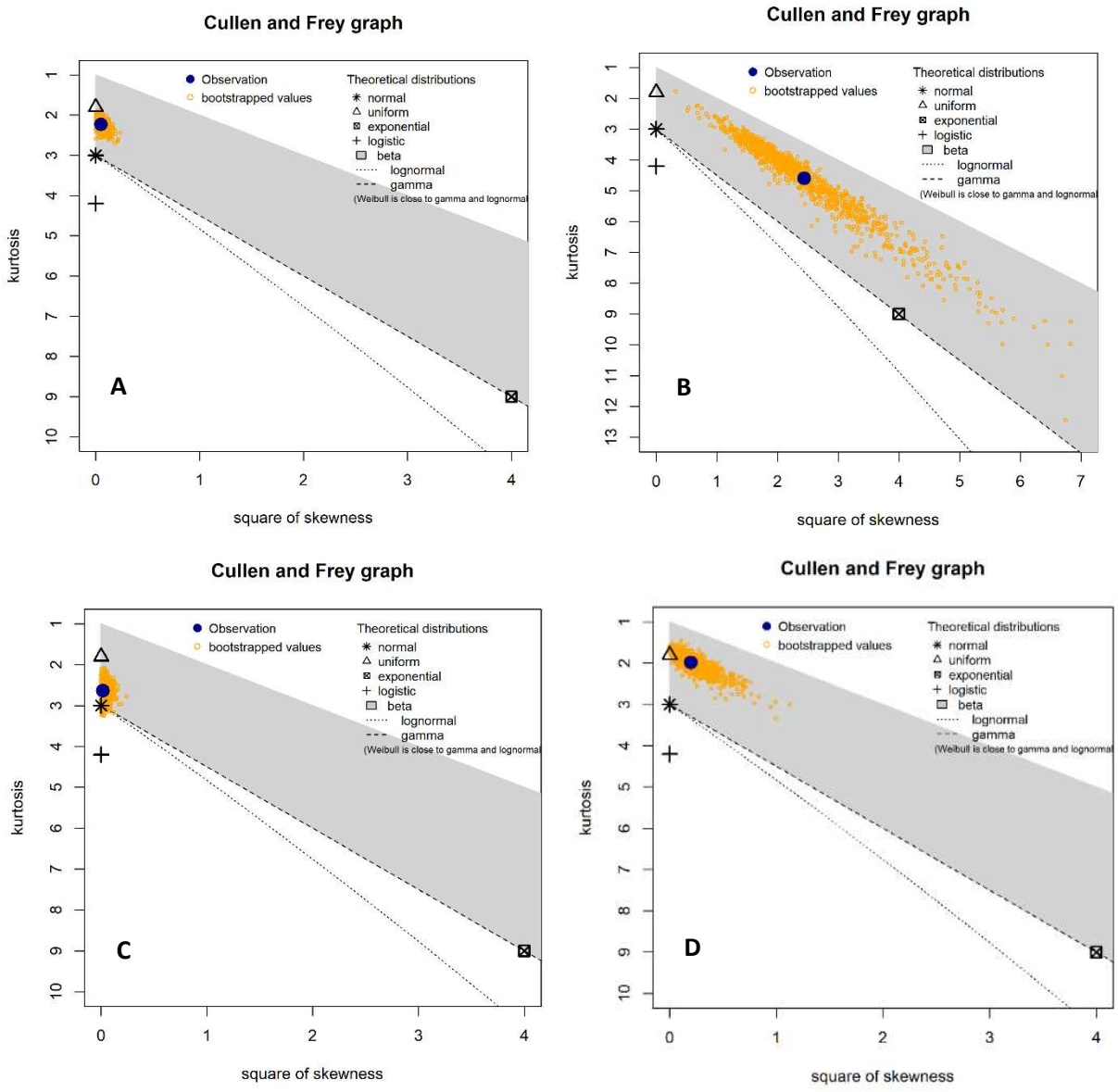

*Figure 7 Skewness and kurtosis results for the volumetric moisture content (VMC) of plot 1; figure **A**: Combined fit results of all three seasons spanning one year, **B**: fit for season 1, **C**: fit for season 2, **D**: fit for season 3*

The annual VMC of plot 1 fit well in the beta and normal region of the graph. The values of kurtosis and the square of skewness were 2.22 and 0.22 respectively, which meant that the distribution was pointier than a normal distribution but symmetrical (skewness <0.5). The validation results of graph A of Figure 7 are presented in Figure 8. The distribution is right skewed.

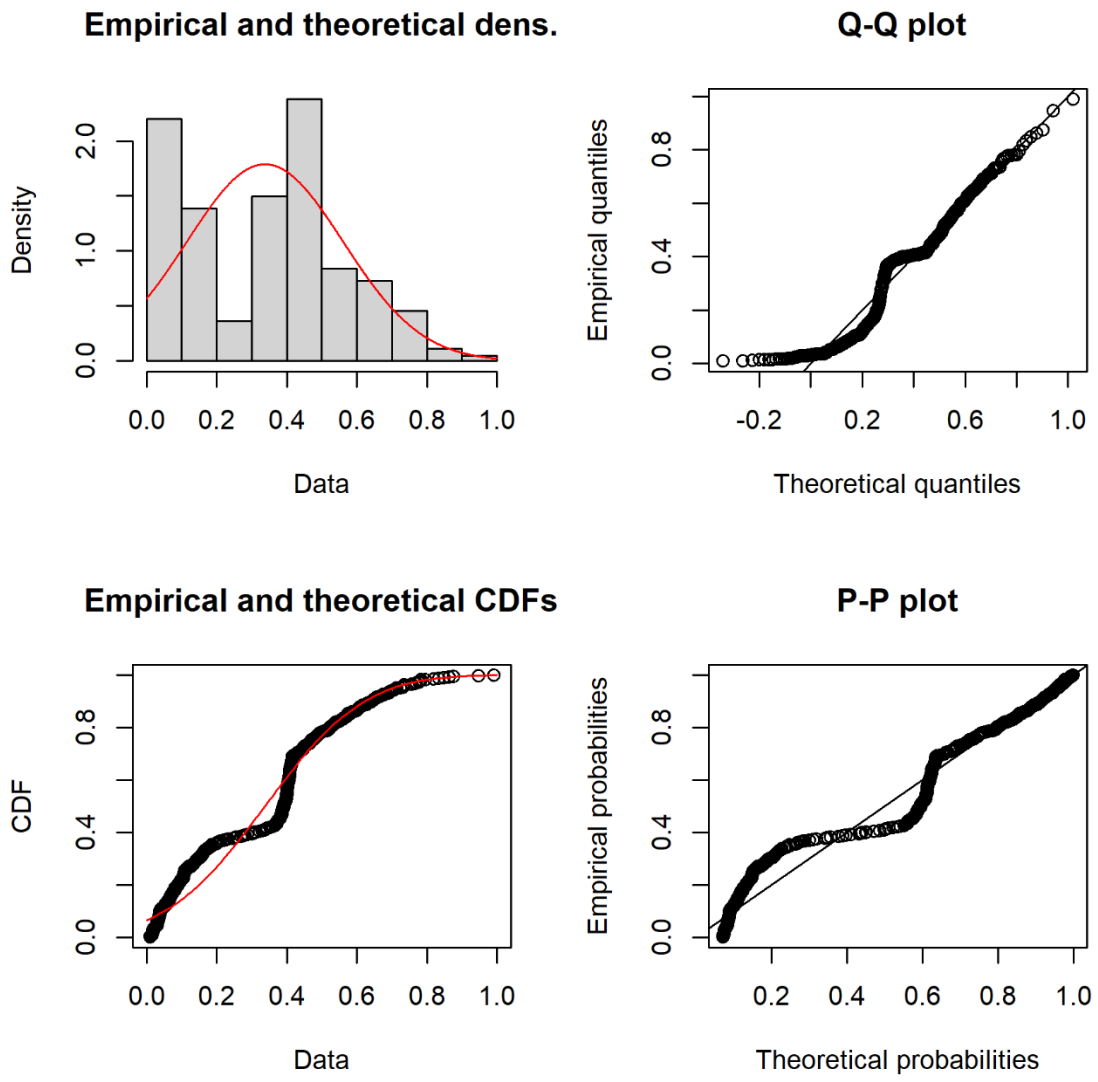

Figure 8 Cross Validation results of the data distribution in the beta region for annual Volumetric Moisture Content (VMC) of Plot 1

Figure 9 presents the fit distribution for the EC of plot 1 annually and seasonally. The data for annual distribution were positively skewed and had a kurtosis of 4.5. The fit distribution graphs for other types of treatments and their validation graphs are present in Appendix section B.

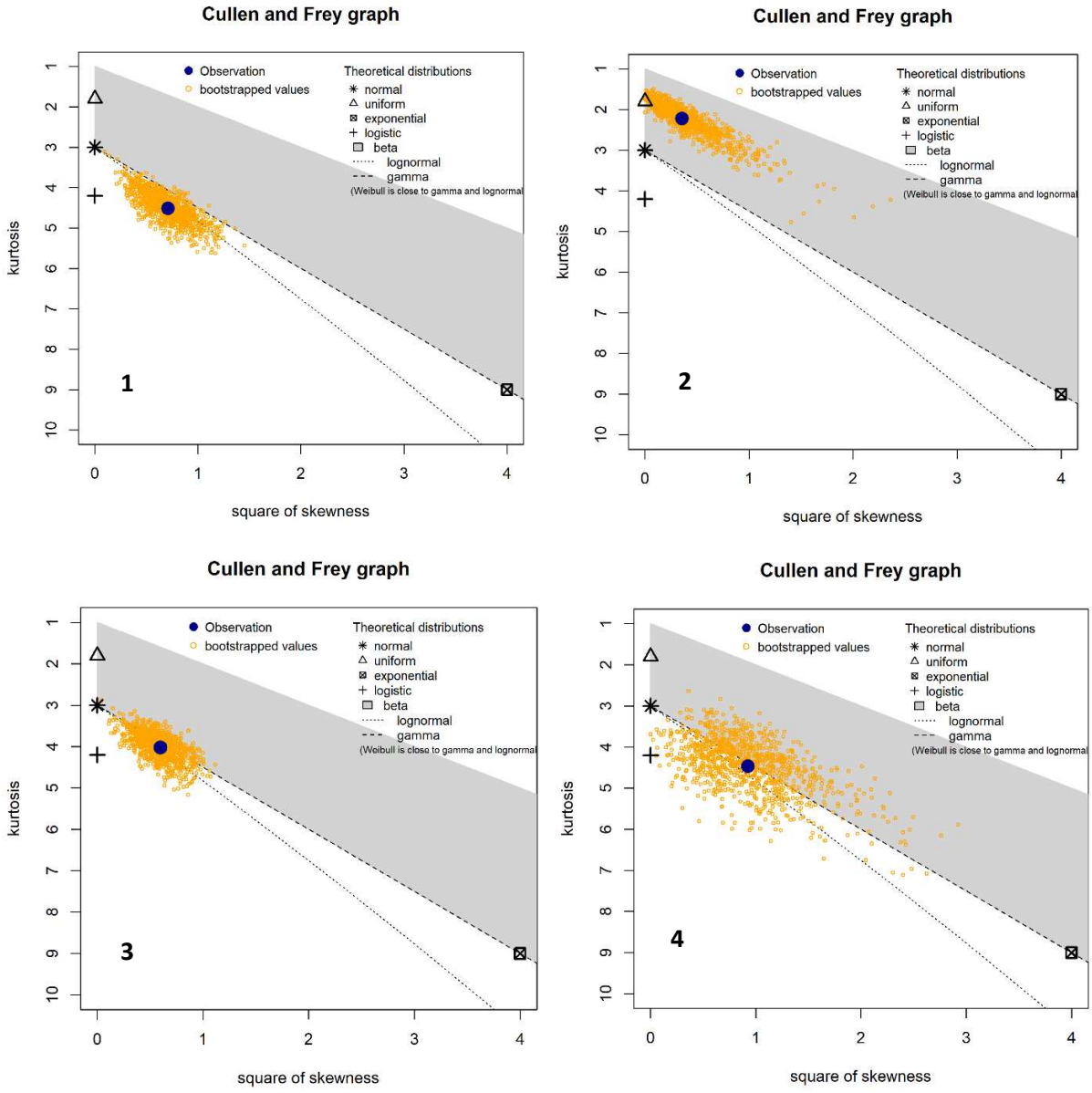

*Figure 9 Skewness and kurtosis results for plot 1 EC; Graph **1:** Combined fit results of all three data spanning one year, **2:** result of season 1, **3**: result of season 2, **4:** result of season 3*

3.3 Long-term effects on Soil Salinity using HYDRUS

3.3.1 Inverse simulation results

The results of the inverse simulations performed on season 1 data of soil moisture content of the 15 simulations are presented in Figures 10 and 11. The modeled data were sparser in the simulations so in the figures, each of the dotted lines do not represent a data point. Even though the model results lack in accurate parameter estimation, overall, the model can predict the water transport for the plots, considering that the input parameters did not go into much detail about the characterization of the soil type in the field and the partition of the potential evapotranspiration. The root-mean-square-error (RMSE) value for each simulation is presented in Table 9, which provides a quantitative measure of the goodness of fit between the data and the simulation. The RMSE values range from 0.08 to 0.295 m^3/m^3. Upon the multiple tests of various parameters, it was found that the sensitivity of the model mainly depended upon the hydraulic conductivity and longitudinal dispersivity of the soil. Although the soil texture was considered the same for all the simulations, there were substantial differences in the simulated hydraulic conductivities, which ranged from 5 cm/day in Plot 9 to a high of 29.53 cm/day in plot 11, both of which were AW plots. The compaction of soil around the sensors due to various reasons might have caused these results. The differences were even more dramatic in the case of linear dispersivity of the soil. It ranged from the lowest value of 0.04 cm in Plot 1 to the highest value of 59.94 cm in Plot 7. The minimum and maximum values for dispersivity were selected as 0 to 60 cm at the start of inverse simulation to produce a better fit. The accuracy of simulations may also be questioned in the absence of the data required to employ the entire neural network model. For our simulations, the inputs to the ROSETTA neural network model might not have been enough or accurate. The values for the estimations of θs, θr, α, Ks and l can be found in the Appendix C in detail.

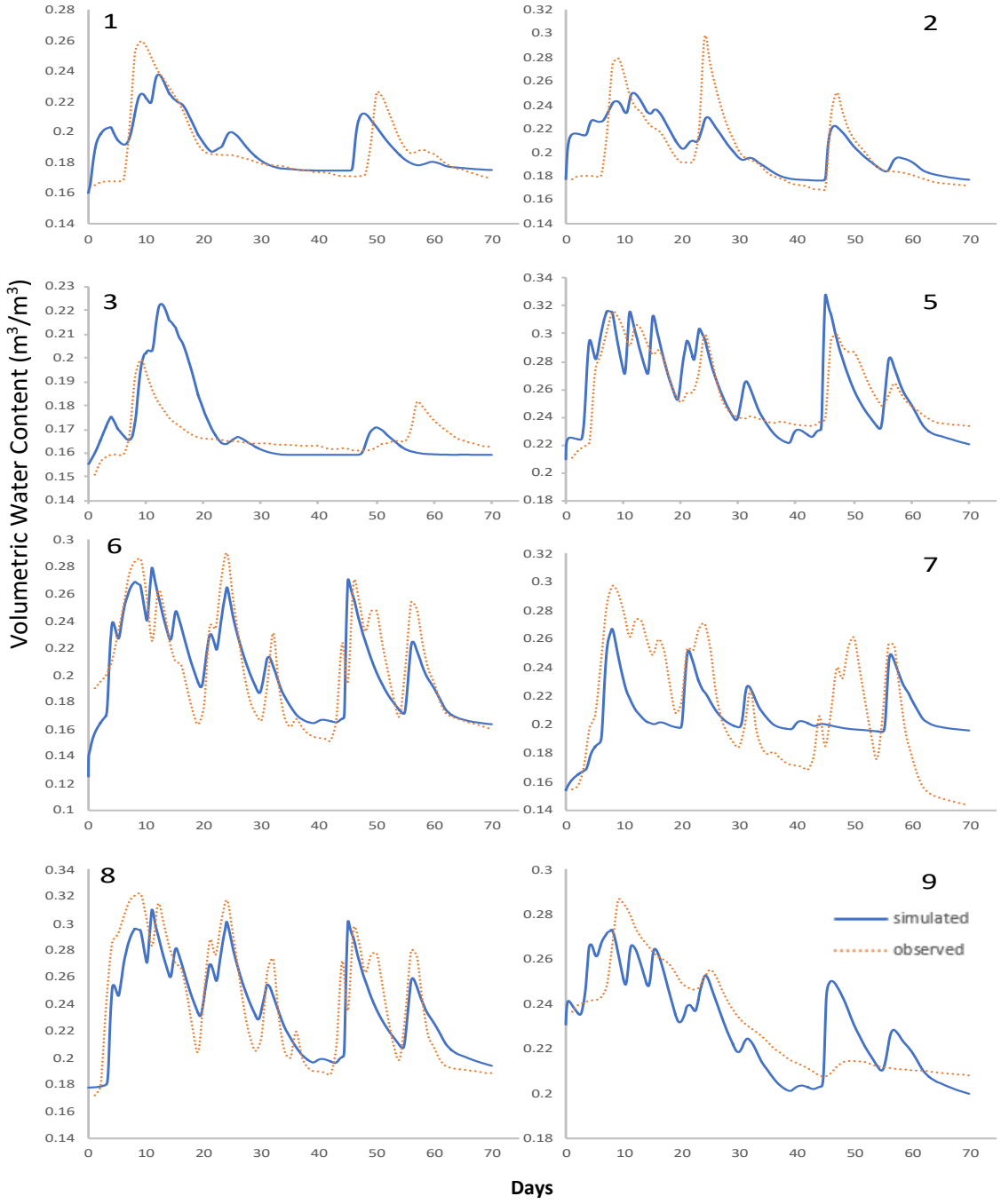

Figure 10 *Measured versus simulated volumetric water contents (VMC) for experimental plots (1 to 9) for season 1 data. The scatter plots compare the observed (dotted lines) and modeled (solid lines) water contents along the season.*

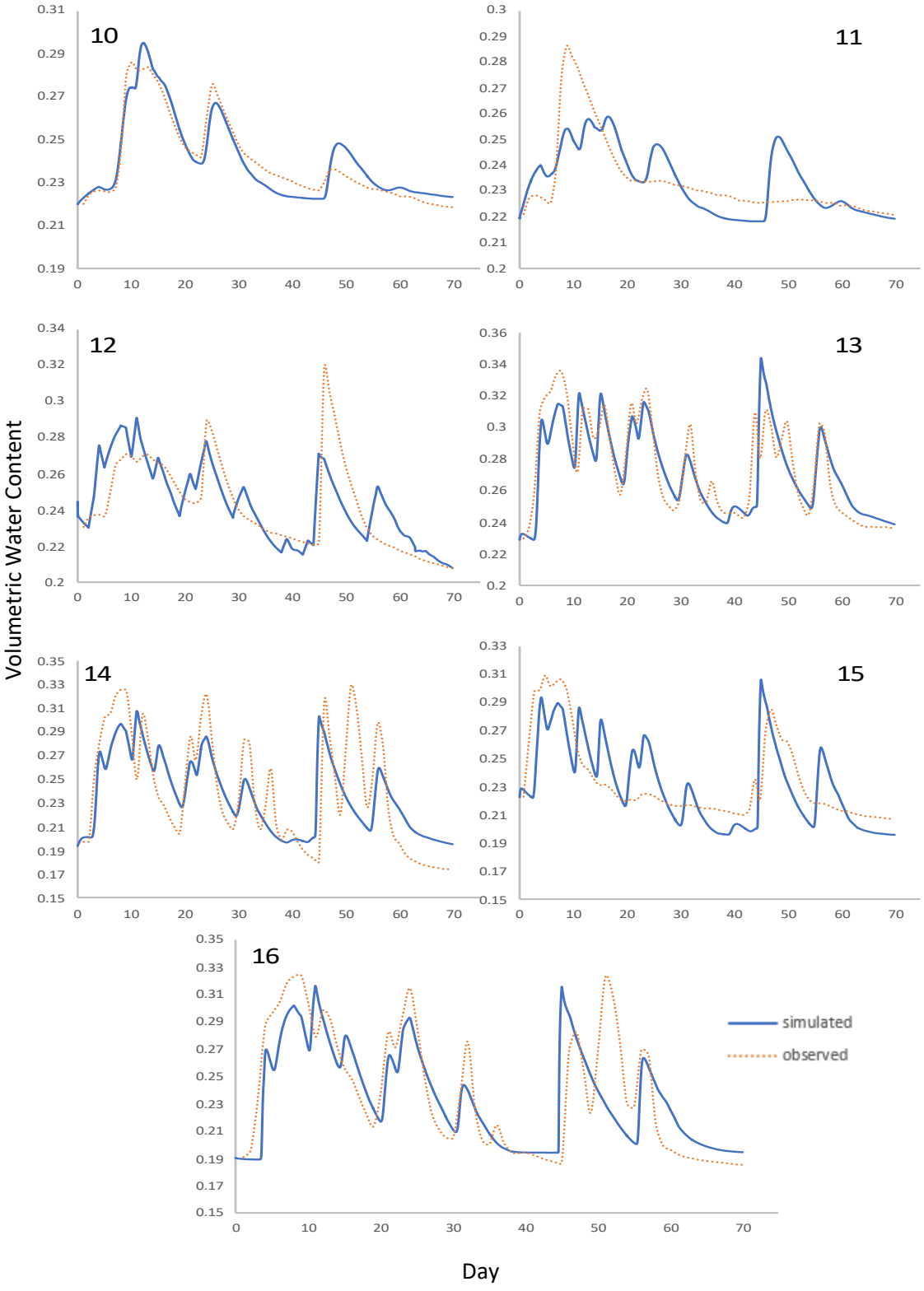

Figure 11 Measured versus predicted volumetric water contents (VMC) for experimental plots (10 to 16) for season 1 data. The scatter plots compare the observed (dotted lines) and modeled (solid lines) water contents along the season.

Table 9: RMSE values of season 1 simulation fit

Plot #	RMSE	Plot #	RMSE
1	0.1282	9	0.1233
2	0.1253	10	0.08
3	0.295	11	0.1386
4	NA	12	0.1312
5	0.1364	13	0.1093
6	0.1127	14	0.1318
7	0.1504	15	0.1504
8	0.1066	16	0.1305

3.3.2 Forecasting the effects on soil moisture and soil salinity

The results for the forecasted VMC of hypothetical dry, average, wet simulations of 6 years are presented in Figure 12. Comparison of weather conditions showed that the wettest period had the highest soil water content, followed by the average year and then the dry year. When AW and WW plots were compared, it was found that plots irrigated with AW had retained higher VMC by 5.9%, 5.6% and 7.26% in the dry, average and wet simulations respectively. The EC results of the model are presented in Figure 13. When EC results of the two AW and WW plots were compared, it was found that on average, the WW plots had 5.7%, 12.8% and 20.5% more salts than the AW plots for the dry, average and wet years, respectively. Figure 11 shows that WW plots also have a faster increase in EC than AW plots, as shown by the steeper slope of their graphs (0.0013 vs 0.0008, 0.0007 vs 0.0004, 0.0005 vs 0.0003 for dry, average and wet respectively).

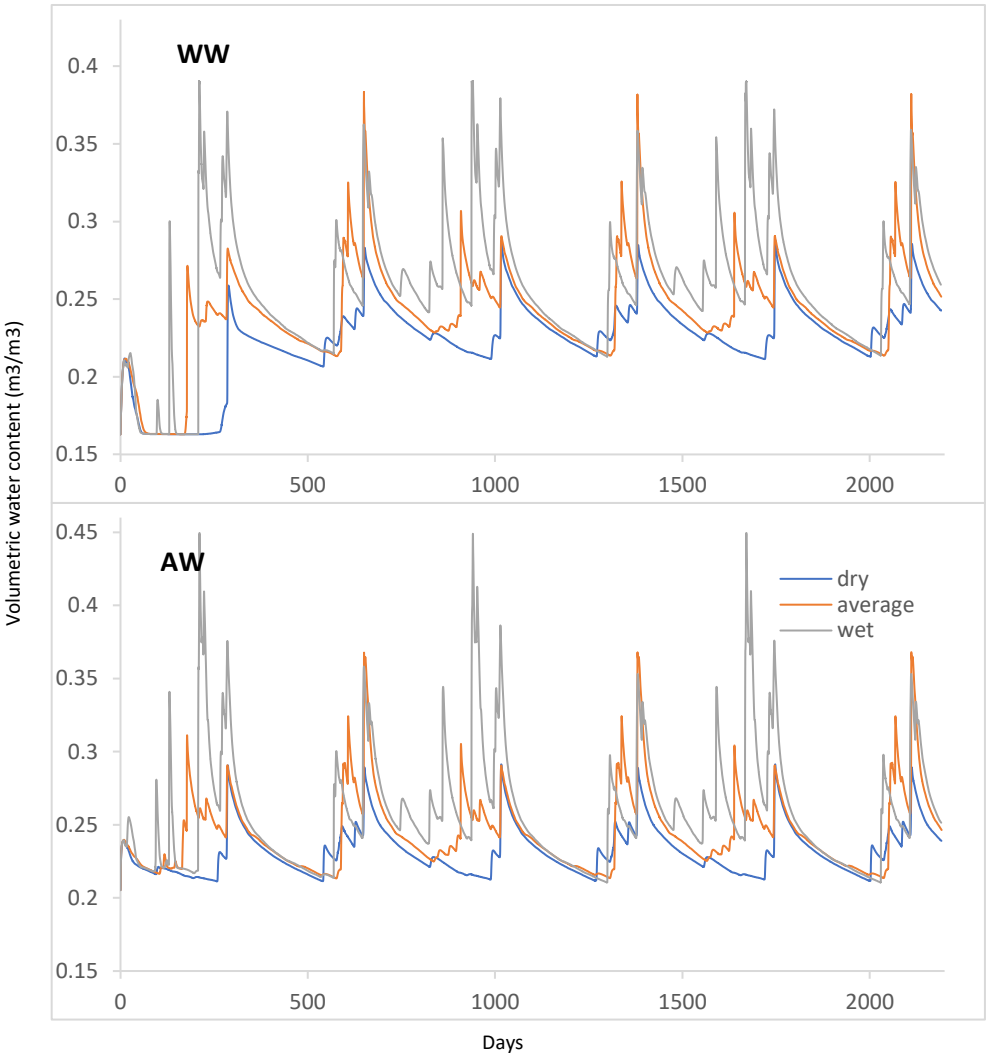

Figure 12 Forecasting results of VMC for the dry, average and wet periods

Unlike the VMC results, the EC results showed a different scenario in case of the three weather conditions (Figure 13). The average precipitation scenario had an overall higher EC, followed by dry and then the wet periods for both kinds of treatments. To check the possible reasons for this, a new set of simulations were run where the precipitation amount was decreased by 10% to 90% for the dry, average and wet years. The results could not provide any meaningful insight as to why the average years simulation produced higher amounts of salts in the soil profile. For the WW plot, the switch between dry and average years was seen when the precipitation amounts were decreased by 70% to only 0.3 times the precipitation.

At that point, the dry period's EC became higher than the average period's EC, then was followed by the wet period. But in the case of AW plot, the switch was seen faster i.e., at 40% decrease in precipitation. The only definitive pattern was shown by wet period simulations, in that they had the lowest amounts of salts throughout all the scenarios, which might be an effect of higher leaching applied by the model due to higher precipitation. The results showing the point of the switch for WW and AW plots are presented in Figure 14.

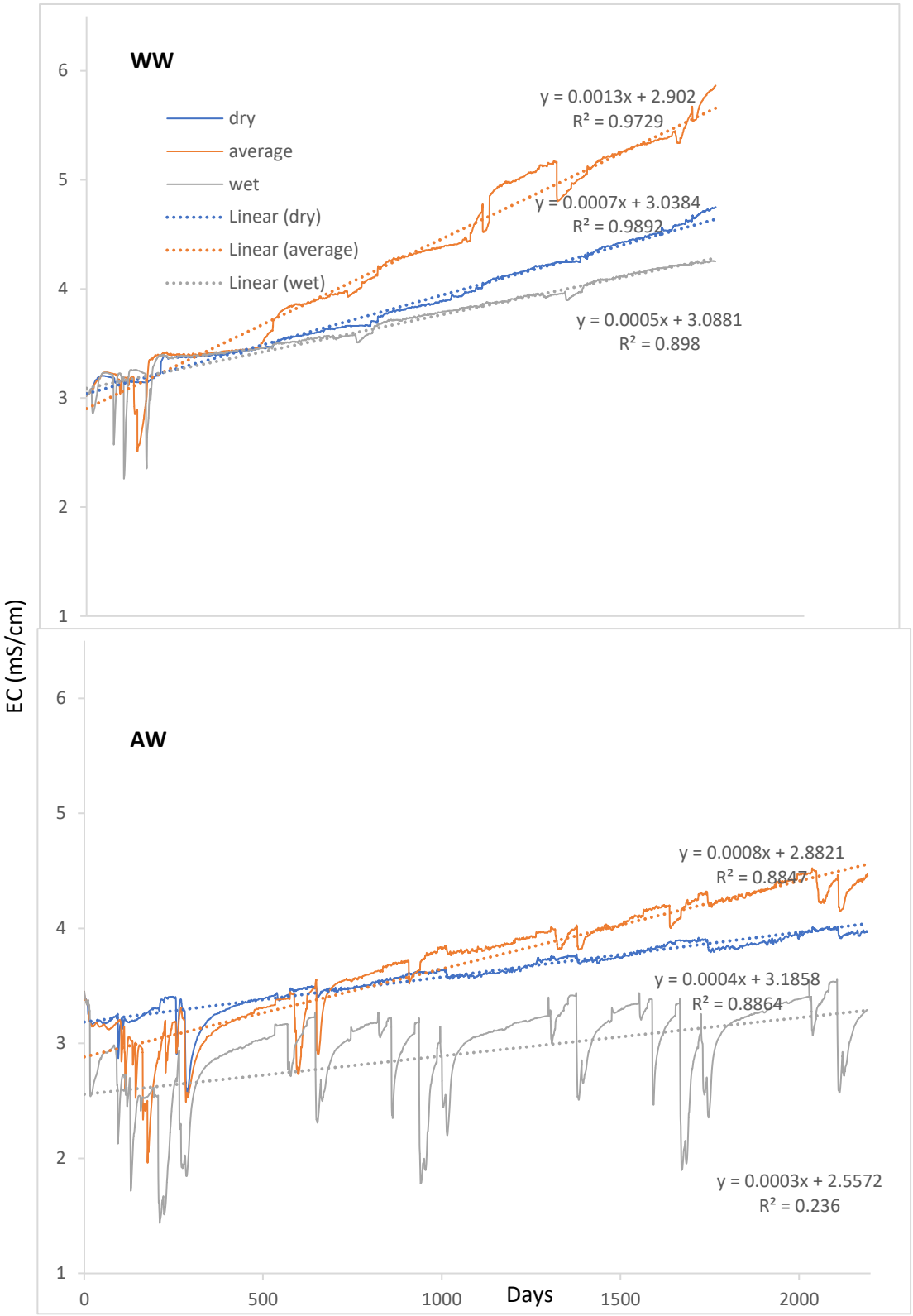

Figure 13 Forecasting results for 6 years of simulation of EC simulating soil conditions at the depth of 30 cm at AVRC plots in the dry, average and wet periods.

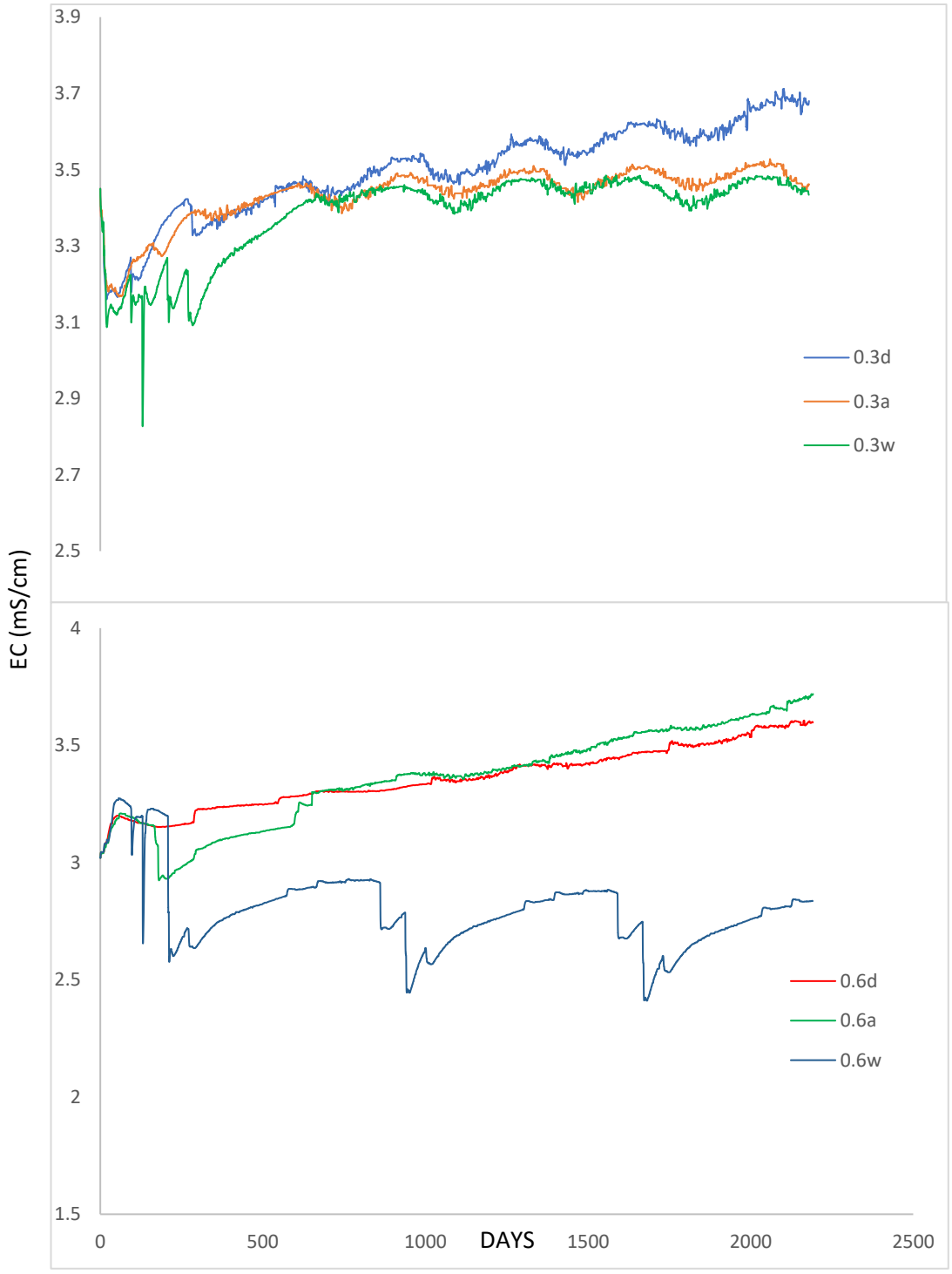

Figure 14 EC results tracking the salts in soil profile with different scenarios of precipitation during the dry, average and wet periods, showcasing the point at which average period's EC overtakes the dry period with same reduction in precipitation. Reductions in precipitations higher than these values showed average period's EC being greater than dry period's

3.4 Limitations of Study

Significant limitations were felt in the modeling portion of the study. The lack of enough data of the processes that govern the plant intake of available water from the root zone like the leaf area index and root ball dimensions and weight were a source of uncertainty in major hydrological processes like root water uptake and water content of the modeled results. The manual harvest at the end of every season and occasional malfunction of sensor wires might have made the fieldwork prone to human errors. Moreover, from the results seen so far, it was inferred that the currently available data is not enough to foretell whether the selected treatments and their application methods are able to reduce the salt load in the irrigated field by a significant amount and that a multiyear progression of the study should occur.

3. SUMMARY AND CONCLUSIONS

Biomass harvesting, soil testing and monitoring, and numerical modeling were used to quantify the impact of on-farm desalination systems on crop yield and soil salinity in a semi-arid, irrigated region. The Arkansas Valley Research Center in Rocky Ford, CO, was used the experimental site. 16 experimental plots were assigned 4 different combinations of treatments, which included irrigation with RO permeate mixed water, direct saline well water, application of compost while seeding and no application of compost. Each plot had a soil sensor installed at 6 and 12 inches which recorded continuous data of moisture, EC and temperature. Combining the results of the three approaches, crop yield, soil moisture and EC of the plots were compared. Results did not show significant improvement in soil conditions by the application of desalination for the current period of data. Some highlights include:

1. The volumetric moisture content retained by the plots varied according to the seasons and did not show any significant difference by the type of irrigation water application (0.94% more water in AW plots in season 2 vs WW; 1.06% and 4.09% more VMC in WW plots in season 1 and 3).
2. Smaller noticeable differences were seen in the salt concentrations of the different plots and irrigation applications (20.6% to 26.8% higher salt concentration in WW plots than in AW plots).
3. Marginal differences were seen in the biomass production in the two types of treatments (2.7 to 8% more biomass produced in AW plots in the three seasons).
4. Statistical t-test and distribution of fit were performed on the data. The t-test results showed no significant differences in the VMC, EC and biomass of the plots which were irrigated with different types of water; results of season 3 however encouraged continuation of the fieldwork in order to get clearer results as time proceeds.
5. Application of compost only during the seeding did not increase the crop yield.

6. The numerical model HYDRUS 1D was applied to first season's data and the resulting soil hydraulic properties from the model were used to forecast the VMC and EC in different climatic conditions which showed that drier the climate, more persistent is the soil salinity problem.

The results of the combined field work and numerical modeling approaches and their analysis highlighted the need for a longer study period to be able to accurately predict or quantify the effectiveness of on-farm desalination. Nevertheless, such off-grid, energy-efficient and remotely accessible systems open a new avenue for the effective alliance between scientists, farmers and producers; on top of supporting the research for sustainable consumption of available natural resources. This project has persisted and consistently offered collaboration between multiple universities and disciplines that represents the willingness to address the historical problem of salinity increases in the agricultural fields at the grass-root level. With groundwater pumping and increasing levels of the water table beneath our cultivable land due to intensive irrigation, investment in the on-farm desalination technology can provide a respite to our arable soils choked by excessive salt deposition.

REFERENCES

[1] L. Bernstein, "EFFECTS OF SALINITY AND SODICITY ON PLANT GROWTH," 1975. [Online]. Available: www.annualreviews.org

[2] L. A. Richards, *Soil Science*, vol. 78, no. 2. 1954.

[3] A. Amin, R. Yasin, and M. I. Sarwar, "A review: Impact of salinity on plant growth View project Geochemistry View project", doi: 10.7537/marsnsj170119.06.

[4] A. R. Flowers T. S. and Yeo, "Effects of Salinity on Plant Growth and Crop Yields," in *Environmental Stress in Plants*, 1989, pp. 101–119.

[5] H. I. Mohamed and E. Z. Gomaa, "Effect of plant growth promoting Bacillus subtilis and Pseudomonas fluorescens on growth and pigment composition of radish plants (Raphanus sativus) under NaCl stress," *Photosynthetica*, vol. 50, no. 2, pp. 263–272, 2012, doi: 10.1007/s11099-012-0032-8.

[6] J. R. Acosta-Motos, M. F. Ortuño, A. Bernal-Vicente, P. Diaz-Vivancos, M. J. Sanchez-Blanco, and J. A. Hernandez, "Plant Responses to Salt Stress: Adaptive Mechanisms," *Agronomy*, vol. 7, no. 1, 2017, doi: 10.3390/agronomy7010018.

[7] P. Shrivastava and R. Kumar, "Soil salinity: A serious environmental issue and plant growth promoting bacteria as one of the tools for its alleviation," *Saudi J Biol Sci*, vol. 22, no. 2, pp. 123–131, 2015.

[8] M. G. Pitman and A. Läuchli, "Global Impact of Salinity and Agricultural Ecosystems," in *Salinity: Environment - Plants - Molecules*, A. Läuchli and U. Lüttge, Eds. Dordrecht: Springer Netherlands, 2002, pp. 3–20. doi: 10.1007/0-306-48155-3_1.

[9] J. R. McWilliam, "The National and International Importance of Drought and Salinity Effects on Agricultural Production," *Functional Plant Biology*, vol. 13, no. 1, pp. 1–13, 1986, [Online]. Available: https://doi.org/10.1071/PP9860001

[10] M. Qadir *et al.*, "Economics of salt-induced land degradation and restoration," *Nat Resour Forum*, vol. 38, no. 4, pp. 282–295, Nov. 2014, doi: https://doi.org/10.1111/1477-8947.12054.

[11] M. and H. L. Shahid Shabbir A. and Zaman, "Soil Salinity: Historical Perspectives and a World Overview of the Problem," in *Guideline for Salinity Assessment, Mitigation and Adaptation Using Nuclear and Related Techniques* , Cham: Springer International Publishing, 2018, pp. 43–53. doi: 10.1007/978-3-319-96190-3_2.

[12] T. Jacobsen and Adams Robert M., "Salt and Silt in Ancient Mesopotamian Agriculture," *Science (1979)*, vol. 128, no. 3334, pp. 1251–1258, Nov. 1958.

[13] D. L. Corwin, J. D. Rhoades, and J. Šimůnek, "Leaching requirement for soil salinity control: Steady-state versus transient models," *Agric Water Manag*, vol. 90, no. 3, pp. 165–180, Jun. 2007, doi: 10.1016/j.agwat.2007.02.007.

[14] K. E. Pearson, "Basics of Salinity and Sodicity Effects on Soil Physical Properties."

[15] R. O. Miller, "SOIL TESTING: SATURATED PASTE INTERPRETATION."

[16] Rhoades et al, "US salinity reports." 1989.

[17] R. Mehdaoui, M. Anane, E. E. Cañas Kurz, U. Hellriegel, and J. Hoinkis, "Geospatial Multi-Criteria Approach for Ranking Suitable Shallow Aquifers for the Implementation of an On-Farm Solar-PV Desalination System for Sustainable Agriculture," *Sustainability*, vol. 14, no. 13, 2022, doi: 10.3390/su14138113.

[18] V. Martínez-Alvarez, B. Martin-Gorriz, and M. Soto-García, "Seawater desalination for crop irrigation - A review of current experiences and revealed key issues," *Desalination*, vol. 381. Elsevier, pp. 58–70, Mar. 01, 2016. doi: 10.1016/j.desal.2015.11.032.

[19] O. Lahav and L. Birnhack, "Quality criteria for desalinated water following post-treatment," *Desalination*, vol. 207, no. 1–3, pp. 286–303, Mar. 2007, doi: 10.1016/j.desal.2006.05.022.

[20] Y. Slater, I. Finkelshtain, A. Reznik, and I. Kan, "Large-Scale Desalination and the External Impact on Irrigation-Water Salinity: Economic Analysis for the Case of Israel," *Water Resour Res*, vol. 56, no. 9, Sep. 2020, doi: 10.1029/2019WR025657.

[21] C. Bales, B. Lian, J. Fletcher, Y. Wang, and T. D. Waite, "Site specific assessment of the viability of membrane Capacitive Deionization (mCDI) in desalination of brackish groundwaters for selected crop watering," *Desalination*, vol. 502, Apr. 2021, doi: 10.1016/j.desal.2020.114913.

[22] E. Bresler, B. McNeal, and D. Carter, "Saline and sodic soils: Principle, Dynamics, Modeling," *Advanced series in agricultural sciences*, p. 10.

[23] S. Burn *et al.*, "Desalination techniques — A review of the opportunities for desalination in agriculture," *Desalination*, vol. 364, pp. 2–16, 2015, doi: https://doi.org/10.1016/j.desal.2015.01.041.

[24] National Research Council and others, "Desalination: a national perspective," *Committee on Advancing Desalination Technology*, p. 298, 2008.

[25] M. Mickley, "Treatment of concentrate," US Department of the Interior, Bureau of Reclamation, Technical Service, 2009.

[26] "'The Arid West—Where Water Is Scarce .' Water: No Longer Taken For Granted".

[27] "Production Agricultural in the Western."

[28] T. K. Gates, L. A. Garcia, R. A. Hemphill, E. D. Morway, and A. Elhaddad, "Irrigation Practices, Water Consumption, & Return Flows in Colorado's Lower Arkansas River Valley Field and Model Investigations." [Online]. Available: www.cwi.colostate.edu.

[29] T. K. Gates, L. A. Garcia, and J. W. Labadie, "Toward Optimal Water Management in Colorado's Lower Arkansas River Valley: Monitoring and Modeling to Enhance Agriculture and Environment Colorado Agricultural Experiment Station."

[30] E. v Maas and S. Grattan, "Crop yields as affected by salinity," in *Agricultural Drainage. Agron. Monograph 38*, 1999, pp. 55–108.

[31] J. Šimůnek, M. Šejna, G. Brunetti, and M. Th van Genuchten, "The HYDRUS Software Package for Simulating the One-, Two-, and Three-Dimensional Movement of Water, Heat, and Multiple Solutes in Variably-Saturated Porous Media Technical Manual I Hydrus 1D."

[32] "Market Value of Agricultural Products Sold Sales ($1,000) Rank in State b." [Online]. Available: www.nass.usda.gov/go/cropnames.pdf.

[33] B. Smithers, K. Mallory, P. Xu, D. Johnson, and R. Bailey, "Integration of Renewable Energy, Desalination, Agriculture, and Aquaculture Projects and Motivation Food-Energy-Water," 2019.

[34] S. Tavakoli-Kivi, R. T. Bailey, and T. K. Gates, "A salinity reactive transport and equilibrium chemistry model for regional-scale agricultural groundwater systems," *J Hydrol (Amst)*, vol. 572, pp. 274–293, May 2019, doi: 10.1016/j.jhydrol.2019.02.040.

[35] IDS Group, "Arkansas River Basin Salinity Mapping," *The Campaign for Colorado State University*. http://www.ids.colostate.edu/projects.php?project=arkbasin&breadcrumb=Arkansas+River+Basin+Salinity+Mapping (accessed Nov. 22, 2022).

[36] E. D. Morway, T. K. Gates, and R. G. Niswonger, "Appraising options to reduce shallow groundwater tables and enhance flow conditions over regional scales in an irrigated alluvial aquifer system," *J Hydrol (Amst)*, vol. 495, pp. 216–237, Jul. 2013, doi: 10.1016/j.jhydrol.2013.04.047.

[37] "Project Description-NSF-INFEWST2-2018-UNT-CSU-NMSU_final_v4".

[38] P. I. Gubiani and L. R. Mentges, "Using root water uptake estimated by a hydrological model to evaluate the least limiting water range," *Rev Bras Cienc Solo*, vol. 44, 2020, doi: 10.36783/18069657rbcs20190096.

[39] J. S. Boyer, "Plant Productivity and Environment," *Science (1979)*, vol. 218, no. 4571, pp. 443–448, Oct. 1982, doi: 10.1126/science.218.4571.443.

[40] R. T. Bailey, S. Tavakoli-Kivi, and X. Wei, "A salinity module for SWAT to simulate salt ion fate and transport at the watershed scale," *Hydrol Earth Syst Sci*, vol. 23, no. 7, pp. 3155–3174, Jul. 2019, doi: 10.5194/hess-23-3155-2019.

[41] "simulation_of_field_water_use_and_crop_yield-wageningen_university_and_research_172222".

[42] "Rocky Ford Series," *Established Series*, Jan. 2014.

APPENDIX

A. Results and Calculations for the soil chemistry

1. Soil tests results for salt ions except major ions (Ca^{++}, Mg^{++}, Na^{+}, Cl^{-}, S^{2+})

Ion	Season 2 (mg/L or ppm)		Season 3 (mg/L or ppm)	
	AW	WW	AW	WW
K	187.75	171.25	220	223.5
Zn	2.0125	2.01375	2.2038	2.3413
Fe	4.9375	7.175	5.4125	5.75
Mn	4.5	13.075	2.7875	2.6375
Cu	1.50875	1.61375	1.6713	1.7188
B	0.78625	0.7575	1.4425	1.3638
P	32.5	32.25	38.5	37.875
Total Nitrogen	877.87	882.62		
Total Carbon (%)	1.27	1.3		

2. Calculations for Solute transport: Solution Composition parameters of the Major ion simulations

plot	name	Solution composition (meq/L)						
		Ca	Mg	Na	K	Alk	SO4	Cl
1	AW, NC,12	15.8	6.0	7.0	0.3	2.2	21.0	1.1
2	WW,C,12	23.1	9.0	11.2	0.5	3.2	36.8	3.4
3	AW,C,12	18.2	7.4	8.3	0.3	3.3	23.6	3.6
4	WW,NC,12	17.3	7.0	7.5	0.2	3.3	18.1	3.7
5	AW,NC,6	21.6	8.7	9.2	0.4	4.6	25.6	3.4
6	WW,C,6	19.9	7.6	7.9	0.5	4.1	30.5	2.5
7	AW,C,6	14.6	5.9	6.5	0.4	5.3	19.3	1.9
8	WW,NC,6	16.6	6.9	6.7	0.4	4.5	25.4	2.2
9	AW,NC,12	14.2	5.9	7.7	0.4	3.9	18.3	3.1
10	WW,C,12	29.8	12.6	11.1	0.6	4.6	36.3	5.3
11	AW,C,12	21.4	9.0	9.4	0.4	5.0	26.7	4.2
12	WW,NC,12	23.7	9.9	10.3	0.5	4.3	36.6	3.7
13	AW,NC,6	34.4	14.0	13.3	0.8	4.7	44.2	4.4
14	WW,C,6	29.1	12.0	12.4	0.6	4.4	46.9	4.4
15	AW,C,6	16.1	6.6	6.3	0.5	2.6	22.7	1.9
16	WW,NC,6	34.7	14.2	14.2	0.7	4.0	56.6	2.7

3. Estimated Ionic Strength, Activity Coefficients and Gapon Coefficients

Plot #	Name	Estimated Ionic Strength (mole/L)	Estimated activity coefficient				Gapon Coefficient		
			Ca	Mg	Na	K	Gapon (Ca/Mg)=	Gapon (Ca/Na)=	Gapon (Ca/K)=
1	AW, NC,12	0.09	0.4	0.5	0.8	0.8	0.2	5.9	0.11
2	WW,C,12	0.15	0.4	0.4	0.8	0.7	0.2	3.8	0.15
3	AW,C,12	0.11	0.4	0.4	0.8	0.8	0.2	6.5	0.12
4	WW,NC,12	0.09	0.4	0.5	0.8	0.8	0.2	6.0	0.17
5	AW,NC,6	0.12	0.4	0.4	0.8	0.7	0.2	3.2	0.15
6	WW,C,6	0.12	0.4	0.4	0.8	0.7	0.3	2.8	0.18
7	AW,C,6	0.09	0.4	0.5	0.8	0.8	0.3	2.7	0.16
8	WW,NC,6	0.10	0.4	0.4	0.8	0.8	0.3	2.6	0.16
9	AW,NC,12	0.08	0.4	0.5	0.8	0.8	0.3	3.2	0.15
10	WW,C,12	0.17	0.4	0.4	0.7	0.7	0.3	3.3	0.17
11	AW,C,12	0.12	0.4	0.4	0.8	0.7	0.3	3.2	0.15
12	WW,NC,12	0.15	0.4	0.4	0.8	0.7	0.3	3.4	0.15
13	AW,NC,6	0.20	0.3	0.4	0.7	0.7	0.3	3.6	0.21
14	WW,C,6	0.19	0.3	0.4	0.7	0.7	0.3	3.7	0.17
15	AW,C,6	0.10	0.4	0.5	0.8	0.8	0.3	2.4	0.17
16	WW,NC,6	0.22	0.3	0.4	0.7	0.7	0.3	2.6	0.18

B. Results of distribution of fit

1. Results of VMC fit for plot 1 through 16 (First graph in each set of 4 is for the three seasons combined, 2nd, 3rd and 4th graphs are for seasons 1, 2, 3, respectively.)

Plot 1:

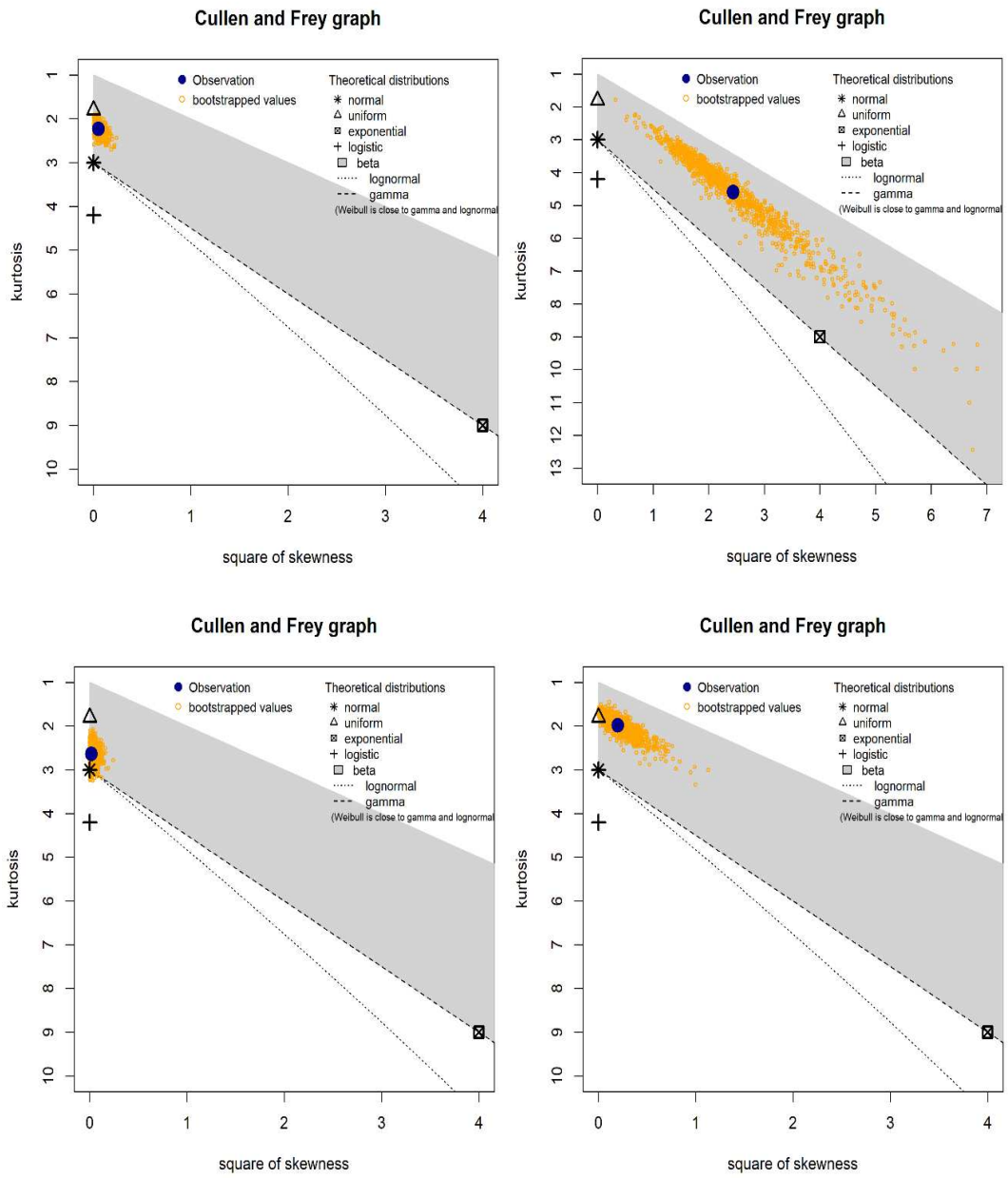

Plot 2:

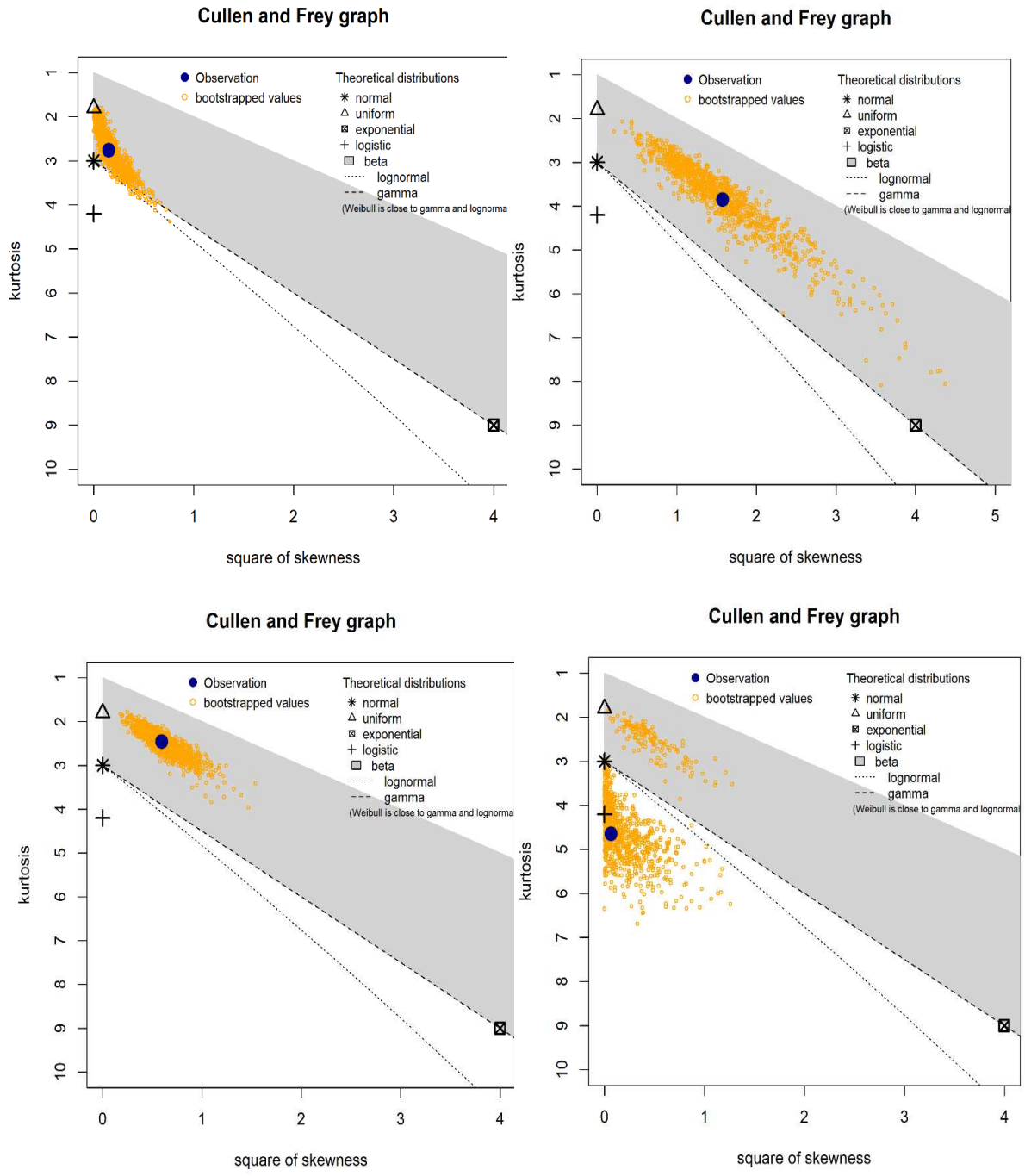
Cullen and Frey graph
Observation
bootstrapped values
Theoretical distributions
normal
uniform
exponential
logistic
beta
lognormal
gamma
(Weibull is close to gamma and lognorma
kurtosis
square of skewness
Cullen and Frey graph
Observation
bootstrapped values
Theoretical distributions
normal
uniform
exponential
logistic
beta
lognormal
gamma
(Weibull is close to gamma and lognormal
kurtosis
square of skewness
Cullen and Frey graph
Observation
bootstrapped values
Theoretical distributions
normal
uniform
exponential
logistic
beta
lognormal
gamma
(Weibull is close to gamma and lognorma
kurtosis
square of skewness
Cullen and Frey graph
Observation
bootstrapped values
Theoretical distributions
normal
uniform
exponential
logistic
beta
lognormal
gamma
(Weibull is close to gamma and lognormal
kurtosis
square of skewness

Plot 3:

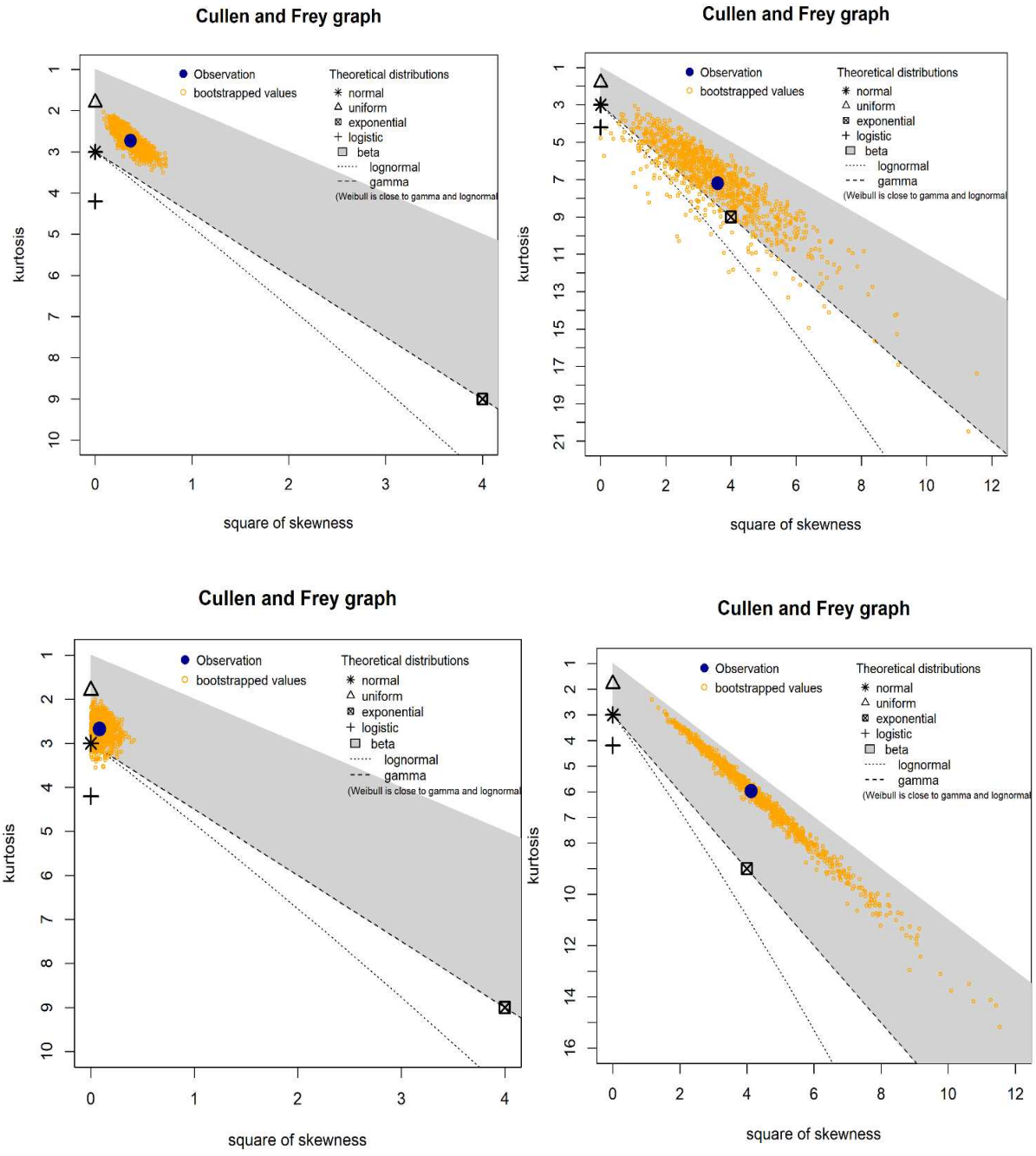
Cullen and Frey graph
Observation
bootstrapped values
Theoretical distributions
normal
uniform
exponential
logistic
beta
lognormal
gamma
(Weibull is close to gamma and lognormal)
kurtosis
square of skewness
Cullen and Frey graph
Observation
bootstrapped values
Theoretical distributions
normal
uniform
exponential
logistic
beta
lognormal
gamma
(Weibull is close to gamma and lognormal)
kurtosis
square of skewness
Cullen and Frey graph
Observation
bootstrapped values
Theoretical distributions
normal
uniform
exponential
logistic
beta
lognormal
gamma
(Weibull is close to gamma and lognormal)
kurtosis
square of skewness
Cullen and Frey graph
Observation
bootstrapped values
Theoretical distributions
normal
uniform
exponential
logistic
beta
lognormal
gamma
(Weibull is close to gamma and lognormal)
kurtosis
square of skewness

Plot 5:

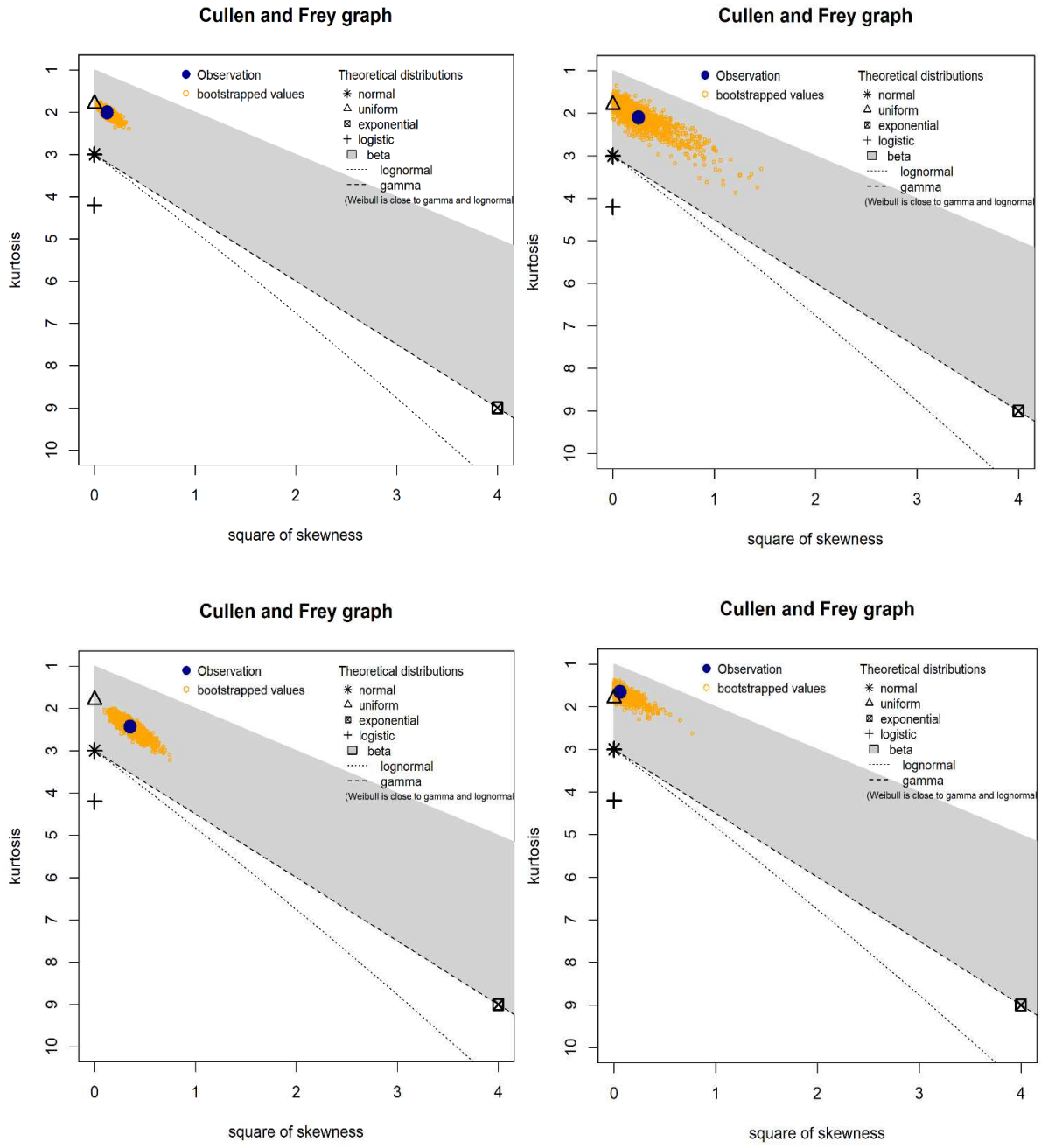
Cullen and Frey graph
Observation
bootstrapped values
Theoretical distributions
normal
uniform
exponential
logistic
beta
lognormal
gamma
(Weibull is close to gamma and lognormal)
kurtosis
square of skewness
0
1
2
3
4
1
2
3
4
5
6
7
8
9
10

Plot 6:

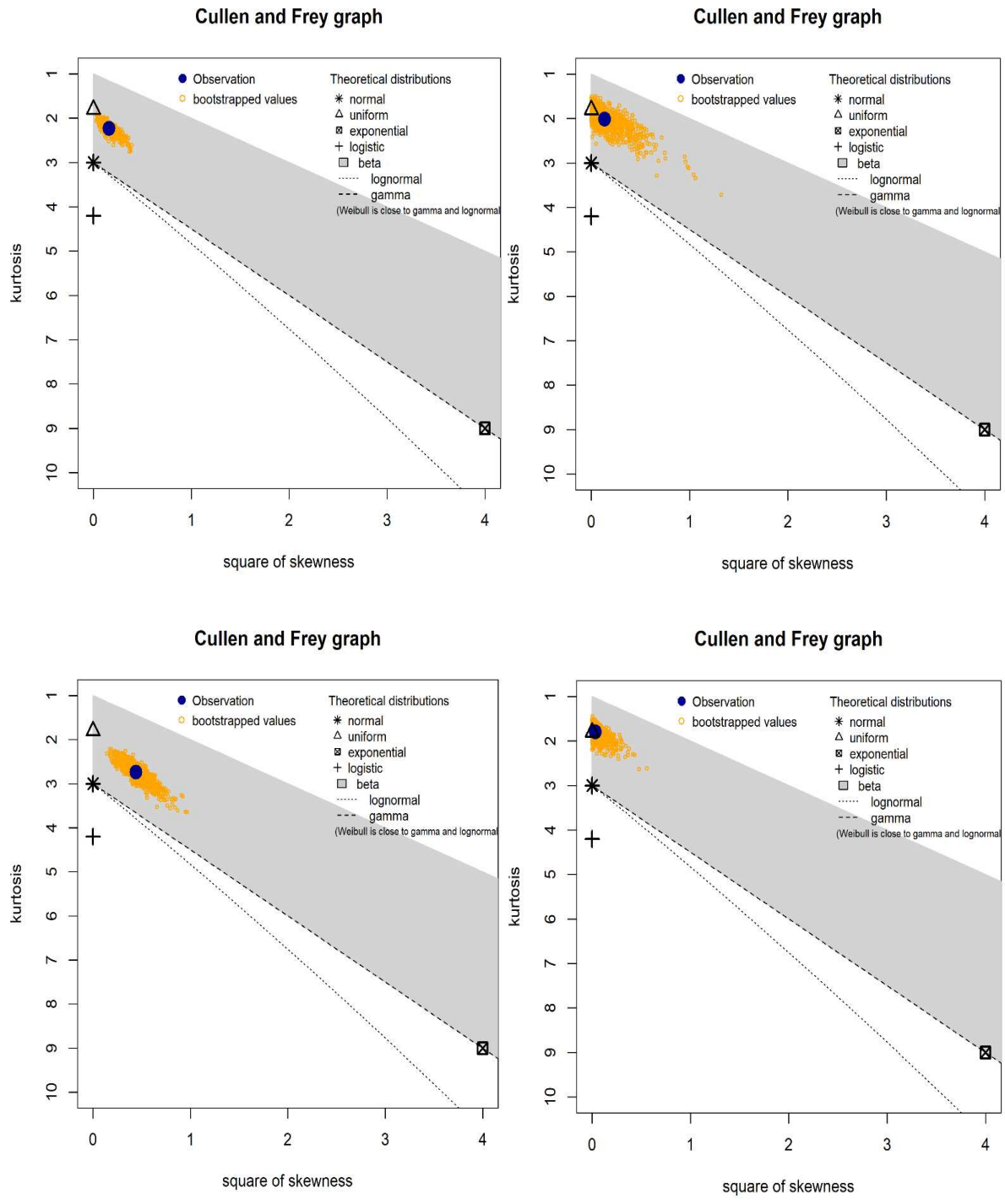
Cullen and Frey graph
Observation
bootstrapped values
Theoretical distributions
normal
uniform
exponential
logistic
beta
lognormal
gamma
(Weibull is close to gamma and lognormal)
kurtosis
square of skewness
Cullen and Frey graph
Observation
bootstrapped values
Theoretical distributions
normal
uniform
exponential
logistic
beta
lognormal
gamma
(Weibull is close to gamma and lognormal)
kurtosis
square of skewness
Cullen and Frey graph
Observation
bootstrapped values
Theoretical distributions
normal
uniform
exponential
logistic
beta
lognormal
gamma
(Weibull is close to gamma and lognormal)
kurtosis
square of skewness
Cullen and Frey graph
Observation
bootstrapped values
Theoretical distributions
normal
uniform
exponential
logistic
beta
lognormal
gamma
(Weibull is close to gamma and lognormal)
kurtosis
square of skewness

Plot 7:

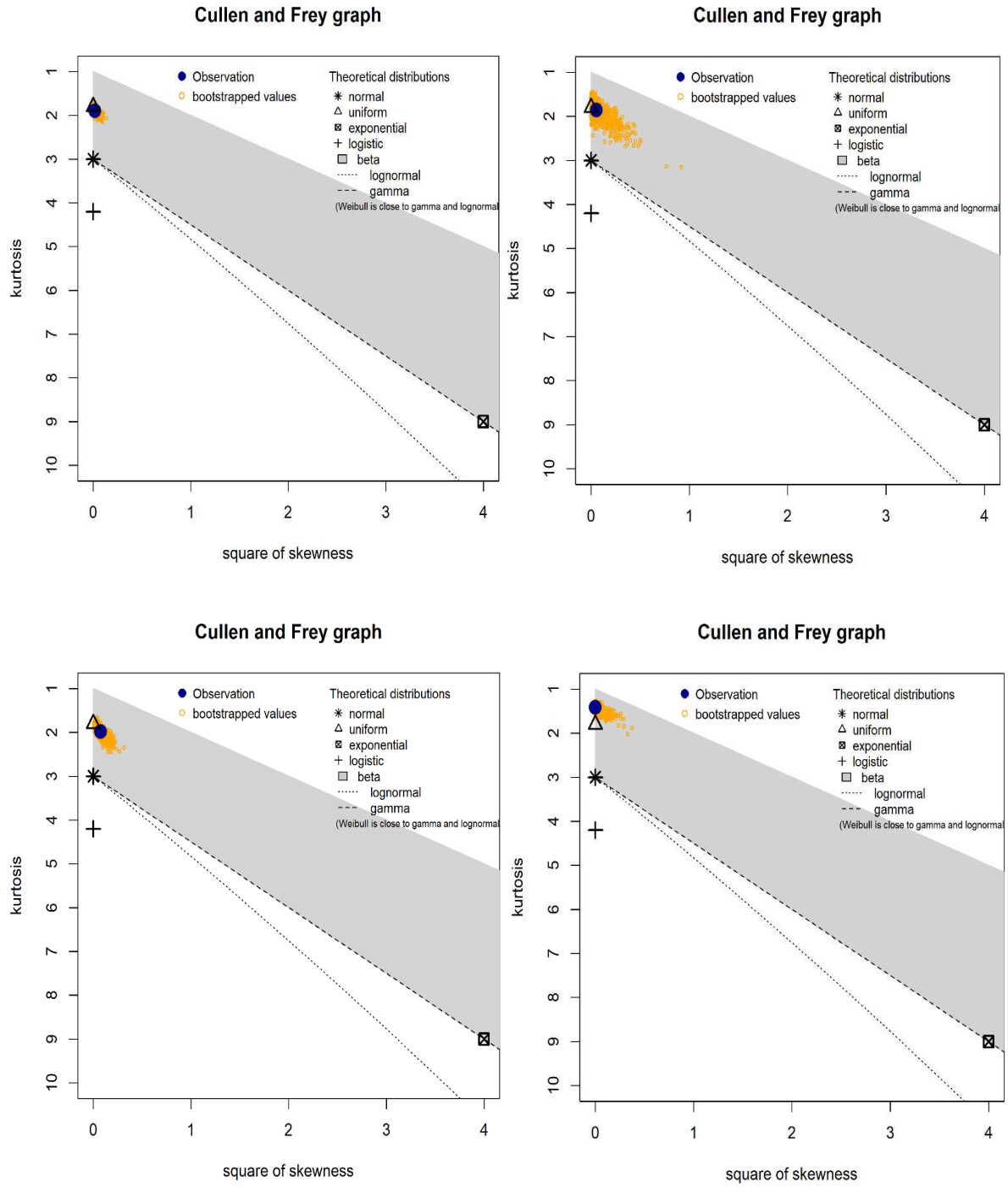
Cullen and Frey graph
Observation
bootstrapped values
Theoretical distributions
normal
uniform
exponential
logistic
beta
lognormal
gamma
(Weibull is close to gamma and lognormal)
kurtosis
square of skewness
0
1
2
3
4
1
2
3
4
5
6
7
8
9
10

Plot 8:

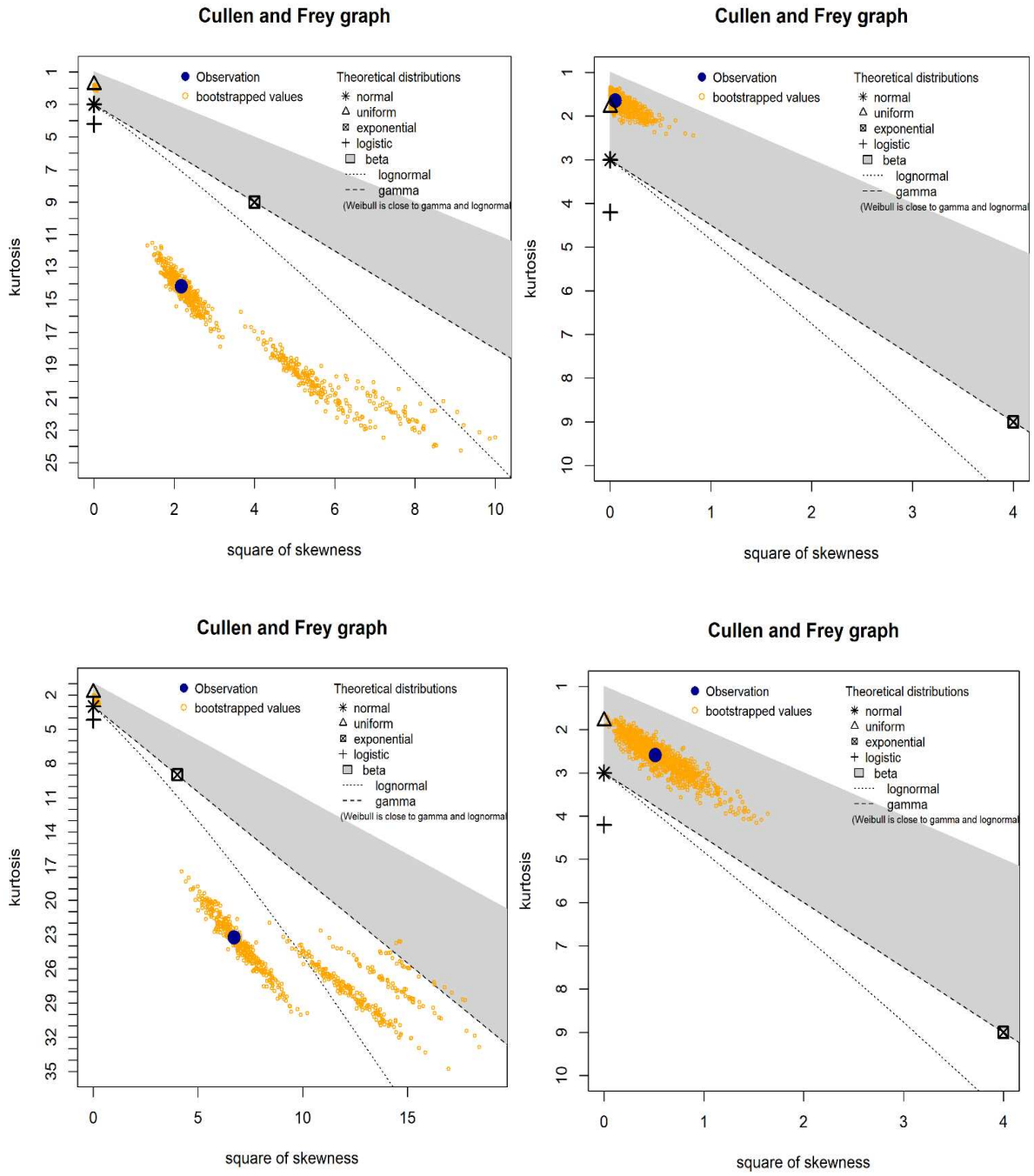
Cullen and Frey graph
Observation
bootstrapped values
Theoretical distributions
normal
uniform
exponential
logistic
beta
lognormal
gamma
(Weibull is close to gamma and lognormal)
kurtosis
square of skewness
Cullen and Frey graph
Observation
bootstrapped values
Theoretical distributions
normal
uniform
exponential
logistic
beta
lognormal
gamma
(Weibull is close to gamma and lognormal)
kurtosis
square of skewness
Cullen and Frey graph
Observation
bootstrapped values
Theoretical distributions
normal
uniform
exponential
logistic
beta
lognormal
gamma
(Weibull is close to gamma and lognormal)
kurtosis
square of skewness
Cullen and Frey graph
Observation
bootstrapped values
Theoretical distributions
normal
uniform
exponential
logistic
beta
lognormal
gamma
(Weibull is close to gamma and lognormal)
kurtosis
square of skewness

Plot 9:

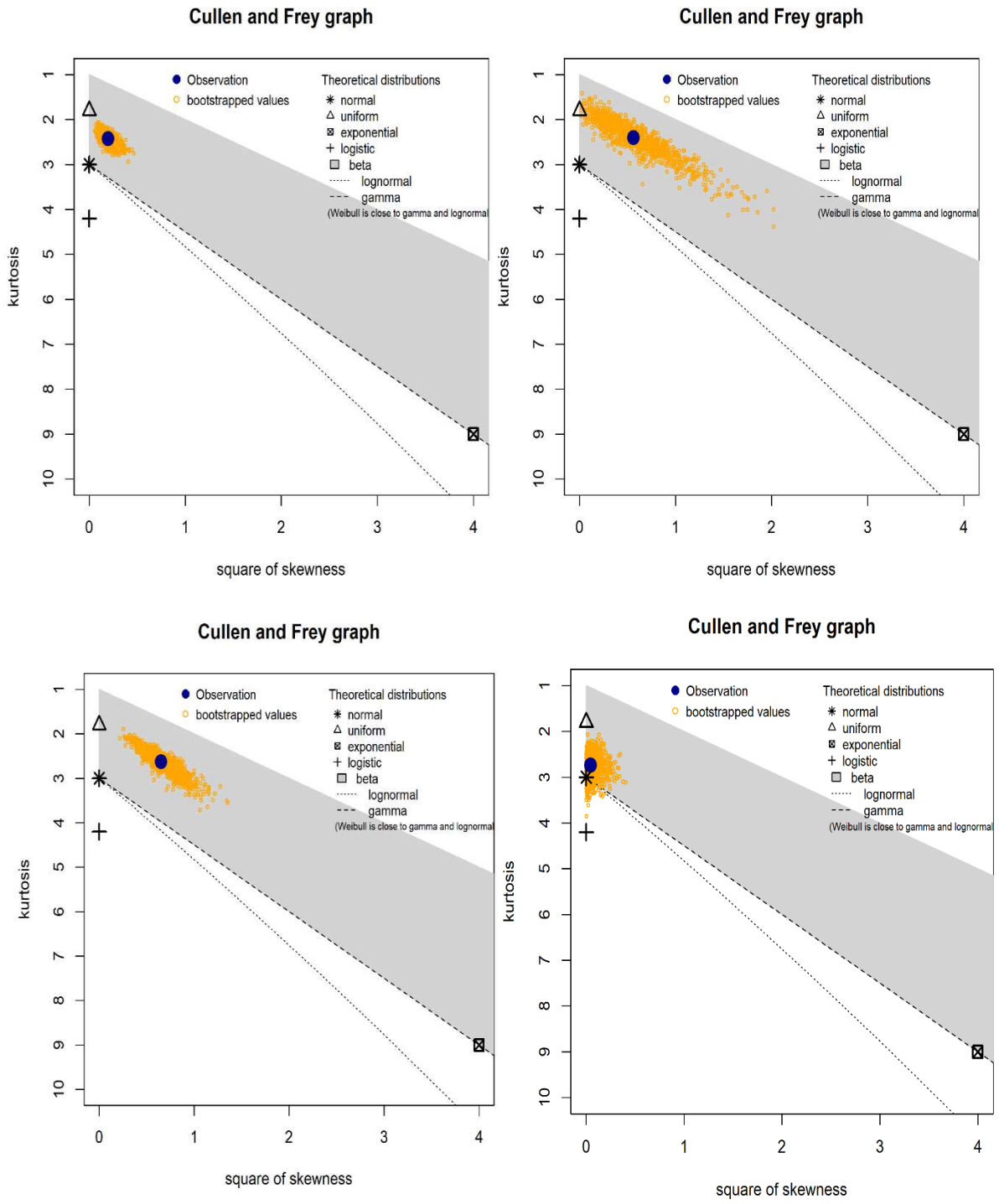
Cullen and Frey graph
Observation
bootstrapped values
Theoretical distributions
normal
uniform
exponential
logistic
beta
lognormal
gamma
(Weibull is close to gamma and lognormal)
kurtosis
square of skewness
Cullen and Frey graph
Observation
bootstrapped values
Theoretical distributions
normal
uniform
exponential
logistic
beta
lognormal
gamma
(Weibull is close to gamma and lognormal)
kurtosis
square of skewness
Cullen and Frey graph
Observation
bootstrapped values
Theoretical distributions
normal
uniform
exponential
logistic
beta
lognormal
gamma
(Weibull is close to gamma and lognormal)
kurtosis
square of skewness
Cullen and Frey graph
Observation
bootstrapped values
Theoretical distributions
normal
uniform
exponential
logistic
beta
lognormal
gamma
(Weibull is close to gamma and lognormal)
kurtosis
square of skewness

Plot 10:

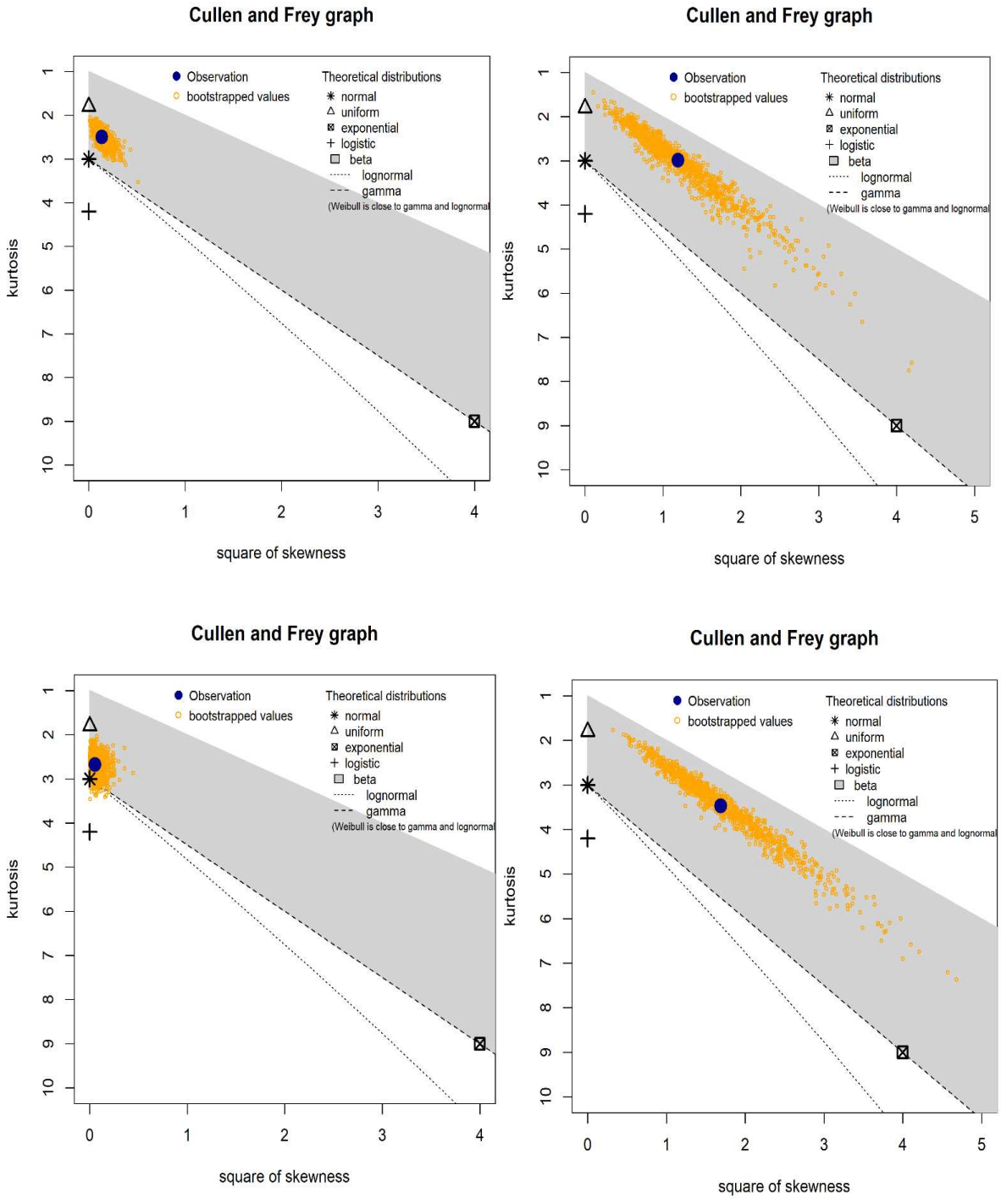
Cullen and Frey graph
Observation
bootstrapped values
Theoretical distributions
normal
uniform
exponential
logistic
beta
lognormal
gamma
(Weibull is close to gamma and lognormal)
kurtosis
square of skewness
Cullen and Frey graph
Observation
bootstrapped values
Theoretical distributions
normal
uniform
exponential
logistic
beta
lognormal
gamma
(Weibull is close to gamma and lognormal)
kurtosis
square of skewness
Cullen and Frey graph
Observation
bootstrapped values
Theoretical distributions
normal
uniform
exponential
logistic
beta
lognormal
gamma
(Weibull is close to gamma and lognormal)
kurtosis
square of skewness
Cullen and Frey graph
Observation
bootstrapped values
Theoretical distributions
normal
uniform
exponential
logistic
beta
lognormal
gamma
(Weibull is close to gamma and lognormal)
kurtosis
square of skewness

Plot 11:

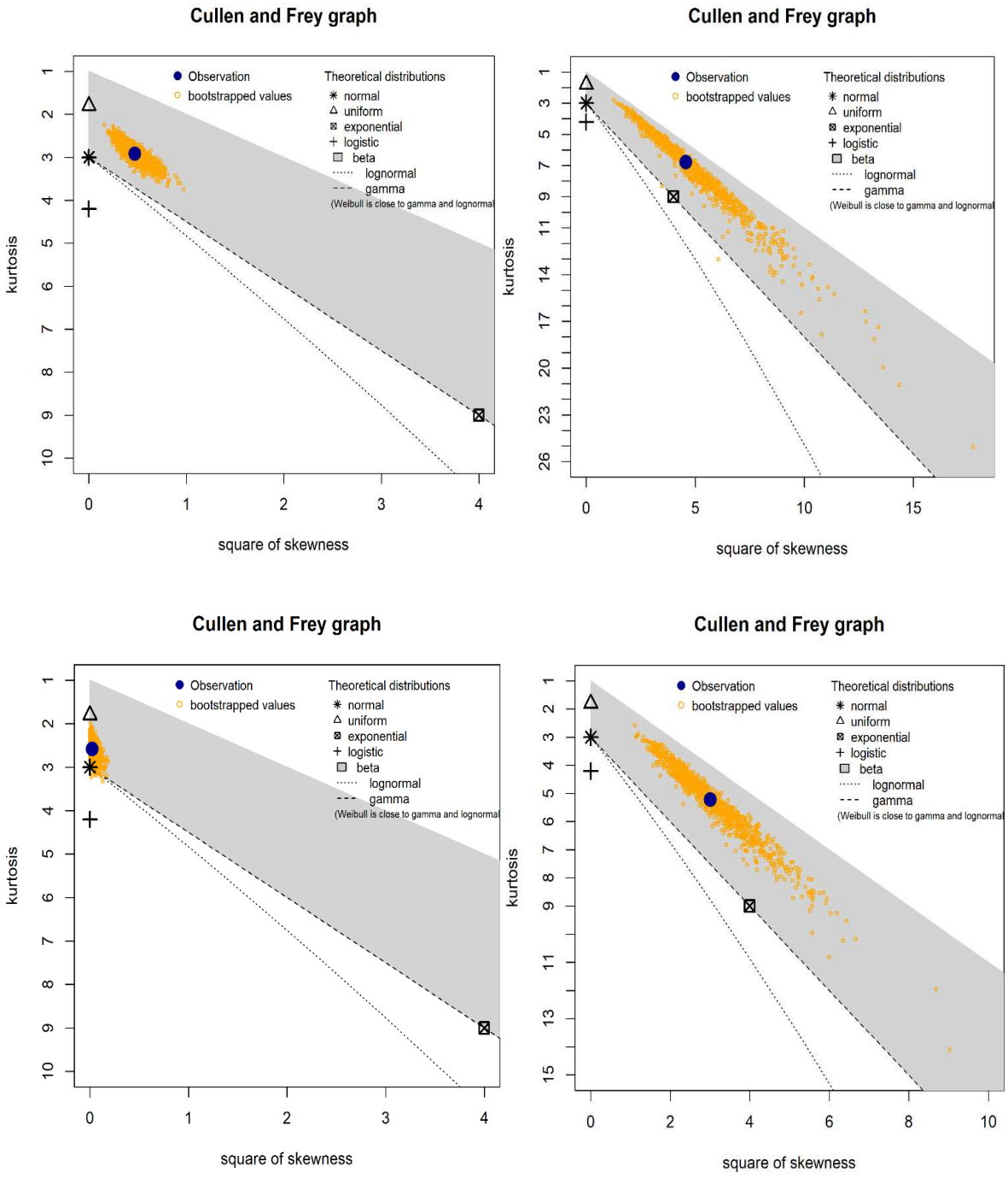
Cullen and Frey graph
Observation
bootstrapped values
Theoretical distributions
normal
uniform
exponential
logistic
beta
lognormal
gamma
(Weibull is close to gamma and lognormal)
kurtosis
square of skewness
Cullen and Frey graph
Observation
bootstrapped values
Theoretical distributions
normal
uniform
exponential
logistic
beta
lognormal
gamma
(Weibull is close to gamma and lognormal)
kurtosis
square of skewness
Cullen and Frey graph
Observation
bootstrapped values
Theoretical distributions
normal
uniform
exponential
logistic
beta
lognormal
gamma
(Weibull is close to gamma and lognormal)
kurtosis
square of skewness
Cullen and Frey graph
Observation
bootstrapped values
Theoretical distributions
normal
uniform
exponential
logistic
beta
lognormal
gamma
(Weibull is close to gamma and lognormal)
kurtosis
square of skewness

Plot 12:

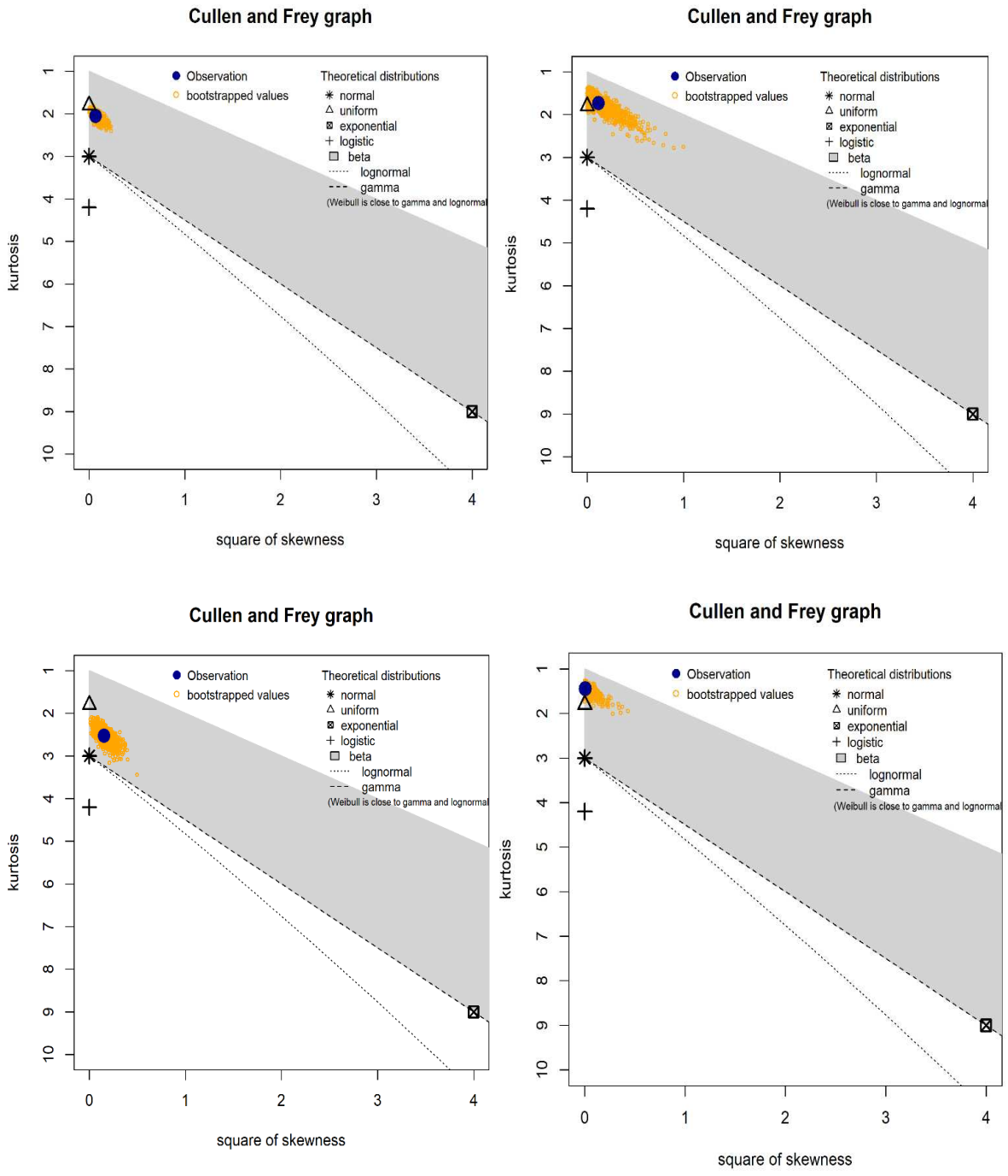
Cullen and Frey graph
Observation
bootstrapped values
Theoretical distributions
normal
uniform
exponential
logistic
beta
lognormal
gamma
(Weibull is close to gamma and lognormal)
kurtosis
square of skewness
0
1
2
3
4
1
2
3
4
5
6
7
8
9
10

Plot 13:

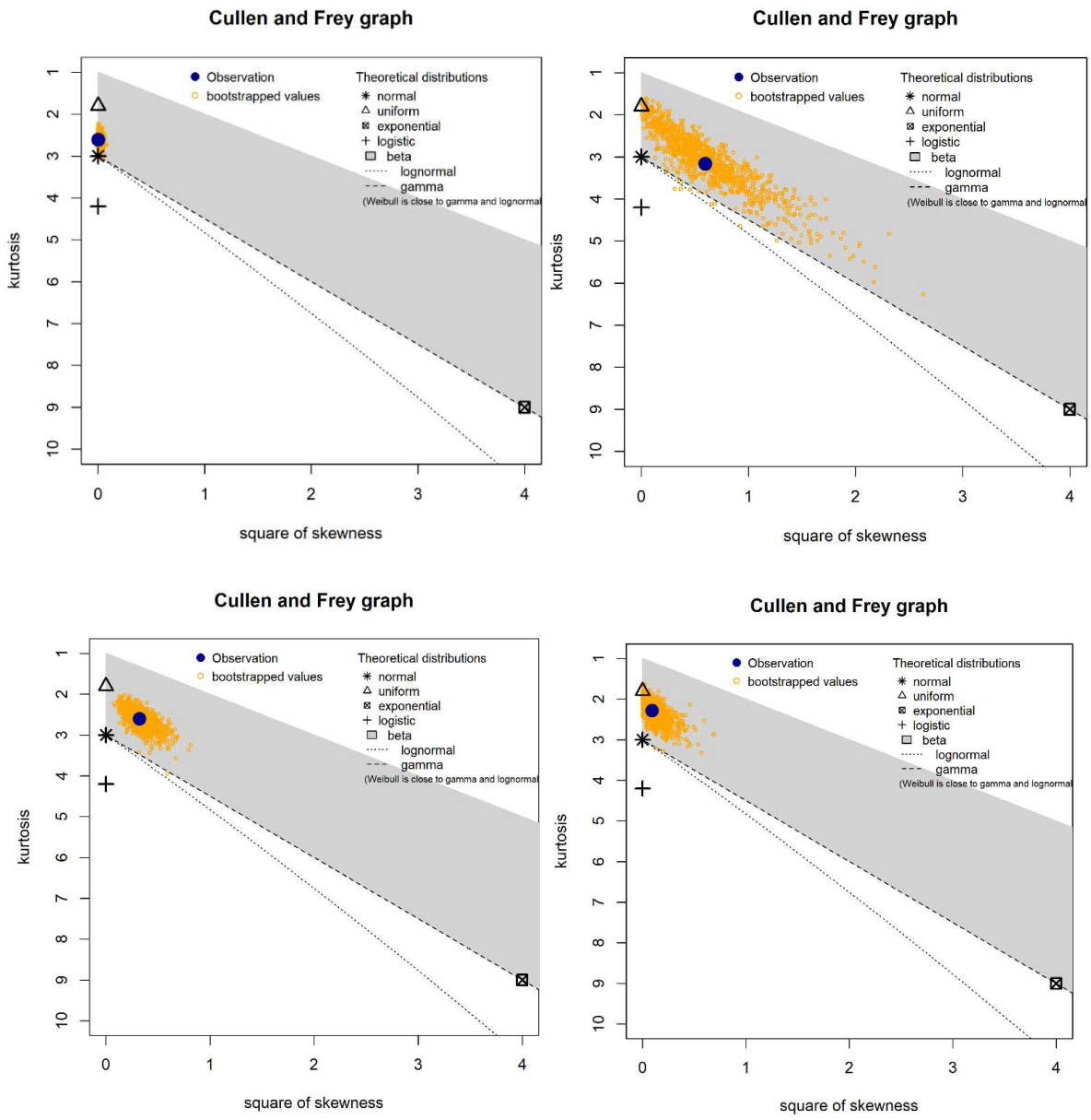
Cullen and Frey graph
Observation
bootstrapped values
Theoretical distributions
normal
uniform
exponential
logistic
beta
lognormal
gamma
(Weibull is close to gamma and lognormal)
kurtosis
square of skewness
Cullen and Frey graph
Observation
bootstrapped values
Theoretical distributions
normal
uniform
exponential
logistic
beta
lognormal
gamma
(Weibull is close to gamma and lognormal)
kurtosis
square of skewness
Cullen and Frey graph
Observation
bootstrapped values
Theoretical distributions
normal
uniform
exponential
logistic
beta
lognormal
gamma
(Weibull is close to gamma and lognormal)
kurtosis
square of skewness
Cullen and Frey graph
Observation
bootstrapped values
Theoretical distributions
normal
uniform
exponential
logistic
beta
lognormal
gamma
(Weibull is close to gamma and lognormal)
kurtosis
square of skewness

Plot 14:

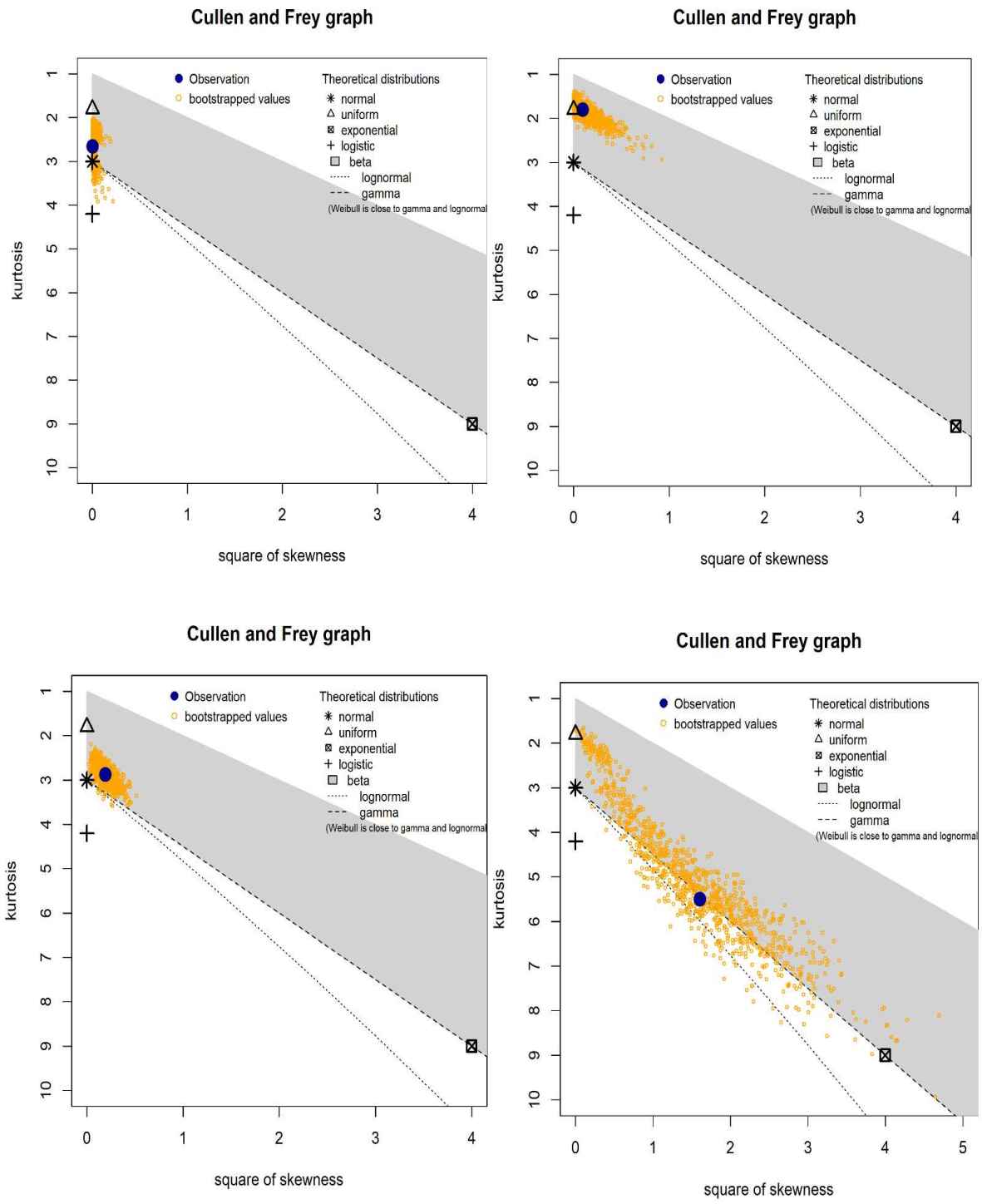
Cullen and Frey graph
Observation
bootstrapped values
Theoretical distributions
normal
uniform
exponential
logistic
beta
lognormal
gamma
(Weibull is close to gamma and lognormal)
kurtosis
square of skewness
Cullen and Frey graph
Observation
bootstrapped values
Theoretical distributions
normal
uniform
exponential
logistic
beta
lognormal
gamma
(Weibull is close to gamma and lognormal)
kurtosis
square of skewness
Cullen and Frey graph
Observation
bootstrapped values
Theoretical distributions
normal
uniform
exponential
logistic
beta
lognormal
gamma
(Weibull is close to gamma and lognormal)
kurtosis
square of skewness
Cullen and Frey graph
Observation
bootstrapped values
Theoretical distributions
normal
uniform
exponential
logistic
beta
lognormal
gamma
(Weibull is close to gamma and lognormal)
kurtosis
square of skewness

Plot 15:

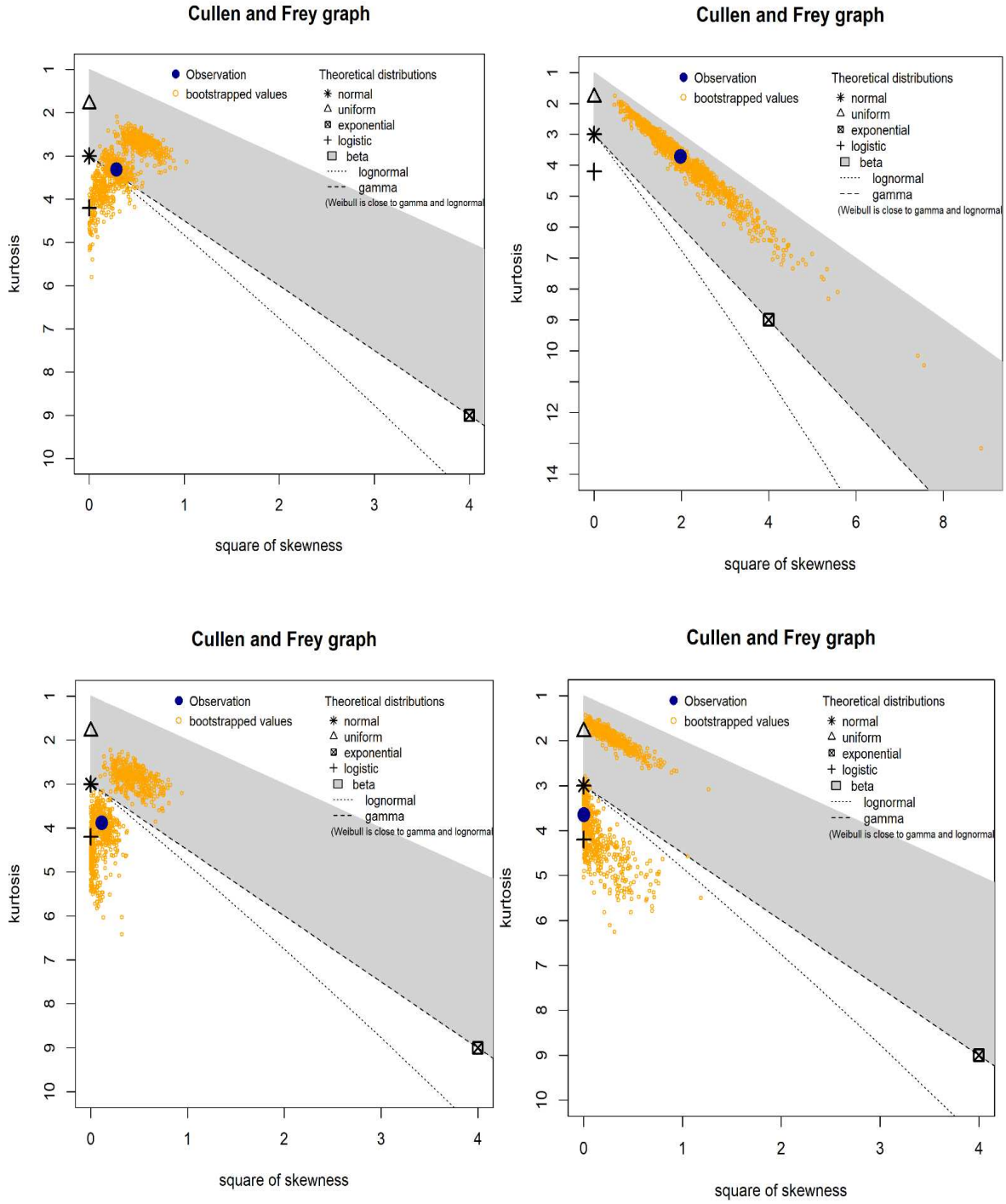
Cullen and Frey graph
Observation
bootstrapped values
Theoretical distributions
normal
uniform
exponential
logistic
beta
lognormal
gamma
(Weibull is close to gamma and lognormal)
kurtosis
square of skewness
Cullen and Frey graph
Observation
bootstrapped values
Theoretical distributions
normal
uniform
exponential
logistic
beta
lognormal
gamma
(Weibull is close to gamma and lognormal)
kurtosis
square of skewness
Cullen and Frey graph
Observation
bootstrapped values
Theoretical distributions
normal
uniform
exponential
logistic
beta
lognormal
gamma
(Weibull is close to gamma and lognormal)
kurtosis
square of skewness
Cullen and Frey graph
Observation
bootstrapped values
Theoretical distributions
normal
uniform
exponential
logistic
beta
lognormal
gamma
(Weibull is close to gamma and lognormal)
kurtosis
square of skewness

Plot 16:

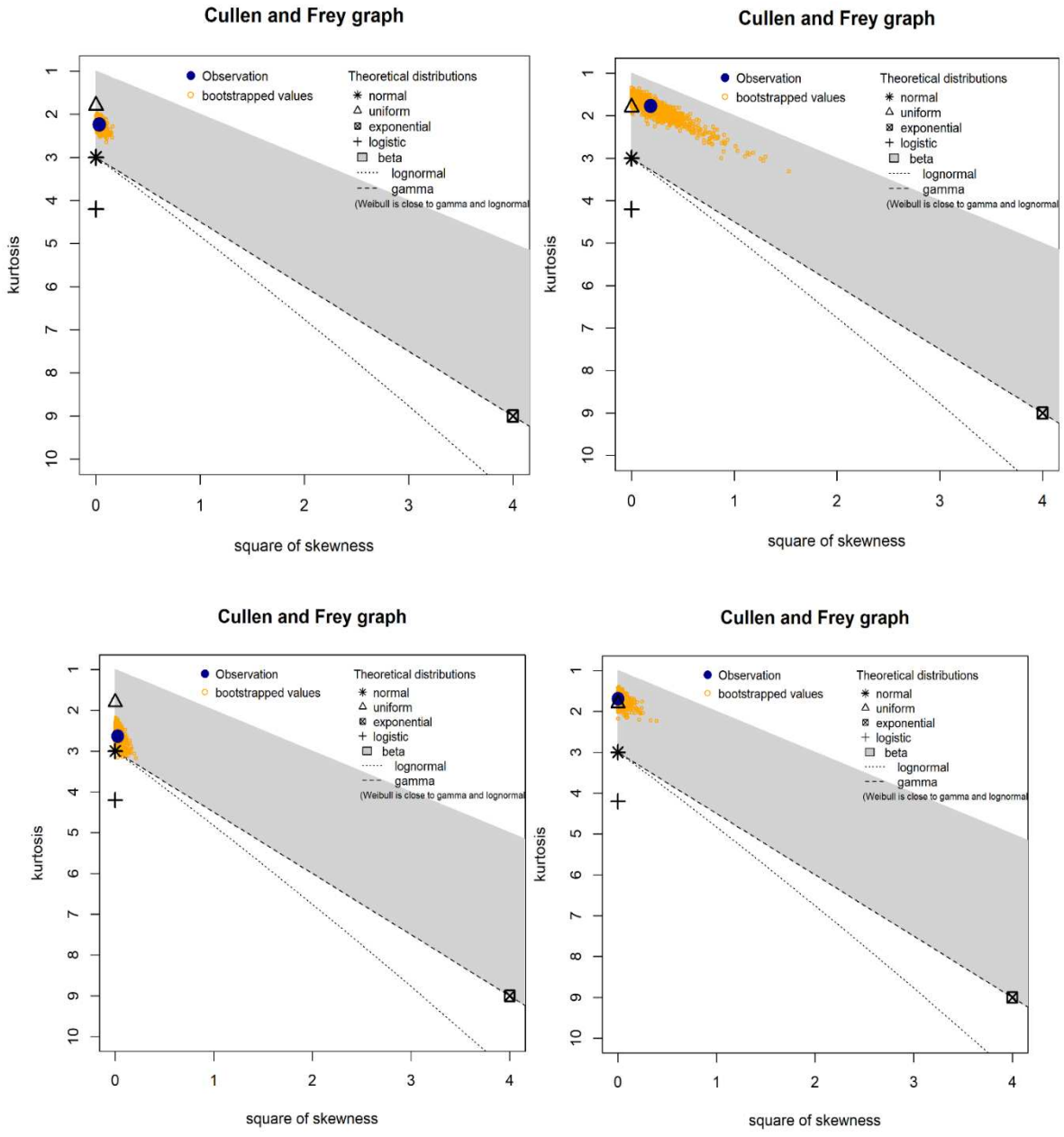
Cullen and Frey graph
Observation
bootstrapped values
Theoretical distributions
normal
uniform
exponential
logistic
beta
lognormal
gamma
(Weibull is close to gamma and lognormal)
kurtosis
square of skewness
0
1
2
3
4
1
2
3
4
5
6
7
8
9
10

1. Results of EC fit for plot 1 through 16

Plot 1:

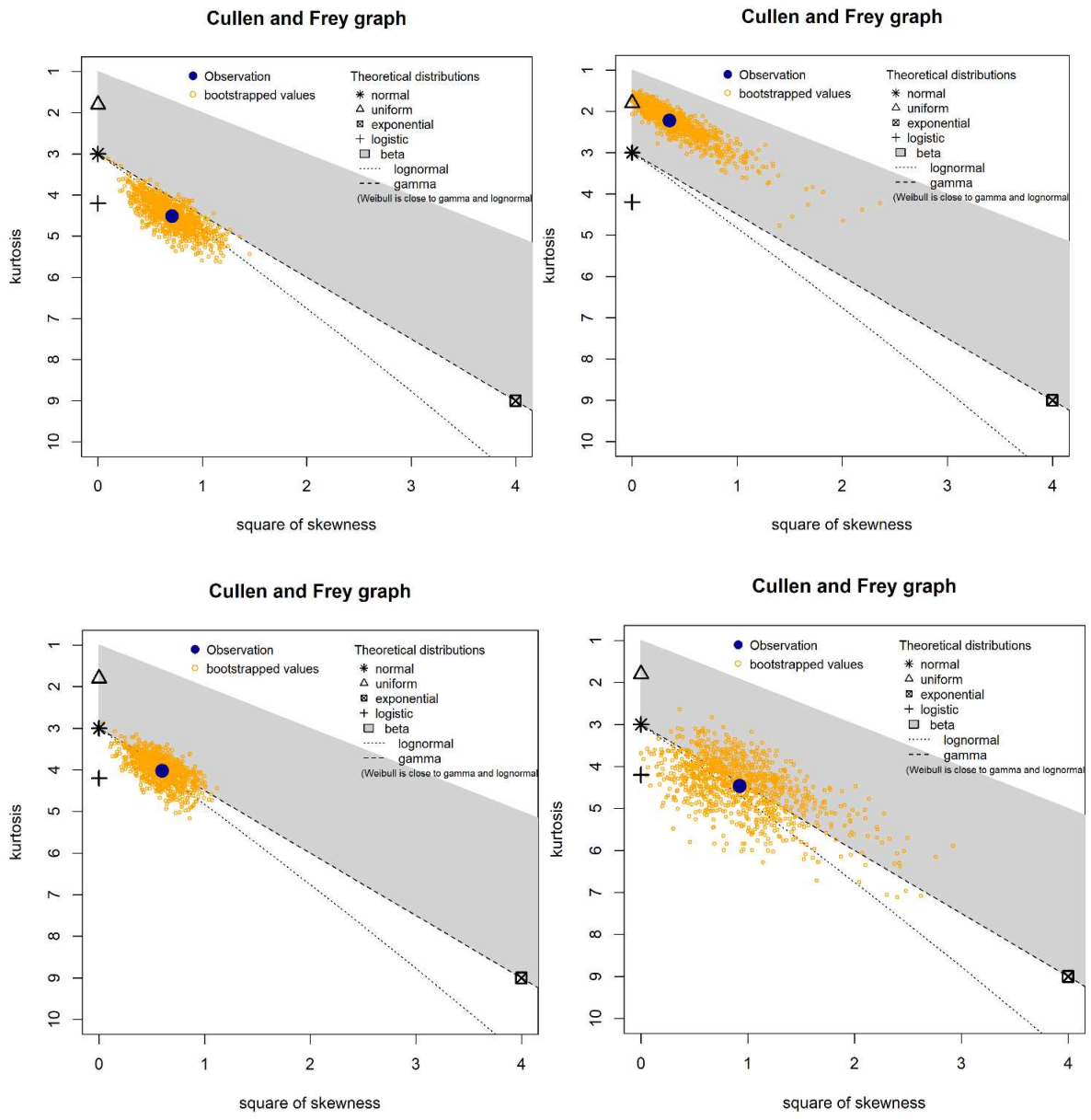

Plot 2:

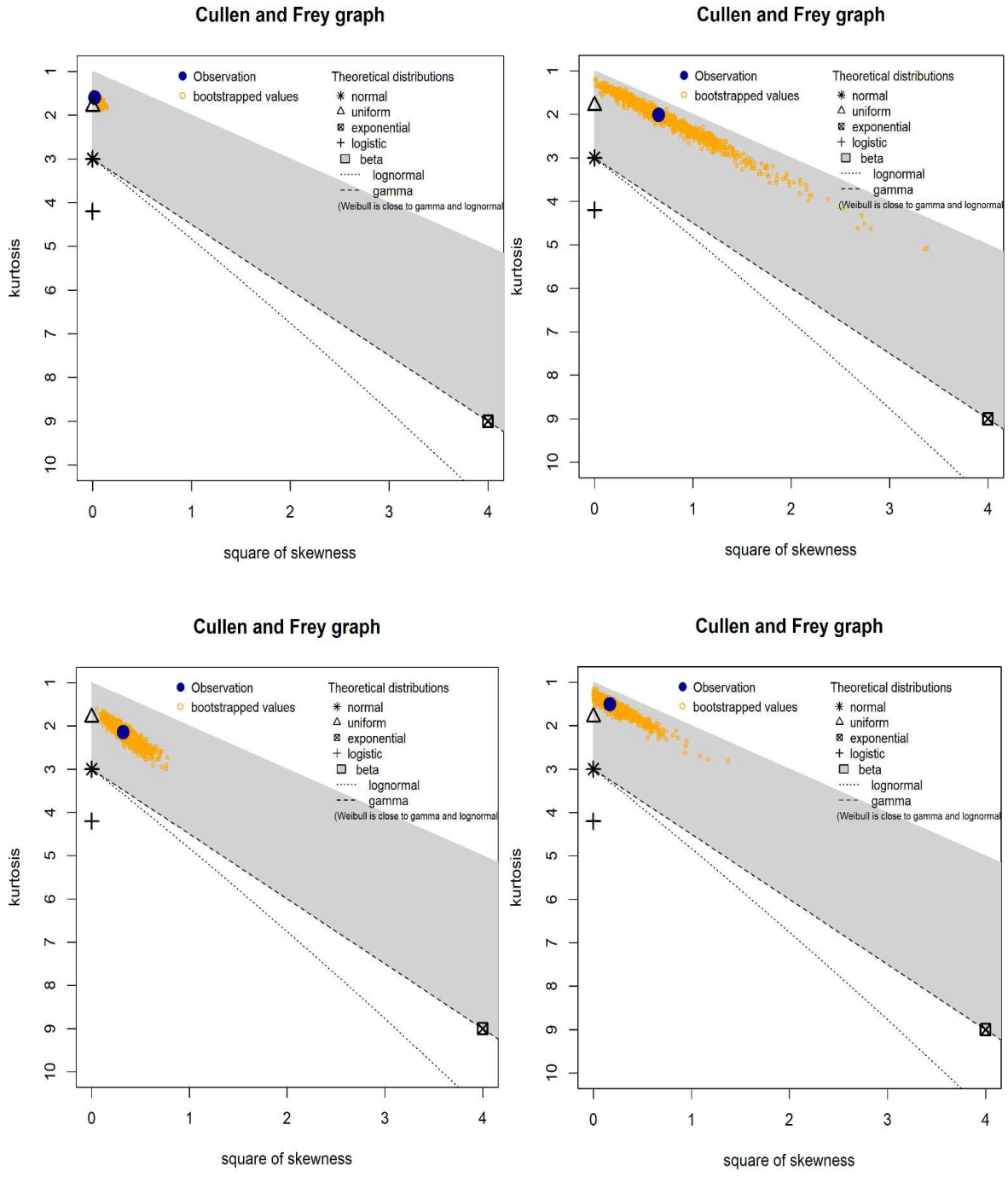
Cullen and Frey graph
Observation
bootstrapped values
Theoretical distributions
normal
uniform
exponential
logistic
beta
lognormal
gamma
(Weibull is close to gamma and lognormal)
kurtosis
square of skewness
Cullen and Frey graph
Observation
bootstrapped values
Theoretical distributions
normal
uniform
exponential
logistic
beta
lognormal
gamma
(Weibull is close to gamma and lognormal)
kurtosis
square of skewness
Cullen and Frey graph
Observation
bootstrapped values
Theoretical distributions
normal
uniform
exponential
logistic
beta
lognormal
gamma
(Weibull is close to gamma and lognormal)
kurtosis
square of skewness
Cullen and Frey graph
Observation
bootstrapped values
Theoretical distributions
normal
uniform
exponential
logistic
beta
lognormal
gamma
(Weibull is close to gamma and lognormal)
kurtosis
square of skewness

Plot 3:

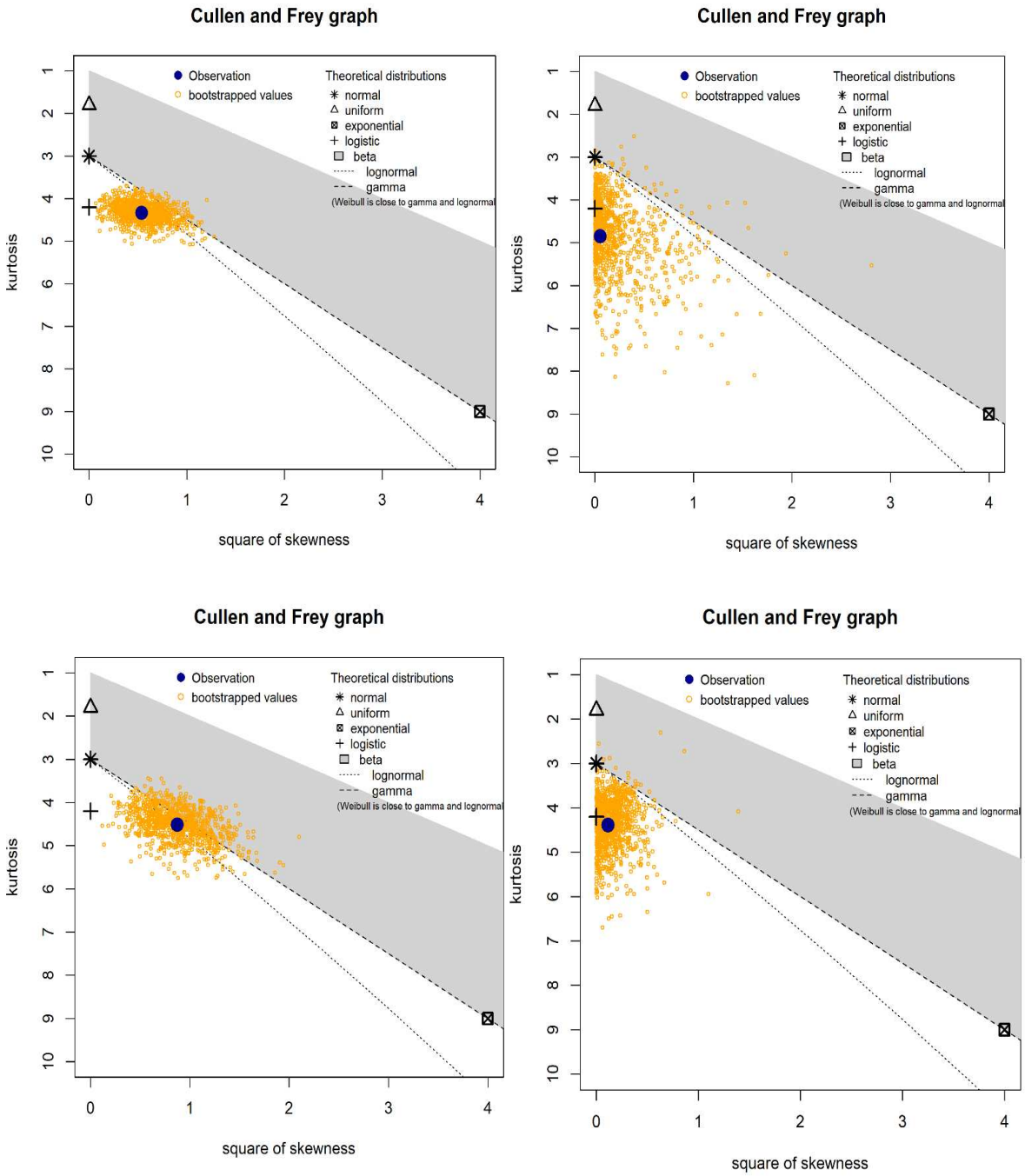
Cullen and Frey graph
Observation
bootstrapped values
Theoretical distributions
normal
uniform
exponential
logistic
beta
lognormal
gamma
(Weibull is close to gamma and lognormal)
kurtosis
square of skewness
Cullen and Frey graph
Observation
bootstrapped values
Theoretical distributions
normal
uniform
exponential
logistic
beta
lognormal
gamma
(Weibull is close to gamma and lognormal)
kurtosis
square of skewness
Cullen and Frey graph
Observation
bootstrapped values
Theoretical distributions
normal
uniform
exponential
logistic
beta
lognormal
gamma
(Weibull is close to gamma and lognormal)
kurtosis
square of skewness
Cullen and Frey graph
Observation
bootstrapped values
Theoretical distributions
normal
uniform
exponential
logistic
beta
lognormal
gamma
(Weibull is close to gamma and lognormal)
kurtosis
square of skewness

Plot 5:

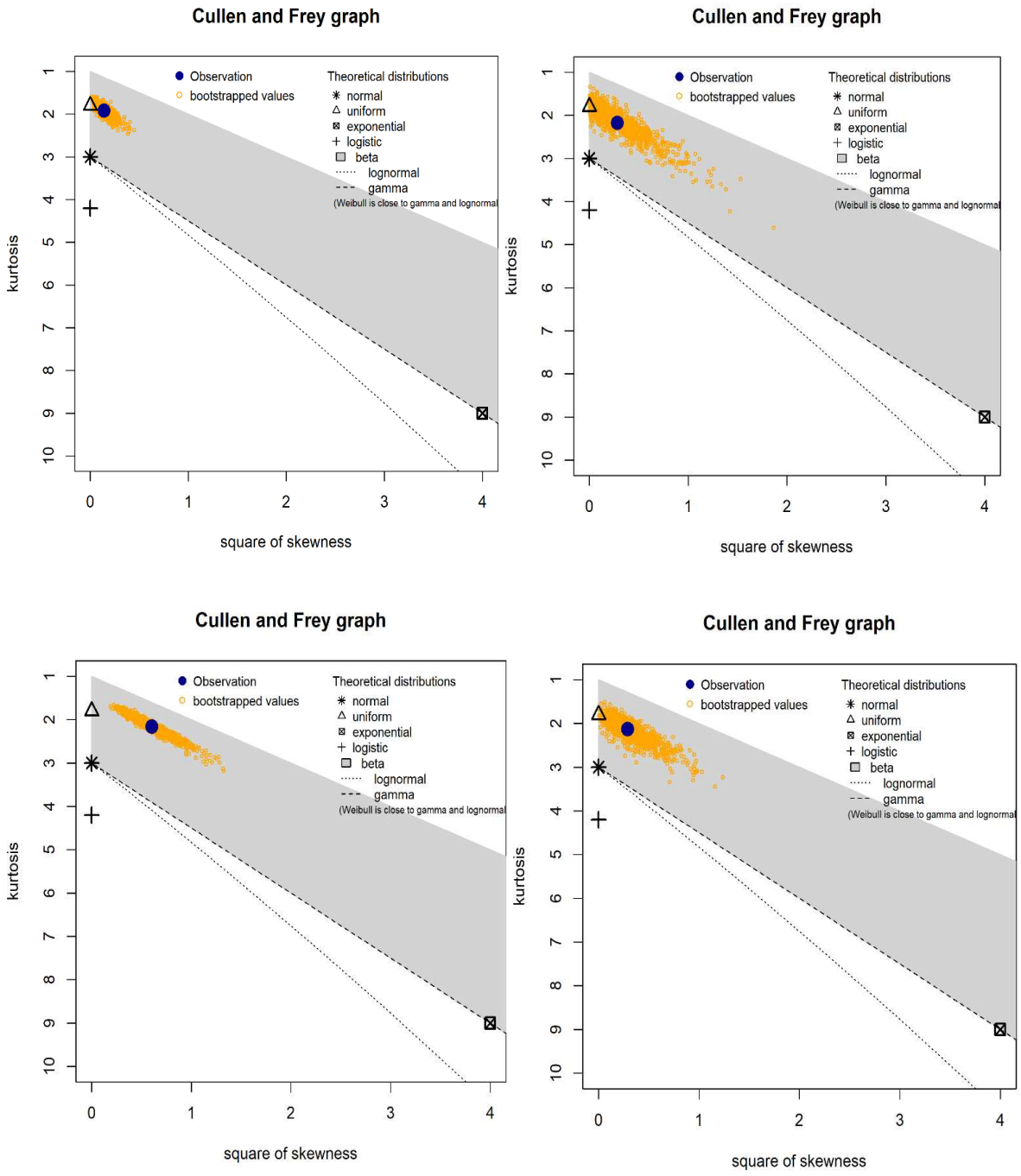
Cullen and Frey graph
Observation
bootstrapped values
Theoretical distributions
normal
uniform
exponential
logistic
beta
lognormal
gamma
(Weibull is close to gamma and lognormal)
kurtosis
square of skewness
0
1
2
3
4
1
2
3
4
5
6
7
8
9
10

Plot 6: Distribution of EC for entire the study period, season 1 and season 2 respectively.

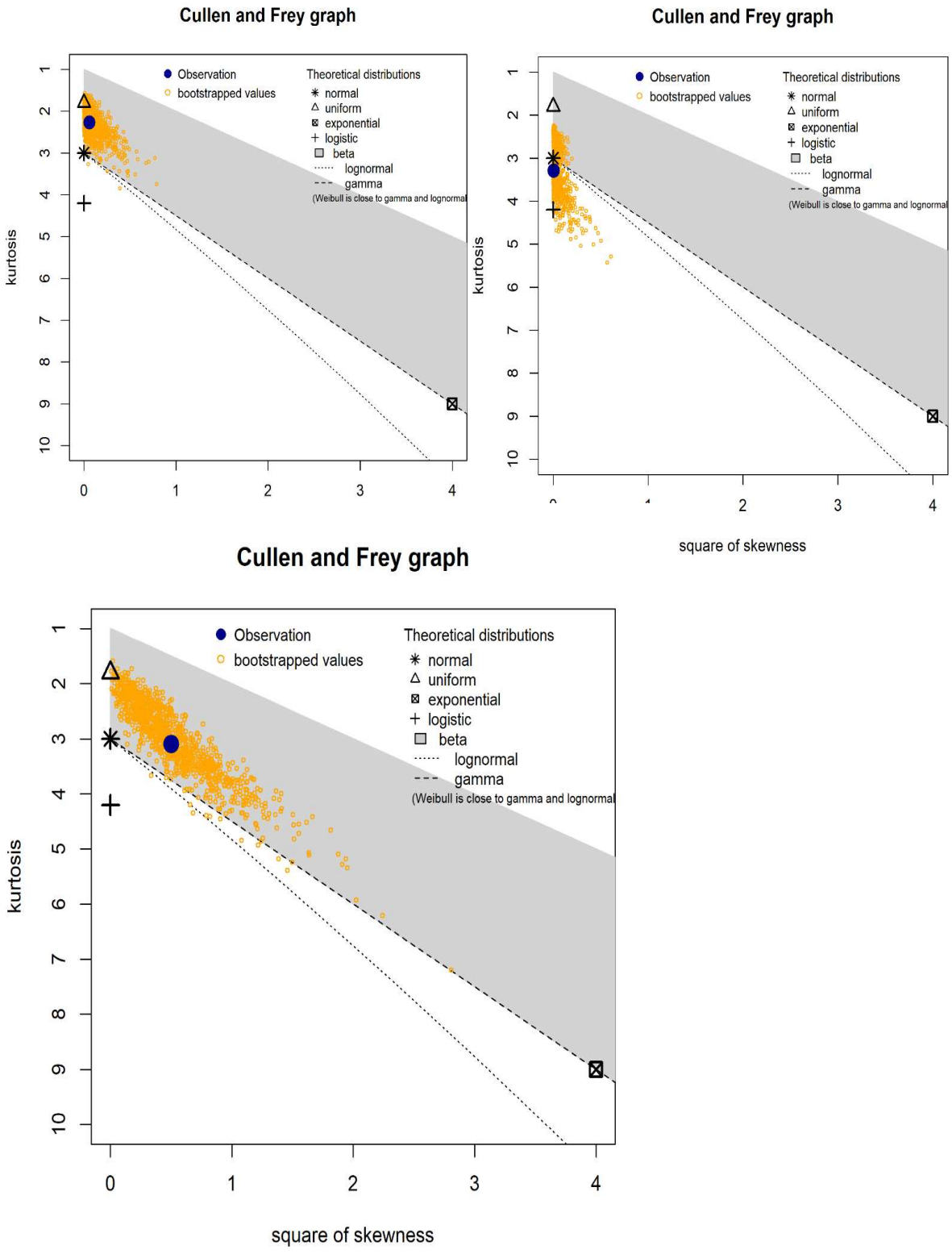

Plot 7: Season 1 and season 2 EC data distribution

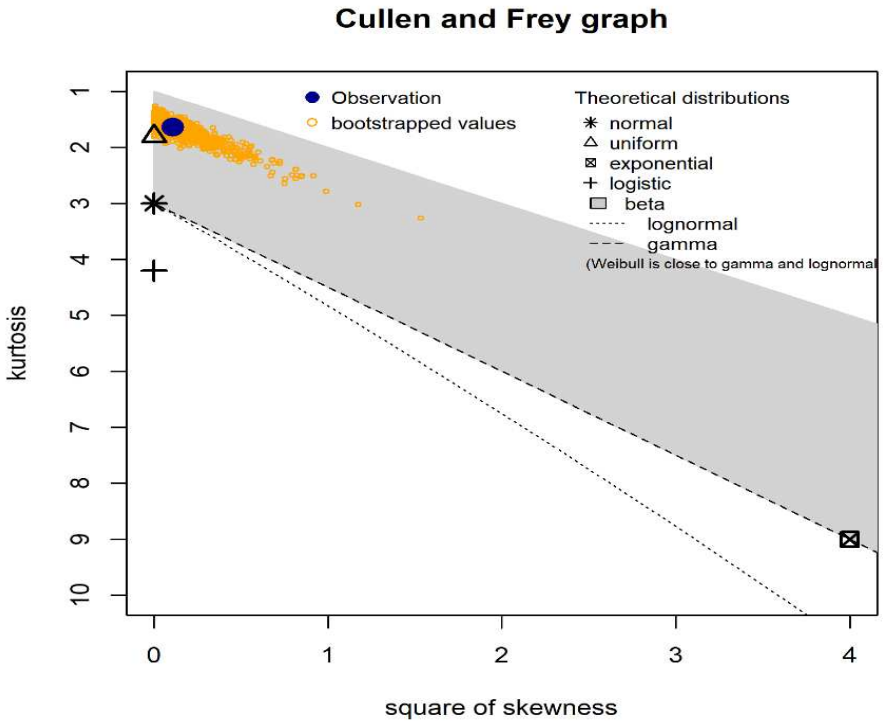

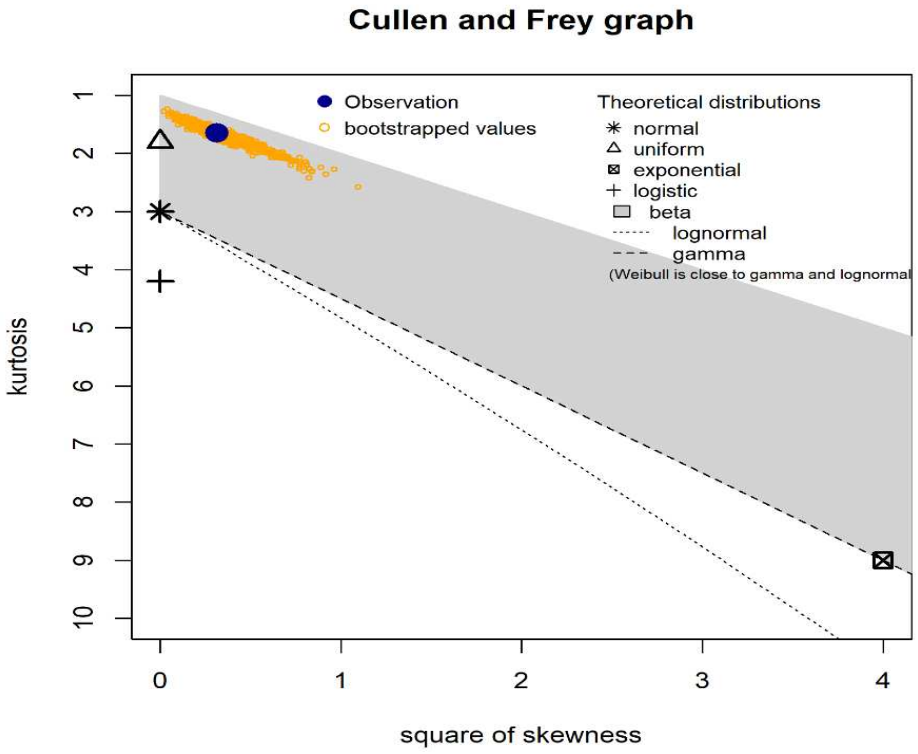

Plot 8:

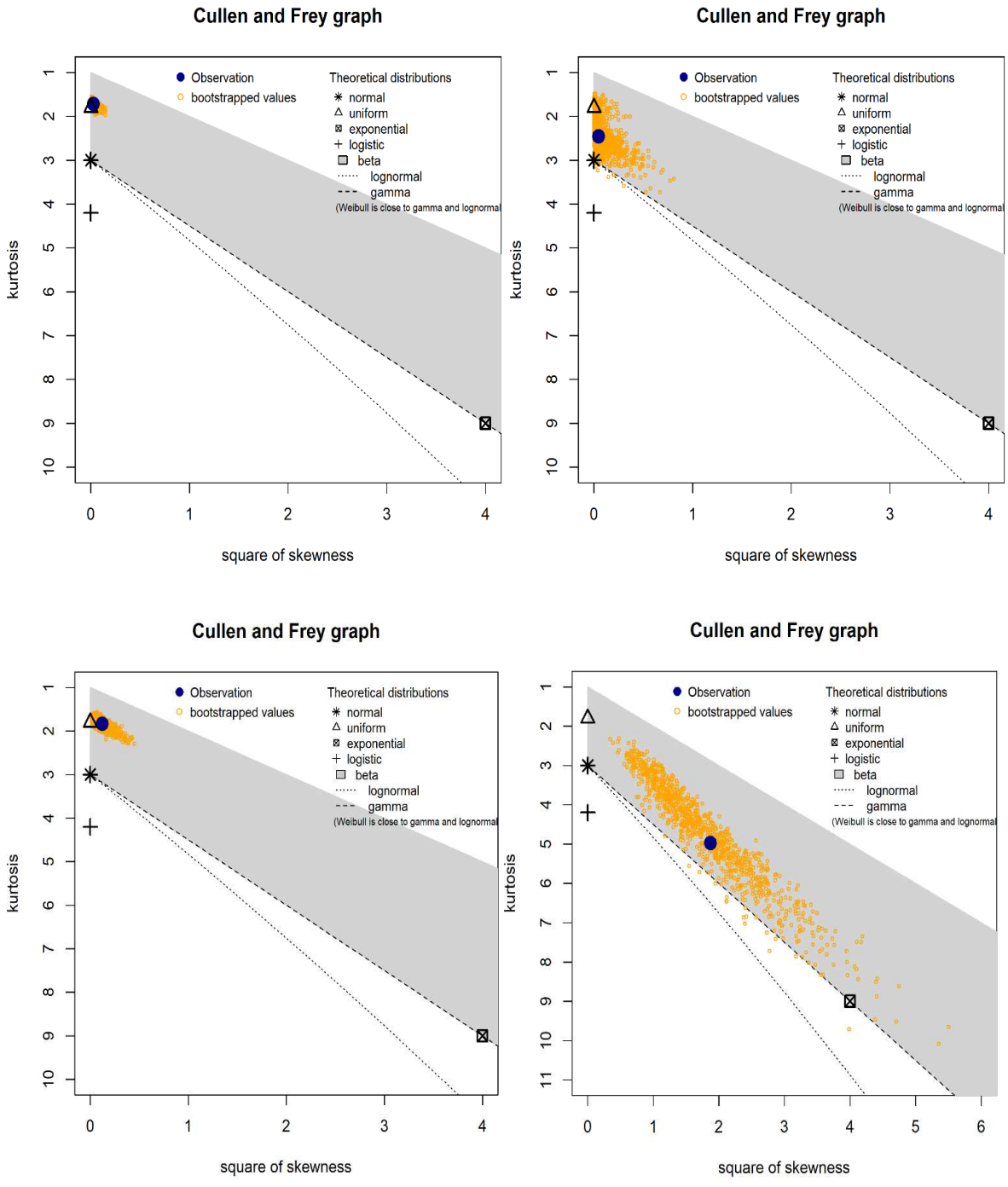
Cullen and Frey graph
Observation
bootstrapped values
Theoretical distributions
normal
uniform
exponential
logistic
beta
lognormal
gamma
(Weibull is close to gamma and lognormal)
kurtosis
square of skewness
Cullen and Frey graph
Observation
bootstrapped values
Theoretical distributions
normal
uniform
exponential
logistic
beta
lognormal
gamma
(Weibull is close to gamma and lognormal)
kurtosis
square of skewness
Cullen and Frey graph
Observation
bootstrapped values
Theoretical distributions
normal
uniform
exponential
logistic
beta
lognormal
gamma
(Weibull is close to gamma and lognormal)
kurtosis
square of skewness
Cullen and Frey graph
Observation
bootstrapped values
Theoretical distributions
normal
uniform
exponential
logistic
beta
lognormal
gamma
(Weibull is close to gamma and lognormal)
kurtosis
square of skewness

Plot 9:

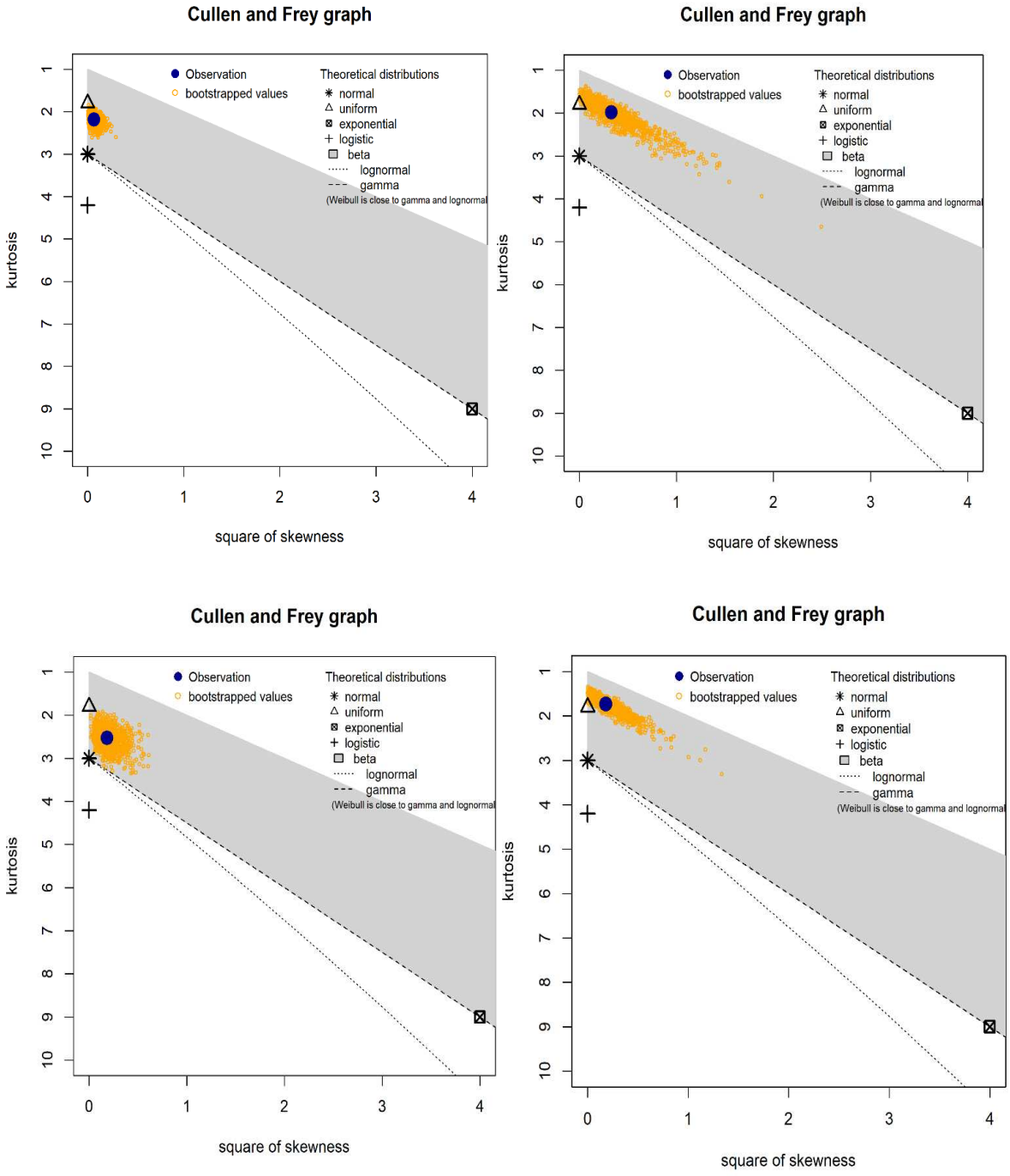
Cullen and Frey graph
Observation
bootstrapped values
Theoretical distributions
normal
uniform
exponential
logistic
beta
lognormal
gamma
(Weibull is close to gamma and lognormal)
kurtosis
square of skewness
Cullen and Frey graph
Observation
bootstrapped values
Theoretical distributions
normal
uniform
exponential
logistic
beta
lognormal
gamma
(Weibull is close to gamma and lognormal)
kurtosis
square of skewness
Cullen and Frey graph
Observation
bootstrapped values
Theoretical distributions
normal
uniform
exponential
logistic
beta
lognormal
gamma
(Weibull is close to gamma and lognormal)
kurtosis
square of skewness
Cullen and Frey graph
Observation
bootstrapped values
Theoretical distributions
normal
uniform
exponential
logistic
beta
lognormal
gamma
(Weibull is close to gamma and lognormal)
kurtosis
square of skewness

Plot 10:

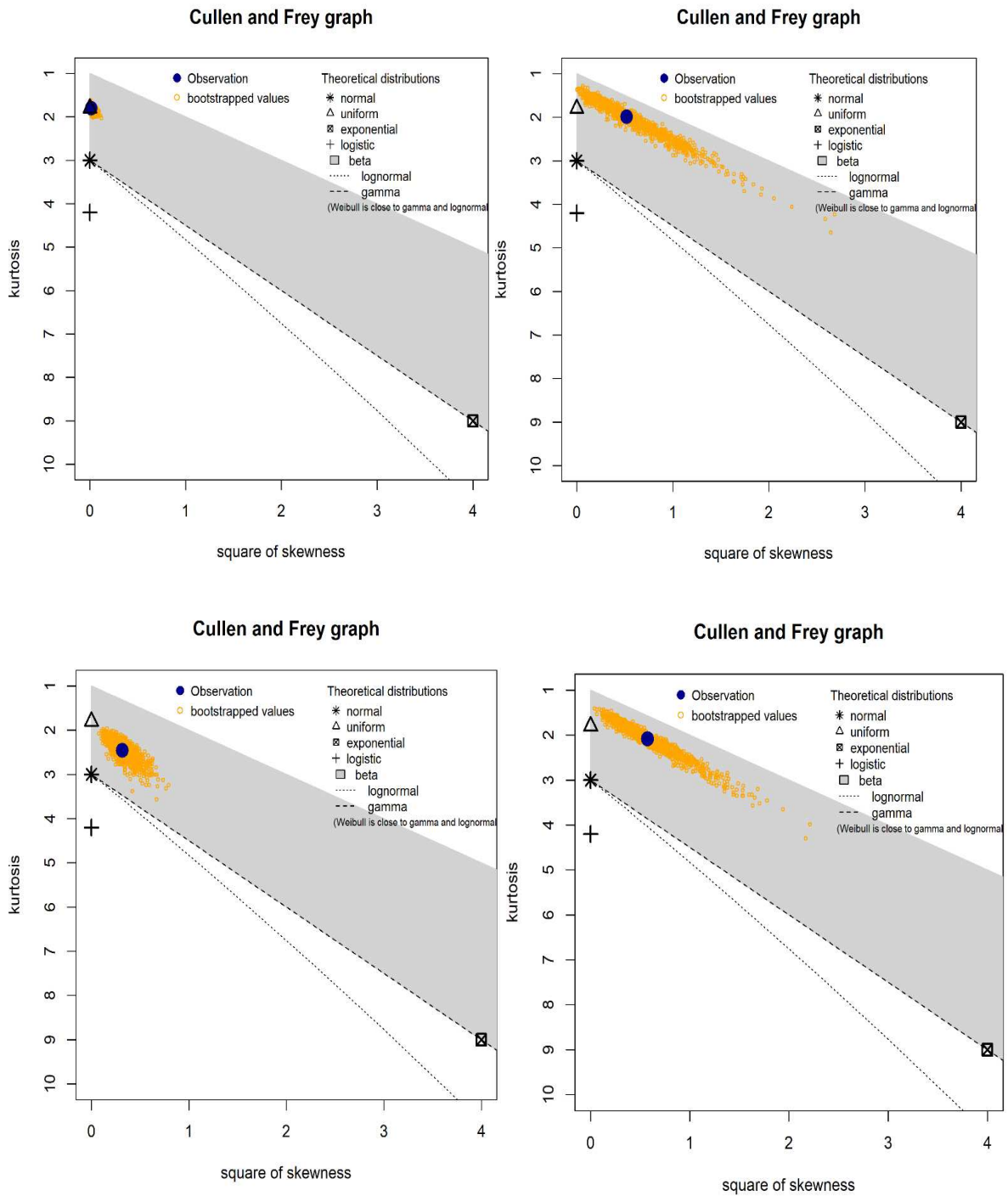
Cullen and Frey graph
Observation
bootstrapped values
Theoretical distributions
normal
uniform
exponential
logistic
beta
lognormal
gamma
(Weibull is close to gamma and lognormal)
kurtosis
square of skewness
Cullen and Frey graph
Observation
bootstrapped values
Theoretical distributions
normal
uniform
exponential
logistic
beta
lognormal
gamma
(Weibull is close to gamma and lognormal)
kurtosis
square of skewness
Cullen and Frey graph
Observation
bootstrapped values
Theoretical distributions
normal
uniform
exponential
logistic
beta
lognormal
gamma
(Weibull is close to gamma and lognormal)
kurtosis
square of skewness
Cullen and Frey graph
Observation
bootstrapped values
Theoretical distributions
normal
uniform
exponential
logistic
beta
lognormal
gamma
(Weibull is close to gamma and lognormal)
kurtosis
square of skewness

Plot 11:

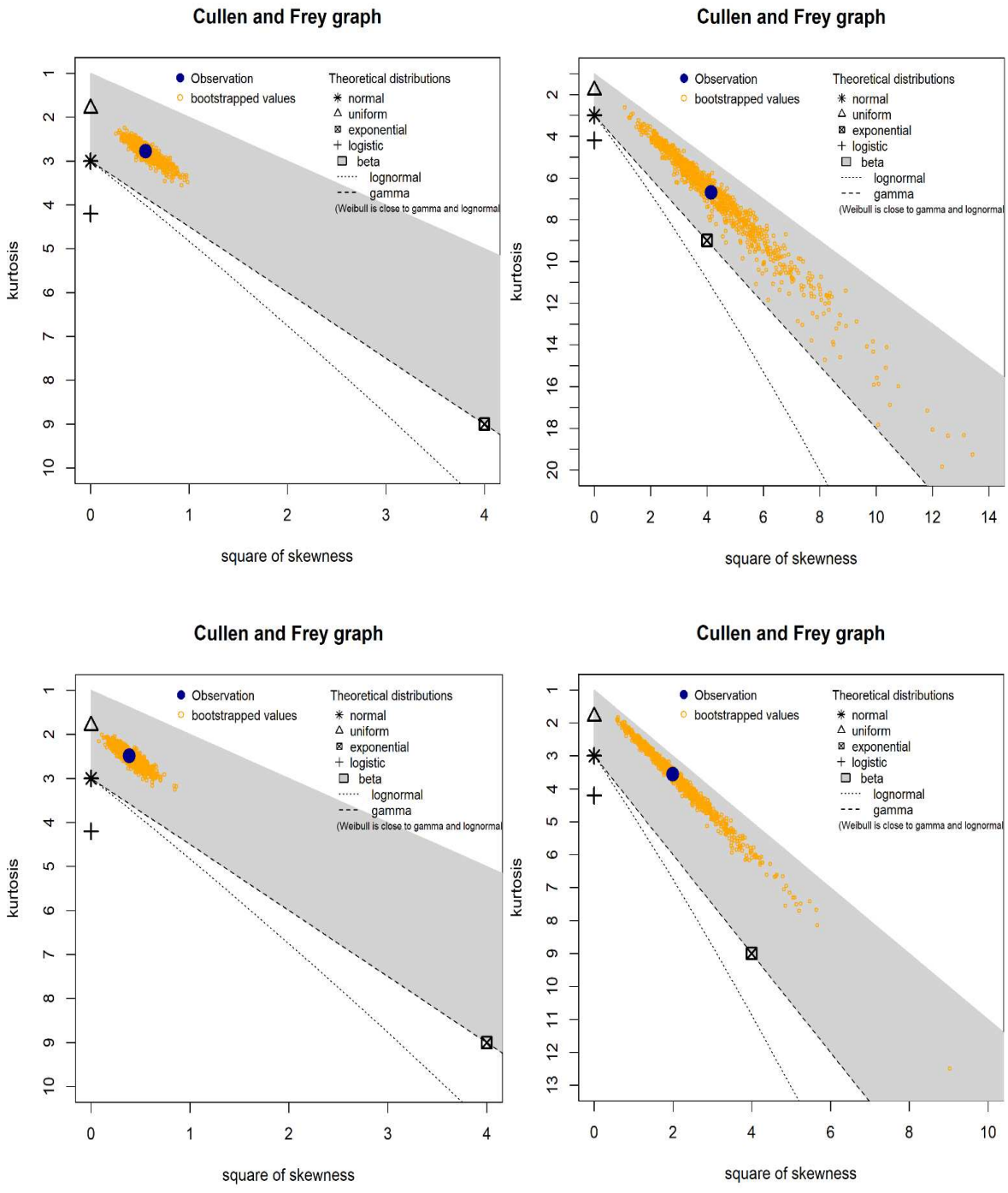
Cullen and Frey graph
Observation
bootstrapped values
Theoretical distributions
normal
uniform
exponential
logistic
beta
lognormal
gamma
(Weibull is close to gamma and lognormal)
kurtosis
square of skewness
Cullen and Frey graph
Observation
bootstrapped values
Theoretical distributions
normal
uniform
exponential
logistic
beta
lognormal
gamma
(Weibull is close to gamma and lognormal)
kurtosis
square of skewness
Cullen and Frey graph
Observation
bootstrapped values
Theoretical distributions
normal
uniform
exponential
logistic
beta
lognormal
gamma
(Weibull is close to gamma and lognormal)
kurtosis
square of skewness
Cullen and Frey graph
Observation
bootstrapped values
Theoretical distributions
normal
uniform
exponential
logistic
beta
lognormal
gamma
(Weibull is close to gamma and lognormal)
kurtosis
square of skewness

Plot 12:

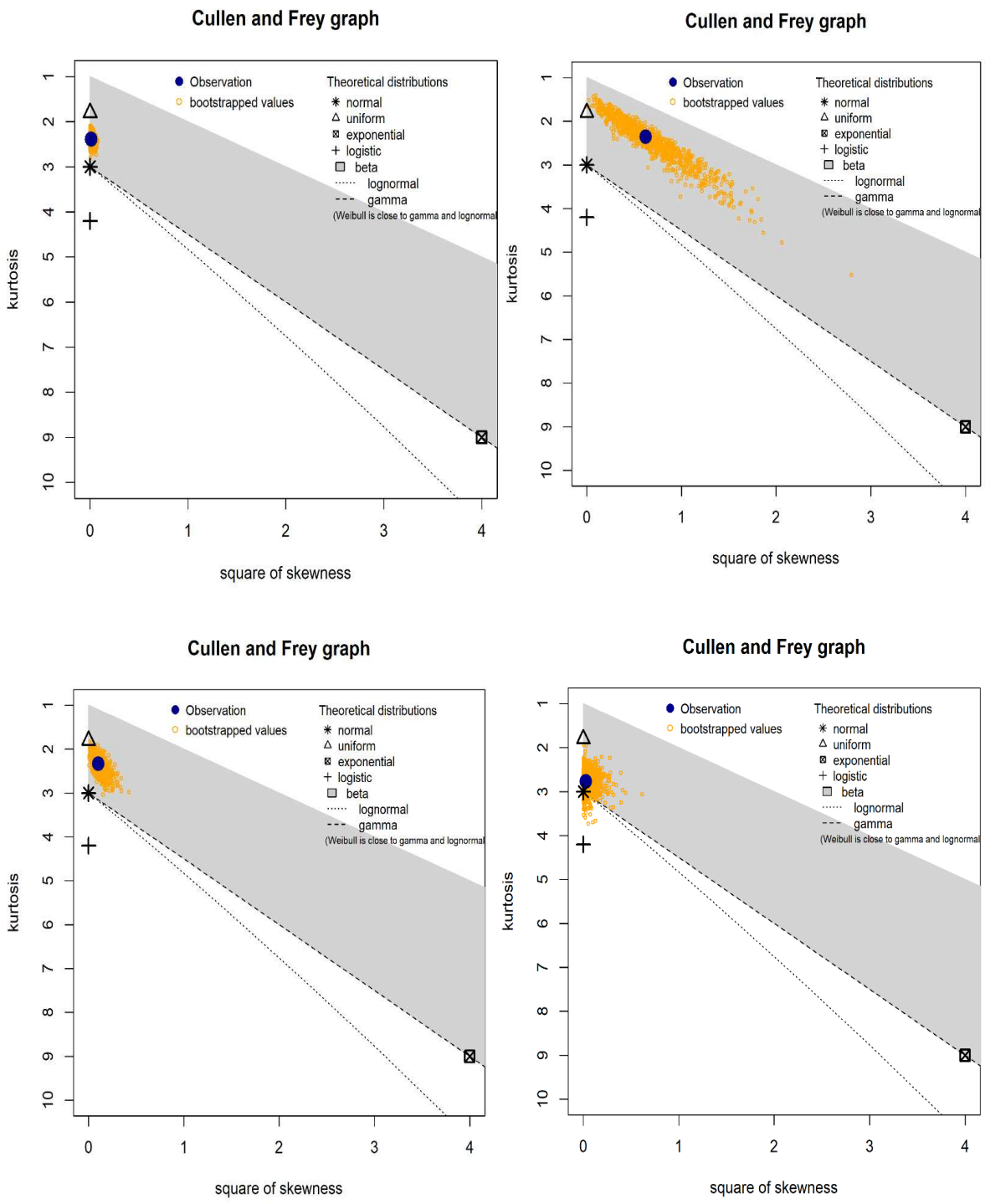
Cullen and Frey graph
Observation
bootstrapped values
Theoretical distributions
normal
uniform
exponential
logistic
beta
lognormal
gamma
(Weibull is close to gamma and lognormal)
kurtosis
square of skewness
Cullen and Frey graph
Observation
bootstrapped values
Theoretical distributions
normal
uniform
exponential
logistic
beta
lognormal
gamma
(Weibull is close to gamma and lognormal)
kurtosis
square of skewness
Cullen and Frey graph
Observation
bootstrapped values
Theoretical distributions
normal
uniform
exponential
logistic
beta
lognormal
gamma
(Weibull is close to gamma and lognormal)
kurtosis
square of skewness
Cullen and Frey graph
Observation
bootstrapped values
Theoretical distributions
normal
uniform
exponential
logistic
beta
lognormal
gamma
(Weibull is close to gamma and lognormal)
kurtosis
square of skewness

Plot 13:

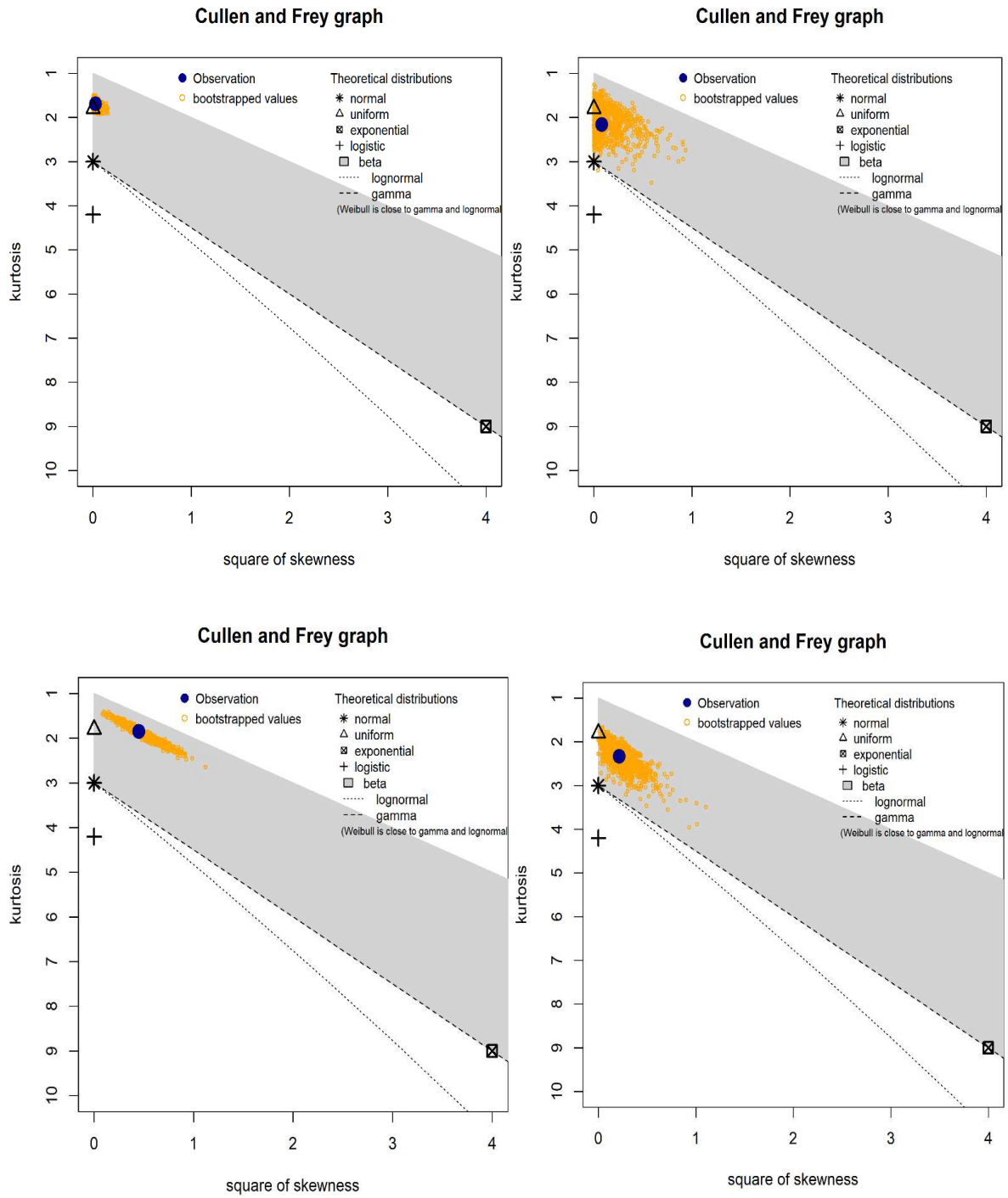
Cullen and Frey graph
Observation
bootstrapped values
Theoretical distributions
normal
uniform
exponential
logistic
beta
lognormal
gamma
(Weibull is close to gamma and lognormal)
kurtosis
square of skewness
Cullen and Frey graph
Observation
bootstrapped values
Theoretical distributions
normal
uniform
exponential
logistic
beta
lognormal
gamma
(Weibull is close to gamma and lognormal)
kurtosis
square of skewness
Cullen and Frey graph
Observation
bootstrapped values
Theoretical distributions
normal
uniform
exponential
logistic
beta
lognormal
gamma
(Weibull is close to gamma and lognormal)
kurtosis
square of skewness
Cullen and Frey graph
Observation
bootstrapped values
Theoretical distributions
normal
uniform
exponential
logistic
beta
lognormal
gamma
(Weibull is close to gamma and lognormal)
kurtosis
square of skewness

Plot 14:

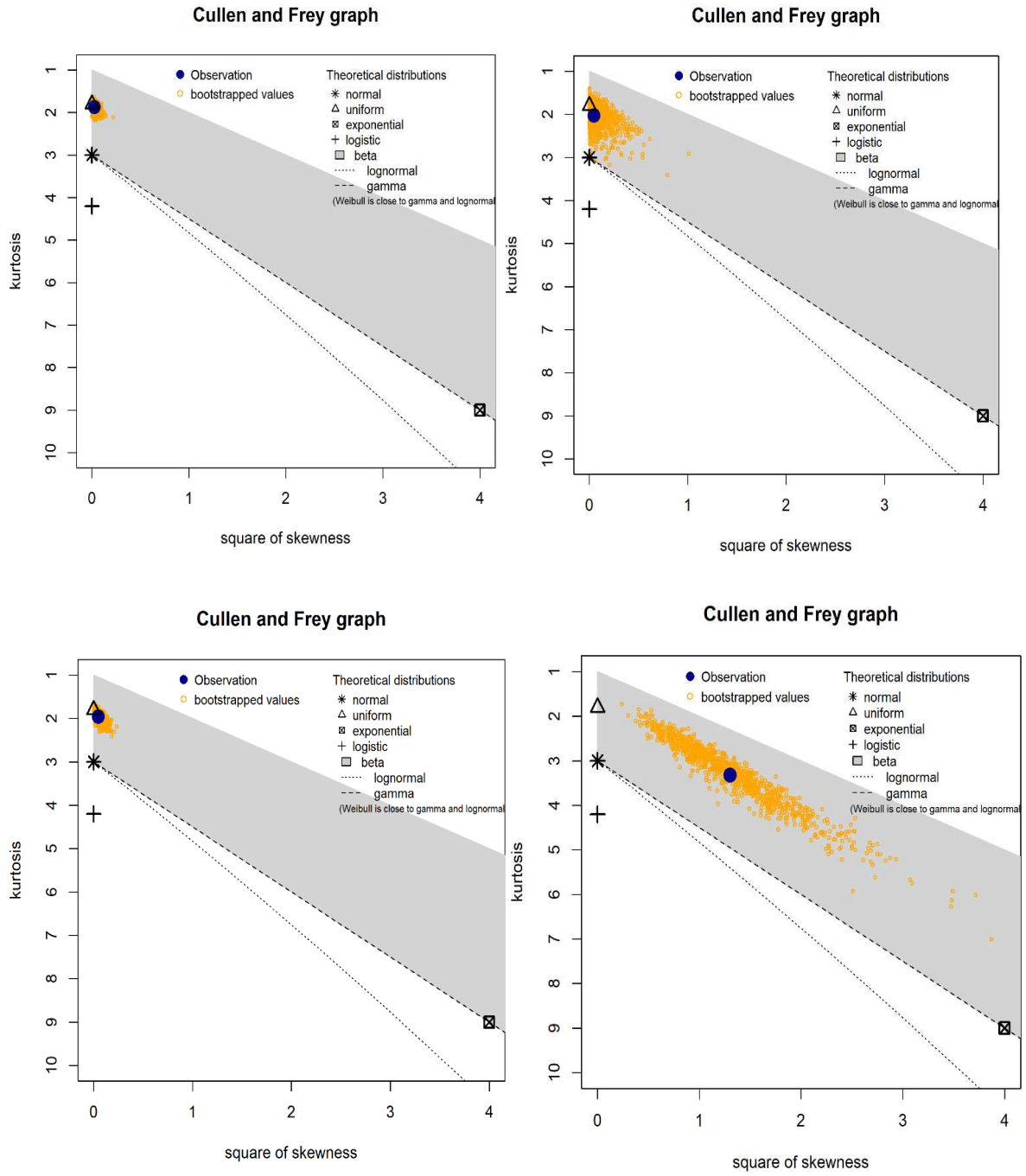
Cullen and Frey graph
Observation
bootstrapped values
Theoretical distributions
normal
uniform
exponential
logistic
beta
lognormal
gamma
(Weibull is close to gamma and lognormal)
kurtosis
square of skewness
Cullen and Frey graph
Observation
bootstrapped values
Theoretical distributions
normal
uniform
exponential
logistic
beta
lognormal
gamma
(Weibull is close to gamma and lognormal)
kurtosis
square of skewness
Cullen and Frey graph
Observation
bootstrapped values
Theoretical distributions
normal
uniform
exponential
logistic
beta
lognormal
gamma
(Weibull is close to gamma and lognormal)
kurtosis
square of skewness
Cullen and Frey graph
Observation
bootstrapped values
Theoretical distributions
normal
uniform
exponential
logistic
beta
lognormal
gamma
(Weibull is close to gamma and lognormal)
kurtosis
square of skewness

Plot 15:

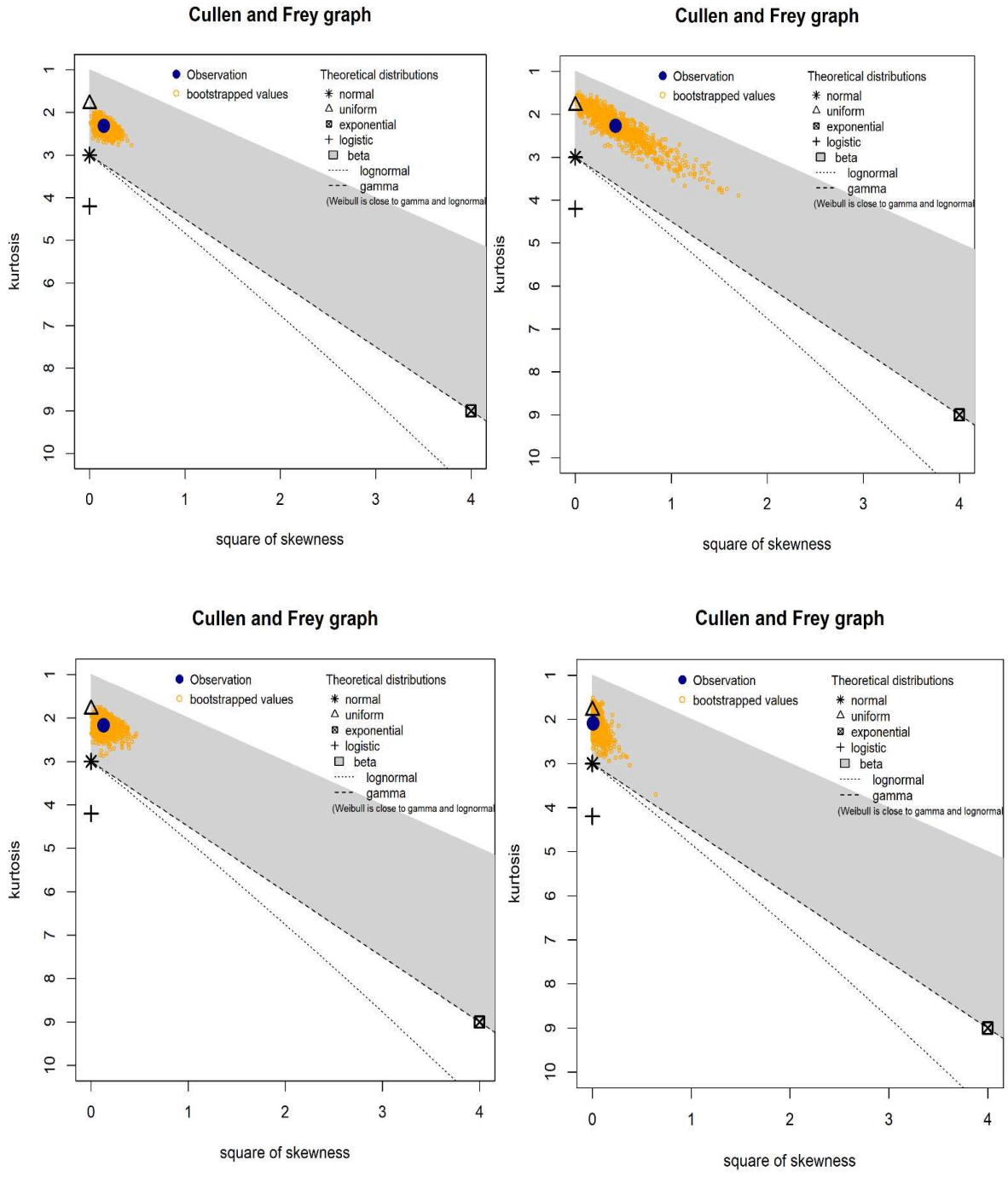
Cullen and Frey graph
Observation
bootstrapped values
Theoretical distributions
normal
uniform
exponential
logistic
beta
lognormal
gamma
(Weibull is close to gamma and lognormal)
kurtosis
square of skewness
Cullen and Frey graph
Observation
bootstrapped values
Theoretical distributions
normal
uniform
exponential
logistic
beta
lognormal
gamma
(Weibull is close to gamma and lognormal)
kurtosis
square of skewness
Cullen and Frey graph
Observation
bootstrapped values
Theoretical distributions
normal
uniform
exponential
logistic
beta
lognormal
gamma
(Weibull is close to gamma and lognormal)
kurtosis
square of skewness
Cullen and Frey graph
Observation
bootstrapped values
Theoretical distributions
normal
uniform
exponential
logistic
beta
lognormal
gamma
(Weibull is close to gamma and lognormal)
kurtosis
square of skewness

Plot 16:

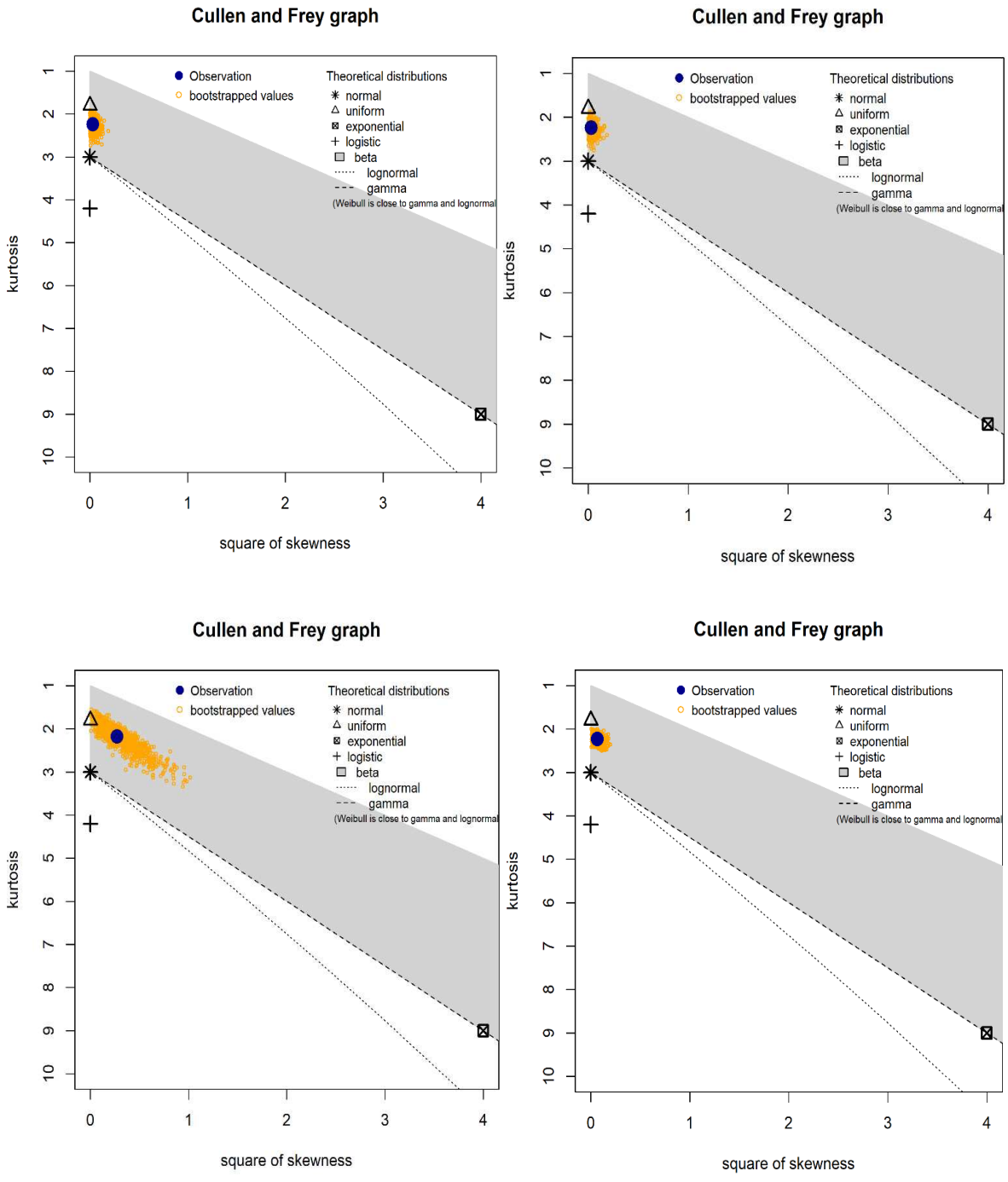
Cullen and Frey graph
Observation
bootstrapped values
Theoretical distributions
normal
uniform
exponential
logistic
beta
lognormal
gamma
(Weibull is close to gamma and lognormal)
kurtosis
square of skewness
0
1
2
3
4
1
2
3
4
5
6
7
8
9
10

C. HYDRUS season 1 simulation, inverse results for soil hydraulic parameters

Plot #1

Variable	Value	S.E.Coef.	95% Confidence limits Lower	Upper
WCR	0.09	0.05	0.00	0.18
WCS	0.46	0.05	0.36	0.56
ALPHA	0.00	0.00	0.00	0.00
N	1.37	0.15	1.08	1.67
COND S	12.25	2.34	7.62	16.88
L	0.56	0.35	-0.14	1.26
Qn	0.58	0.82	-1.04	2.20
Qo	0.01	0.05	-0.08	0.10
DispH	0.04	0.19	-0.33	0.42

Plot #2

Variable	Value	S.E.Coef.	95% Confidence limits Lower	Upper
WCR	0.08	0.06	-0.03	0.19
WCS	0.46	0.06	0.35	0.58
ALPHA	0.00	0.00	0.00	0.00
N	1.45	0.18	1.09	1.82
COND S	5.03	3.36	-1.60	11.67
L	0.60	0.87	-1.12	2.32
Qn	0.60	0.87	-1.11	2.31
Qo	0.05	0.18	-0.31	0.41
DispH	25.00	96.65	-166.21	216.21

Plot #3

Variable	Value	S.E.Coef.	95% Confidence limits Lower	Upper
WCR	0.08	0.02	0.04	0.12
WCS	0.39	0.02	0.35	0.42
ALPHA	0.01	0.00	0.01	0.01
N	1.26	0.03	1.20	1.33
COND S	8.69	0.89	6.93	10.45
L	0.01	0.17	-0.33	0.36
Qn	0.51	1.74	-2.93	3.95
Qo	0.02	0.28	-0.54	0.58
DispH	30.00	355.62	-673.53	733.53

Plot #5

Variable	Value	S.E.Coef.	95% Confidence limits Lower	Upper
WCR	0.09	0.01	0.07	0.10
WCS	0.50	0.06	0.38	0.62
ALPHA	0.00	0.00	0.00	0.00
N	1.32	0.06	1.20	1.44
COND S	7.44	3.39	0.73	14.16
L	0.00	0.00	0.00	0.00
Qn	0.60	1.31	-2.00	3.20
Qo	0.05	0.56	-1.05	1.15
DispH	29.02	263.46	-492.18	550.22

Plot #6

Variable	Value	S.E.Coef.	95% Confidence limits Lower	Upper
WCR	0.10	0.02	0.06	0.14
WCS	0.48	0.08	0.32	0.65
ALPHA	0.00	0.00	0.00	0.01
N	1.44	0.03	1.38	1.50
COND S	17.98	20.83	-23.23	59.19
L	0.01	0.05	-0.09	0.10
Qn	0.60	1.05	-1.49	2.69
Qo	0.05	0.52	-0.98	1.08
DispH	5.56	44.65	-82.78	93.90

Plot #7

Variable	Value	S.E.Coef.	95% Confidence limits Lower	Upper
WCR	0.00	0.00	0.00	0.00
WCS	0.42	0.07	0.28	0.55
ALPHA	0.00	0.00	0.00	0.01
N	1.19	0.06	1.07	1.31
COND S	16.24	4.18	7.97	24.50
L	0.11	1.01	-1.89	2.12
Qn	0.60	1.04	-1.46	2.66
Qo	0.03	0.30	-0.57	0.63
DispH	59.94	643.23	-1212.60	1332.50

Plot #8

Variable	Value	S.E.Coef.	95% Confidence limits Lower	Upper
WCR	0.10	0.01	0.08	0.12

Plot #9

Variable	Value	S.E.Coef.	95% Confidence limits Lower	Upper
WCR	0.02	0.07	-0.11	0.16

Plot #10

Variable	Value	S.E.Coef.	95% Confidence limits Lower	Upper
WCR	0.07	0.03	0.02	0.13

WCS	0.36	0.02	0.32	0.41
ALPHA	0.01	0.00	0.01	0.01
N	1.18	0.02	1.14	1.23
CONDS	21.74	18.79	-15.43	58.91
L	0.34	1.87	-3.35	4.04
Qn	0.60	1.06	-1.49	2.69
Qo	0.05	0.59	-1.11	1.21
DispH	28.08	334.84	-634.34	690.51

WCS	0.40	0.02	0.36	0.44
ALPHA	0.00	0.00	0.00	0.00
N	1.28	0.08	1.11	1.44
CONDS	5.00	4.36	-3.63	13.64
L	0.60	1.66	-2.68	3.88
Qn	0.60	0.75	-0.88	2.08
Qo	0.05	0.14	-0.23	0.33
DispH	5.14	18.00	-30.47	40.74

WCS	0.48	0.02	0.45	0.51
ALPHA	0.00	0.00	0.00	0.00
N	1.25	0.03	1.20	1.31
CONDS	6.54	2.57	1.46	11.63
L	0.54	0.45	-0.34	1.42
Qn	0.60	0.39	-0.17	1.37
Qo	0.01	0.02	-0.03	0.05
DispH	5.00	10.24	-15.26	25.26

Plot #11

Variable	Value	S.E.Coef.	95% Confidence limits Lower	Upper
WCR	0.05	0.03	0.00	0.10
WCS	0.44	0.01	0.42	0.46
ALPHA	0.01	0.00	0.01	0.01
N	1.16	0.01	1.13	1.19
CONDS	29.53	3.04	23.53	35.54
L	0.00	0.00	0.00	0.00
Qn	0.60	0.77	-0.92	2.12
Qo	0.01	0.03	-0.06	0.08
DispH	6.82	23.39	-39.46	53.09

Plot #12

Variable	Value	S.E.Coef.	95% Confidence limits Lower	Upper
WCR	0.10	0.05	0.01	0.19
WCS	0.45	0.03	0.40	0.51
ALPHA	0.00	0.00	0.00	0.00
N	1.27	0.08	1.11	1.42
CONDS	13.60	3.91	5.87	21.33
L	0.00	0.01	-0.01	0.01
Qn	0.60	0.58	-0.56	1.76
Qo	0.01	0.02	-0.04	0.06
DispH	50.00	139.70	-226.37	326.37

Plot #13

Variable	Value	S.E.Coef.	95% Confidence limits Lower	Upper
WCR	0.10	0.07	-0.03	0.23
WCS	0.49	0.07	0.34	0.63
ALPHA	0.00	0.00	0.00	0.00
N	1.27	0.13	1.02	1.53
CONDS	12.46	6.49	-0.37	25.29
L	0.08	0.50	-0.90	1.07
Qn	0.60	0.97	-1.33	2.53
Qo	0.03	0.28	-0.52	0.59
DispH	19.59	121.35	-220.47	259.65

Plot #14

Variable	Value	S.E.Coef.	95% Confidence limits Lower	Upper
WCR	0.09	0.04	0.01	0.18
WCS	0.50	0.08	0.34	0.66
ALPHA	0.00	0.00	0.00	0.00

Plot #15

Variable	Value	S.E.Coef.	95% Confidence limits Lower	Upper
WCR	0.13	0.03	0.07	0.20
WCS	0.45	0.04	0.37	0.54
ALPHA	0.01	0.00	0.00	0.01

Plot #16

Variable	Value	S.E.Coef.	95% Confidence limits Lower	Upper
WCR	0.09	0.06	-0.03	0.22
WCS	0.37	0.03	0.31	0.42
ALPHA	0.01	0.00	0.00	0.01

N	1.40	0.07	1.25	1.54
COND				
S	12.00	14.58	-16.85	40.85
L	0.57	0.43	-0.28	1.41
Qn	0.55	0.81	-1.04	2.14
Qo	0.05	0.33	-0.61	0.71
DispH	8.71	70.35	-130.45	147.88

N	1.35	0.14	1.07	1.63
COND				
S	22.64	8.00	6.82	38.47
L	0.00	0.00	-0.01	0.01
Qn	0.60	0.77	-0.92	2.12
Qo	0.05	0.33	-0.60	0.70
DispH	5.30	34.60	-63.16	73.75

N	1.21	0.10	1.01	1.41
COND				
S	11.44	6.41	-1.25	24.12
L	0.59	1.76	-2.90	4.08
Qn	0.60	0.85	-1.08	2.28
Qo	0.05	0.41	-0.76	0.86
DispH	5.00	43.66	-81.37	91.37

ABBREVIATIONS

AVRC: Arkansas Valley Research Centre

AW: Agricultural Water

CEX: Cation Exchange Resins

CEC: Cation Exchange Capacity

CIP: Cleaning in Practice

DSW: Desalinated Seawater

EC: Electrical Conductivity

FAO: Food and Agricultural Organization

IC: Inoculation with compost

LARV: Lower Arkansas River Valley

LBC: Lower Boundary Condition

mCDI: Membrane Capacitive Desalination

NC: No Compost

NF: Nano-filtration

PLC: Programmable Logic Controller

PV: Photo-voltaic

RO: Reverse Osmosis

SAR: Sodium Adsorption Rate

SPE: Saturation Paste Extract

SWDPs: Sea-Water Desalination Plants

TWW: Treated Wastewater

UBC: Upper Boundary Condition

VMC: Volumetric Moisture Content

WW: Well Water